University of Alberta

Extending HCCI Low Load Operation Using Chaos Prediction and Feedback Control

by

Ahmad Ghazimirsaied

A thesis submitted to the Faculty of Graduate Studies and Research in partial fulfillment of the requirements for the degree of Doctor of Philosophy.

Department of Mechanical Engineering

Spring 2012
Edmonton, Alberta

Abstract

Homogenous Charge Compression Ignition (HCCI) is a promising technology that offers high fuel economy and low oxides of nitrogen and particulate emission for automotive and stationary engines. A significant challenge with HCCI is the large number of partial burn/misfire cycles within the lean operation and the control of the combustion phasing. A detailed experimental and modeling investigation into the patterns of HCCI ignition timing and control based on deterministic structure of data points in HCCI combustion to reduce the high cyclic variations for operating conditions near misfire and to extend the HCCI operating range is the focus of this thesis.

Nonlinear dynamics and chaos theory applied to a wide range of engine operating conditions show that unstable operation of HCCI with higher cyclic variations with a non-Gaussian distribution is observed near the partial burn and misfire region of the engine. In order to predict and control the ignition timing in the partial burn region of HCCI, the temporal dynamics of cyclic variation in HCCI engine near misfire is analyzed using chaotic theory methods. Closed loop ignition timing control is used to reduce cyclic combustion variations for an unstable operating range of the engine near misfire using fuel octane as the control input.

Table of Contents

List of Tables

List of Figures

Nomenclature

Acronyms

aBDC	after Bottom Dead Center.
aTDC	after Top Dead Center.
AFR	Air Fuel Ratio.
BD	Burn Duration.
bTDC	before Top Dead Center.
CAD	Crank Angle Degree.
CAI	Controlled Auto-Ignition.
CDF	Cumulative Distribution Function.
CF	Cool Flame.
CFD	Computational Fluid Dynamics.
CFR	Cooperative Fuels Research.
CI	Compression Ignition.
CO	Carbon Monoxide.
CO_2	Carbon Dioxide.
COM	Control Oriented Model.
COV	Coefficient of Variations.
CV	Control Volume.

DFM	Dual Fuel Modulation.
dp3Lim	Threshold Limit for 3^{rd} Derivative of Pressure Trace.
ECU	Engine Control Unit.
EGR	Exhaust Gas Recirculation.
EIA	Energy Input Air.
EIF	Energy Input Fuel.
EOC	End of Combustion.
EVC	Exhaust Valve Closing.
EVO	Exhaust Valve Opening.
FPGA	Field-Programmable Gate Array.
GEV	Generalized Extreme Value.
GHG	Greenhouse Gas.
HC	Hydrocarbons.
HCCI	Homogeneous Charge Compression Ignition.
H_2O	Water Vapor.
HL	Heat Loss.
HRR	Heat Release Rate.
HTR	High Temperature Reactions.
IMEP	Indicated Mean Effective Pressure.
IVC	Intake Valve Closing.
IVO	Intake Valve Opening.
KIM	Knock Integral Model.

LTR	Low Temperature Reactions.
MIMO	Multi-Input Multi-Output.
MFB	Mass Fraction Burned.
MKIM	Modified Knock Integral Model.
NASA	National Aeronautics & Space Administration.
N_2	Nitrogen Gas.
ND	Normal Distribution.
NOx	Oxides of Nitrogen.
O_2	Oxygen Gas.
ON	Octane Number.
P	Products.
PCM	Phase-Change Materials.
PDF	Probability Density Function.
PFI	Port Fuel Injection.
PM	Particulate Matter.
PRBS	Pseudo-Random Binary Sequence.
PRF	Primary Reference Fuel.
R	Reactants.
RPM	Revolution per Minute.
SI	Spark Ignition.
SOC	Start Of Combustion.
STD	Standard Deviation.

TDC	Top Dead Center.
TKM	Thermo-Kinetic Model.
UEGO	Universal Exhaust Gas Oxygen (sensor).
VVA	Variable Valve Actuation.
VCR	Variable Compression Ratio.
VVT	Variable Valve Timing
W/M	Weak/Misfired.

Symbols

A	Area [m^2].
AFR	Air Fuel ratio [-].
B	Bore [m].
CA_X	Crank angle for X% burnt fuel [CAD aTDC].
C_D	Discharge coefficient [-].
C_v	Constant-volume specific heat capacity [$\frac{\text{kJ}}{\text{kg.K}}$].
C_p	Constant-pressure specific heat capacity [$\frac{\text{kJ}}{\text{kg.K}}$].
C_r	Compression ratio [-].
CoC	Completeness of combustion [-].
$\triangle T$	Exhaust gas transport delay [s].
d_v	Exhaust valve diameter [m].
EGR	Fraction of exhaust gas recirculated [-].
f_c	Cutoff frequency [$\frac{1}{\text{CAD}}$].

h	Enthalpy [$\frac{\text{kJ}}{\text{kg}}$].
h_c	Convective heat transfer coefficient [$\frac{\text{W}}{\text{m}^2.\text{K}}$].
k	Ratio of specific heat capacities [-].
L	Instantaneous cylinder height [m].
L_v	Exhaust valve axial lift [m].
LHV	Lower heating value of fuel [$\frac{\text{kJ}}{\text{kg}}$].
N	Engine speed [rpm] ; Number of moles [mole].
Φ	Equivalence ratio [-].
OF	Overlap factor [-].
PW	Pulse width [ms].
P	Pressure [kPa].
Q	Heat [kJ].
R	Gas constant [$\frac{\text{kJ}}{\text{kg.K}}$]
ρ	Density [$\frac{\text{kg}}{\text{m}^3}$].
S	Stroke [m].
S_p	Piston speed [$\frac{\text{m}}{\text{s}}$].
t	Time [s].
τ_f	Mean evaporation time for the fuel film flow [s].
τ_m	AFR sensor measurement time constant [s].
θ	Crank angle [CAD].
U	Internal energy [kJ].
V	Volume [m^3].

W	Work [kJ].
x	Fuel split parameter [-].
X_r	Residual gas mass fraction [-].
X_d	Mixture dilution fraction [-].
y	Mass fraction [-].

Subscripts

a	air.
b	burned ; base point.
c	compression.
ce	(flow) from cylinder to exhaust.
ch	charge (air+fuel+EGR).
d	duration.
dis	displacement.
e	expansion.
ec	(flow) from exhaust to cylinder.
exh	exhaust.
egr	exhaust gas recirculated.
eoc	end of combustion.
evc	exhaust valve closing.
evo	exhaust valve opening.
f	fuel.

ff	fuel film.
fi	fuel injected.
fv	fuel vapor.
g	cylinder gas.
i	cycle/specie number.
iso	isooctane.
inj	injected.
ivc	intake valve closing.
ivo	intake valve opening.
m	(intake) manifold .
mix	mixture.
mot	motoring.
s	(in-cylinder) surface.
soc	start of combustion.
t	total gas.
T	downstream of exhaust valves.
u	universal.
v	(exhaust) valve.
w	cylinder walls.

Chapter 1

Introduction

Global warming, limited fossil fuels resources and local pollution problems are three serious worldwide energy and environmental concerns of this era [4]. Considering the large number of vehicles manufactured worldwide (estimated 15-20 million road vehicles per year), automobiles are one of the largest consumers of fossil fuels [5], and subsequently one of the largest producers of carbon dioxide. A mid-term solution is to reduce fuel consumption and emissions through the use of efficient and clean combustion in engines. HCCI (Homogenous Charge Compression Ignition) is a promising technology offering high fuel economy and low NOx emission [6, 7]. HCCI combustion has the potential to have high thermodynamic efficiency and produce low emissions. HCCI can have efficiencies as high as Compression Ignition (CI) engines, while producing low NOx and PM emissions [8].

HCCI engine fundamentals, history, challenges and proposed solutions are introduced in this chapter. The main HCCI problem is then identified for this study and the research goals and the scope of this study are outlined. An overview of the structure of this thesis concludes this chapter.

1.1 BACKGROUND

1.1.1 HCCI Fundamentals

HCCI is considered as a high-efficiency alternative to Spark Ignited (SI) gasoline operation and as a low-emissions alternative to traditional diesel compression ignition (CI) combustion, particularly at part load and near the partial burn/misfire limit. HCCI combustion has the potential for improved fuel economy, very low oxides of nitrogen (NOx) and low particulate emissions [7]. HCCI is achieved by uniform auto-ignition of a homogeneous mixture of combustion gases. This leads to a low post-combustion temperature, which significantly reduces NOx emissions [9].

HCCI combustion combines the best features of both Spark Ignition (SI) and Compressed Ignition (CI) engines. Similar to an SI engine, the charge is well mixed which minimizes the NOx and particulate matter emissions. Like a CI engine, the combustion is compression ignited and has no throttling losses, which leads to high efficiency [10, 11, 8]. A schematic of the three types of combustion is shown in Figure 1.1.

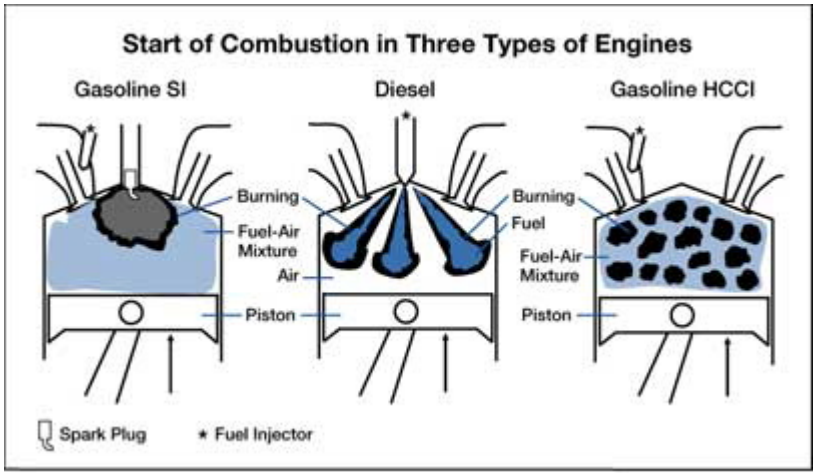

Figure 1.1: HCCI Engine versus SI and CI Engines.[3]

Unlike SI or diesel engines, where the combustion is initiated via spark and fuel injection respectively, HCCI has no defined input that initiates combustion. Therefore, ensuring that combustion occurs with acceptable timing, or at all, is more complicated than in the case of either SI or CI combustion. Combustion phasing in HCCI is dominated by chemical kinetics, which depend on the in-cylinder concentrations of reactants and products, their temperature and the amount of time that mixing takes place [12].

There are several methods used to initiate HCCI, such as heating or precompressing the intake air [13], trapping exhaust gases from the previous cycle by closing the exhaust valve early [14] and modulating intake and exhaust flows using variable valve actuation (VVA) to reinduct exhaust from the previous cycle [15]. As in a SI engine, a homogeneous air/fuel mixture is drawn into the cylinder and compressed. Ignition of the mixture does not depend on a spark but rather on the compression of the mixture, through which the temperature and pressure of the mixture are such that it will autoignite [16]. For HCCI engines which employ trapped hot residual as means of initiating combustion, it is necessary to operate the engine in SI mode first. Thus the HCCI mode is used at part and medium loads and the SI mode is used at cold start and high loads. As such, understanding the engine behavior in SI/HCCI mode transitions and the management of these transitions are critical to the successful implementation of HCCI in these engines [17, 18, 19]. Burning of premixed lean mixtures and the absence of diffusion-limited combustion remove the potential for soot formation in HCCI engines [20, 21]. The combination of both high efficiency and ultra-low PM and NOx emissions makes the HCCI engine an attractive alternative to traditional engines.

1.1.2 HCCI History

HCCI or controlled auto-ignition (CAI) combustion has been introduced as a new combustion process in reciprocating internal combustion engines through research papers over the last few decades. However, the age of this concept is the same as spark ignition (SI) combustion in gasoline engine and compression ignition (CI) combustion in diesel engines [22]. Diesel engines were developed over 100 years ago. Kerosene was injected onto the surface of a heated chamber in these engines partway early through compression stroke giving lots of time for mixing and vaporization of fuel with air. During the start-up, a burner heats a hot bulb on the outside. Vaporization of the injected fuel happens very quickly as it comes in contact with the surface because of hot bulb. The auto-ignited homogenous charge combustion was later found, when there were modifications on the main chamber so that a homogenous charge could be formed [23]. The Russian scientist Nikolai Semonov and his colleagues established the first theoretical and practical exploitation of chemical-kinetics controlled combustion for diesel engines in the 1930s [24]. Later in the 1970s, Semonov and Gussak [25] built the first CAI engine and controlled combustion by using active species which are discharged from a partially burned mixture in a separate prechamber. The original efforts on HCCI/CAI were done to control the combustion irregularities caused by the auto-ignition of the cylinder charge to obtain stable combustion in a conventional 2-stroke gasoline engine running lean [26, 27]. Subsequently, mainly in the late 1980s, several attempts were made to explore the fundamental principles of HCCI combustion. The first studies focused on the basic understanding of HCCI combustion and combustion mechanisms, chemical reactions, and the effects of the main engine input parameters on HCCI combustion. At this time, researchers found that HCCI combustion is influenced mainly by chemical kinetics due to its type of combustion. It was observed that HCCI combustion

produces almost no NOx, while the amounts of HC and CO are usually higher than in conventional engines.

Consequently, Honda introduced their first production CAI automotive engine which realized a fuel consumption reduction of up to 29% by utilizing the thermal energy of residual gases [28]. The subsequent investigation into the application of the new combustion process to a 4-stroke single cylinder engine employing the potential of this type of combustion to reduce emissions and fuel consumption was performed later [11, 8, 29]. Since the 1990s, the HCCI area has grown to a large world wide research topic because of higher fuel prices and the need to meet more stringent EU and US emission regulations [30, 31, 32, 33, 34]. Around the year 2000, it was shown that the CAI combustion is achievable in 4-stroke gasoline engines using early closure of exhaust valve or negative valve overlap [35, 36, 37, 14]. Trapping residual gas and exhaust gas rebreathing for initiating and controlling CAI have been popular in the last few years because no changes to vehicle are required [38]. HCCI technology has a high fuel flexibility ranging from biofuels [39, 40] to hydrocarbon and reforming fuels [41, 42, 43, 44, 45]

1.1.3 HCCI Challenges & Proposed Solutions in Literature

The practical application of HCCI requires overcoming several technical hurdles. HCCI misfire or partial burn is undesirable because it results in increased exhaust emissions and reduces engine power output [46], but it is desirable to run the engine near this limit to maximize the high efficiency HCCI operating range. Misfire and partial-burn criteria using crank angle based engine parameters are needed. The other main challenges of HCCI combustion are limited power output, maintaining constant ignition timing despite no direct mechanism to initiate combustion and to expand the part load region of HCCI near the misfire limit [47, 48]. These challenges are directly linked to normal and partial burn

region recognition, defining an accurate criteria of ignition timing, and cyclic variation characterization in HCCI engines. Under certain operating conditions, HCCI engines can exhibit large cyclic variations in ignition timing.

To increase the limited power output of HCCI engines, dual-mode combustion between SI-HCCI [49, 50, 51] and Diesel-HCCI [52, 53] has been proposed. Supercharging [54, 55, 56, 57] and turbocharging [56, 58, 59] have been used as tools to boost the intake air flow leading to higher power outputs. To prepare the homogenous mixture, early in-cylinder injection has been used for diesel fuels [60, 55]. Fuel injection in highly turbulent flow has been used for gaseous and volatile fuels [30, 61]. VVT and residual/gas trapping including exhaust gas trapping, modulating intake and exhaust flows have been used as actuators to affect the mixture temperature and eventually control the combustion timing [62, 63, 64, 65, 66]. Variable coolant temperature, in-cylinder injection timing, water injection, variable compression ratio (VCR) and variable EGR are among other existing methods to affect the control of combustion timing [67, 68, 69, 70, 71, 72, 64, 57, 73, 49]. Fuel additives, fuel reforming and modulating multiple fuels also affect combustion timing via the mixture reactivity changes[74, 75, 76, 77, 78, 79].

At a fixed fuel octane and engine speed, HCCI operation is limited by partial burn at low load, and knock at high load - both undesirable phenomena [80]. Methods to extend the HCCI operation range have been investigated [81]. Cycle-by-cycle experimental observations of important engine parameters have shown an inherent non-random structure inside a SI engine [82]. The presence of deterministic structures make it possible for real-time control methods to stabilize these unstable operating regions of the engine [83].

A significant challenge with HCCI is the control of the combustion phasing, which is necessary to obtain low fuel consumption and emissions [84]. HCCI lacks a direct combustion trigger making control of combustion timing challenging [85].

If the combustion event occurs too early, the hot combustion gases must be compressed, decreasing the thermal efficiency of the engine, increasing the NOx emissions, and potentially leading to knock. If the combustion event occurs too late, not all of the fuel will react, decreasing the thermodynamic efficiency of the engine and increasing the hydrocarbon and carbon monoxide emissions [86, 87, 88]. Thus, developing stable and robust methods of ignition timing control is paramount to achieving the potential of HCCI engines. There are engine conditions under which HCCI is unstable, so to realize the full potential of HCCI appropriate stabilizing strategies need to be developed to maximize the range of HCCI operation. Several recent publications have begun to address the control issues but have not focused on the fundamental nature of the transition dynamics associated with different operating conditions of HCCI combustion [89, 90, 17, 91]. Non-random cyclic dispersion for unstable HCCI conditions are observed in [37]. The presence of structure in the variations indicates the feasibility for developing real-time control methodologies to stabilize combustion at least in some regions which are unstable.

For closed-loop control of the combustion phasing, a feedback signal is necessary and pressure feedback is, perhaps, the most straightforward approach. In practice, the crank angle of 50 percent burnt fuel (CA50) has proved to be a reliable indicator of on-going combustion [92, 93, 84].

Controlling engine in-cylinder parameters to correspond to the engine operating conditions, results in the expected HCCI combustion phasing being obtained. With the development of control technology for engines, many combustion control approaches have been studied. Some approaches to actuate the combustion phasing are: exhaust gas recirculation (EGR) [94], variable compression ratio (VCR) [95, 96], variable valve timing (VVT) [97, 14, 98], dual fuel supply [99, 93], and thermal management [13]. Using these control methods,

HCCI range, stability and efficiency improvements in HCCI combustion have been achieved [15, 16, 17, 18, 19, 84].

In addition, different types of models have been used in modeling the combustion timing of HCCI engines in literature. These models range from simple control-oriented models [100, 101] to complex multi-zone models [102, 103] and multi-dimensional CFD models [104, 105].

Developing new methods to control ignition timing and extend the limited operating range of HCCI combustion requires an accurate comparison between the performance of different ignition timing criteria and characterizing the cyclic variation at various modes of operation. The accurate definition of ignition timing criteria, partial burn characterization and cyclic variations using chaotic methods are investigated in this thesis using collected experimental data at over 500 HCCI steady state operating points each with at least 300 consecutive engine cycles. This study, to the author's knowledge, is the first detailed analysis of performance of ignition timing at partial burn operation of HCCI engines.

1.2 Problem Identification and Research Scope

With lean combustion and exhaust gas recirculation to minimize NOx emissions, engine combustion cyclic variability (CV), also known as cyclic dispersion, becomes important. Recent examples of this interest can be found in [106, 107, 108, 109, 110]. Cyclic variations in HCCI combustion directly influence the operating range of HCCI. The operating range of HCCI is limited by knock at high load and by misfire/instability at low load where cyclic variations are unacceptably high [111]. High cyclic variations in HCCI engines makes the control of ignition timing more difficult [9]. Hence, it is critical to understand the cyclic variation characteristics and dynamics in order to find proper strategies for ignition timing control and extending the limited operating range of HCCI

engines.

One of the major constraints to practical lean operation has been the large number of misfires and partial burns. A misfire event is capable of destroying modern catalytic converters [112]. Misfires and partial burns are caused when cyclic variations are large enough to push the local in-cylinder equivalence ratio for a cycle very near to or less than the lean limit. Therefore, minimization of cyclic variations is a key requirement for operating near to or extending the effective lean limit [112].

The analysis of cyclic combustion variations is made difficult by the existence of interrelated contributing phenomena. Under idle conditions in which the air-fuel mixture stoichiometry is lean, the combination of residual cylinder gas and parametric variations (such as variations in fuel preparation) gives rise to significant combustion instabilities that may lead to engine roughness and transient emissions spikes. Such combustion instabilities may preclude operation at air-fuel ratios that would otherwise be advantageous for fuel economy and emissions [113]. HCCI combustion lacks features for direct control of ignition timing and it is mainly dependant on the charge properties which are influenced by the temperature of residual gas from a previous cycles [114].

A good understanding of the dynamics of HCCI combustion can be used to reduce the high cyclic variations under certain operating conditions and thus extend the operating range. This understanding, embodied in a mathematical model is used to recognize the deterministic structure inherent in the data points and can then be used to predict the cycles ahead. This prediction model can then be used to implement control applications on ignition timing of the HCCI engine [115].

The main causes of engine cyclic variations are grouped in two categories: linear random flow processes and deterministic coupling between consecutive cycles

which has been mostly analyzed using nonlinear and chaotic theory [116], [109], [82].

Cycle-by-cycle experimental observations of important engine parameters have shown an inherent non-random structure inside the SI engine [82]. The presence of deterministic structures suggests that techniques for real-time control to stabilize the unstable operating regions of the engine can be implemented [83].

The transition between spark ignition and HCCI combustion has been found to follow a relatively low-dimensional deterministic dynamics [83]. There the internal EGR (Exhaust Gas Recirculation) is varied by changing the timing and lift of the intake and exhaust valve. In [117], the connection between past and future combustion events are investigated using experimental nonlinear mapping functions. Their results confirm that the deterministic component of lean combustion variations can be approximated by fitting the data to a low-order nonlinear map. Chaotic behavior in a production internal combustion engine has also been documented in [118]. Different patterns of cyclic variation of combustion patterns have been observed in [119] including normal, periodic and cyclic variations with weak/misfired ignitions.

In [112], the development of period-doubling and bifurcation in the experimental measurements of spark ignition engine is investigated as the fuel is made leaner. Transition from stochastic behavior to a relatively deterministic structure has been recognized as λ is increased to very lean conditions. In [120], a method is proposed based on symbolic approach to measure temporal irreversibility in time series. In [121], a new method is introduced to detect and quantify the time irreversibility. Recent developments for applying a time-series analysis technique called symbolic time series analysis is summarized in [122]. In [123], the symbolic method is analyzed in a different way. It is declared in their work that symbolization can directly enhance signal-to-noise ratio. Onset of combustion instabilities

under lean fueling mixture condition was studied using symbolic methods for observed in-cylinder pressure measurements in SI engine [124], [125] and [120]. In [126], the observation of time irreversibility in cycle-resolved combustion measurements of SI engines is discussed and the advantage of their model to those linear gaussian random processes is expressed. The transition dynamics from conventional SI engines to HCCI engines is described using nonlinear tools in [127]. In their work, the cyclic combustion oscillations occurring in transition between the SI and HCCI engine as a sequence of bifurcations in a low-dimensional map is described.

Control of ignition timing, has been recognized as the most challenging problem in HCCI engines [128, 129]. Since ignition timing is the main control parameter in HCCI engines, the quality of the system used to control ignition timing affects the HCCI operation [130, 131]. The absence of a specific event to initiate the combustion and high sensitivity of HCCI to the variations in the charge properties are the reasons ignition timing control is so crucial [114].

The fuels that are used in this work include blends of n-Heptane and iso-Octane. These two fuels (n-Heptane and iso-Octane) are Primary Reference Fuels (PRFs) for octane rating in internal combustion engines, and have octane number of 0 (100% n-Heptane) and 100 (100% iso-Octane), with cetane number of approximately 56 and 15, which is very similar to the cetane number of conventional gasoline and diesel fuel, respectively.

The purpose of the work is to reduce cyclic variations of HCCI engine in order to extend the lean limit operating range. The focus of this thesis is to perform a detailed experimental and modeling investigation into the patterns of HCCI ignition timing. This requires identifying patterns of cyclic variations in HCCI ignition timing and determining different HCCI operating regions with deterministic cyclic variation characteristics. A chaotic predictive model is developed to

predict cycle-to-cycle combustion timing for an HCCI engine. The goal is to have a model that: can predict HCCI combustion timing one cycle ahead, has a good accuracy and has one physical input that can be used as the feedback parameter in the closed loop control of HCCI. The model predicted values will be used to control and regulate the desired engine parameters. The main emphasis is to employ the model outputs in order to control cyclic combustion variations for very unstable operating ranges of engine near misfire. One important feature of these regions which are close to misfire limit is very high cyclic variations which results in unstable operation. The model predicted cycle ahead ignition timing should be accurate enough for use as a feedback parameter to design subsequent control strategies in HCCI engines. Controlling and reducing high cyclic variations results in being able to extend the limited operating region of HCCI especially at misfire limit.

1.3 THESIS ORGANIZATION

This thesis is organized into eight chapters as schematically depicted in Figure 1.2. Chapter 1 contains the introduction and background method. The research target and scope of this work are described in this chapter. In chapter 2 the experimental setup used in this study is documented. The testing procedure and operation limits are then described. In addition, ignition timing definitions are also discussed in chapter 2, since ignition timing criteria will be used several times throughout the thesis. Categories of cyclic variability in HCCI engine ranging from stochastic to deterministic patterns are introduced in Chapter 3. This chapter focuses on studying how nonlinear scattering patterns of ignition timing cyclic variation develop in an HCCI engine. Several techniques applied in nonlinear dynamics and chaos theory are used in this chapter to observe possible deterministic structures inherent in the experimental data due to the experimen-

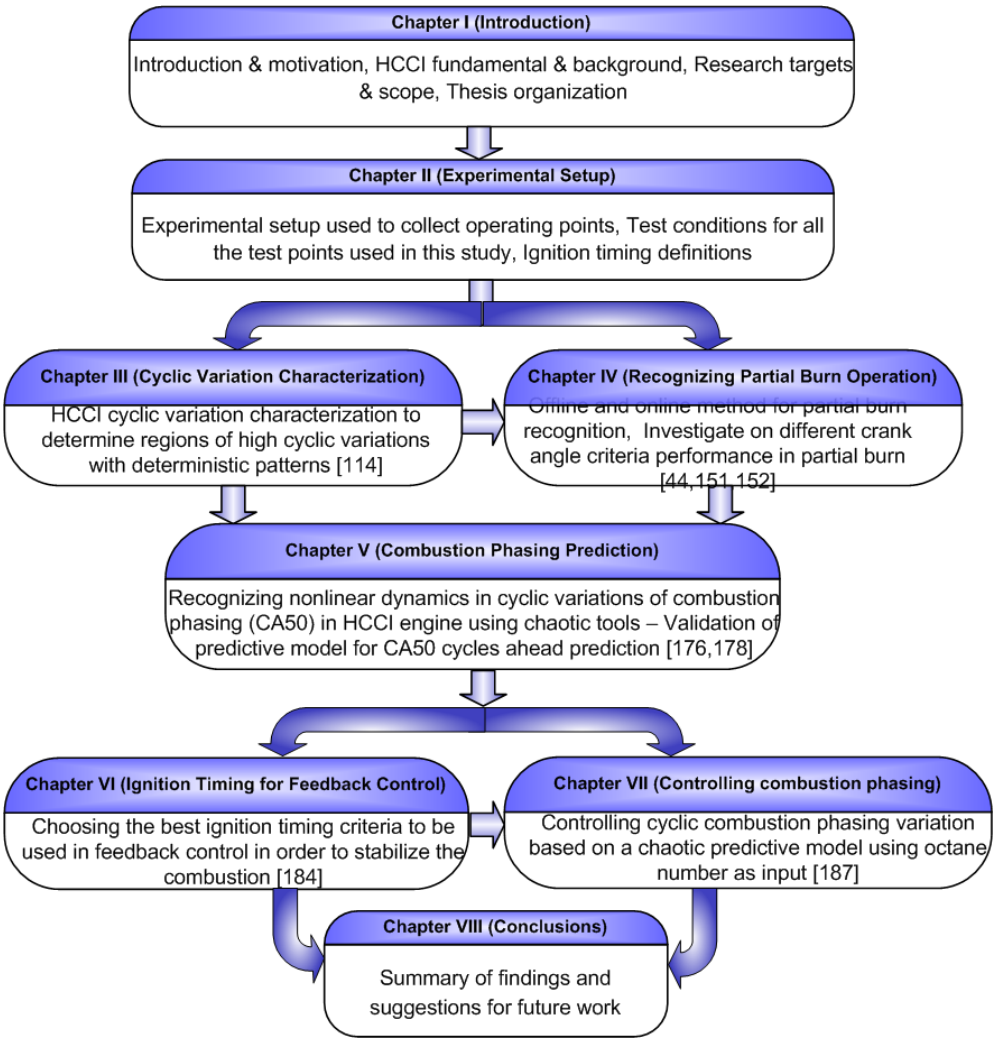

Figure 1.2: Schematic of the thesis organization. (Numbers in brackets refer to our work in conference and journal papers that is the basis for each chapter)

tal HCCI data ranges from the misfire limit to the knock limit varying intake manifold temperature. Dominant deterministic patterns are observed in some of the data near the misfire limit. The results show that unstable operation of HCCI with higher cyclic variations in ignition timing is observed closer to the misfire region of the engine. A wide range of engine operating conditions are also analyzed in Chapter 3 using normal distribution variation statistical tests. These results show that unstable operation of HCCI with higher cyclic variations of non-gaussian distribution is observed closer to the partial burn and misfire region of

the engine. Thus, partial burn/misfire region of HCCI will be the main focus of interest in order to extend the HCCI limited operating range and controlling the combustion instabilities for the following chapters. The results of this chapter provide a basis for recognizing the engine operation near partial burn and misfire in Chapter 4. They will also be used in Chapter 7 in order to extend the HCCI limited operating range and controlling the combustion instabilities.

To predict and control the ignition timing in partial burn region of HCCI, accurate offline and online estimates of ignition timing in that region of HCCI are needed. Offline and online methods to recognize partial burn are developed and discussed in Chapter 4. For offline operating condition ignition timing, a new method is proposed which combines the Coefficient of Variation of Indicated Mean Effective Pressure (COVImep) and percentage of cycles with less than 90 percent heat release of previous cycle. Particularly near the partial burn/misfire limit, this method is more reliable than just COVImep. In addition, different crankangle based methods for determining the start of combustion for each of the two regions of normal and partial burn are compared in Chapter 4. The different crank angle dependant methods used to characterize combustion timing can exhibit inaccurate results near the partial burn region of HCCI. The start and duration of combustion are compared for a wide range of operating conditions and the relative merits of each method are discussed. Finally, an online ignition timing estimate, defined as the ratio between peak of main stage of heat release and the sum of peak of main stage and cool flame stage of heat release is introduced in this chapter to more accurately identify the operating region of the engine. Using this, normal and partial burn engine cycles can be determined in realtime (engine cycle to cycle) for fuels exhibiting a cool flame. This criterion is used to understand the performance of each of the crank angle based methods that are analyzed. The performance of each method is investigated for both the low cyclic

variation and the high cyclic variation (unstable) region of the engine.

Temporal dynamics of cyclic variation in HCCI engine near misfire is analyzed using chaotic theory methods in Chapter 5. The analysis of variation of consecutive cycles of ignition timing is performed for a test point near the misfire condition. A symbol-statistic approach is used to find the occurrence of possible probabilities of the data points under the same operating conditions. These techniques are then used to predict ignition timing one cycle ahead. The predictive method for ignition timing cycles ahead prediction is also validated with experimental engine data in Chapter 5.

The crank angle where the maximum pressure occurs (θ_{Pmax}) is proposed as a robust criteria for distinguishing between normal and misfire HCCI combustion modes in Chapter 6. Particularly near the partial burn/misfire limit, this method is found to be more reliable than other existing methods. The performance of this new criteria is then analyzed for different engine loads at both constant fueling and constant equivalence ratio at 329 HCCI experimental operating points. The results from Chapter 6 are used in Chapter 7 in a feedback control algorithm that stabilizes ignition timing in these regions thus extending the useful operating range of HCCI. Variation of consecutive cycles of θ_{Pmax} is analyzed near misfire operation for five test points with similar conditions but different octane numbers. Predicted θ_{Pmax} has similar dynamical behavior to the experimental measurements. Based on this cycle ahead prediction, and using fuel octane as the input, feedback control is used to stabilize the instability of θ_{Pmax} variations at this engine condition near misfire. Finally, Chapter 8 summarizes the major results from this thesis and provides recommendations for further research.

1.4 Thesis Contributions

The major thesis contributions are summarized below:

- Characterized the cyclic variability of HCCI combustion using both chaotic and statistical methods. Studied the development of nonlinear scattering patterns of ignition timing cyclic variation in HCCI engine. Analyzed a wide range of engine operating conditions to determine which conditions have have a normal distribution for ignition timing [115].

- Defined two criteria (offline and online method) for partial burn operation using experimental data from HCCI engine collected at 115 operating points. Investigated and compared the performance of five methods for characterizing the combustion timing based on the two criteria [132, 46, 133].

- Found a comprehensive ignition timing that works for both normal and partial burn operating conditions [134].

- Captured the deterministic structure inherent in the data points. Performed an analysis of variation of consecutive cycles of ignition timing for an n-heptane fueled engine near the misfire condition in order to predict the following cycles using the identified dynamics. Predicted the next cycle ahead combustion timing [135, 136].

- Developed and implemented a feedback control scheme to stabilize the high cyclic variations of ignition timing. Reduced combustion timing variations resulting in a more stable engine operation with fewer misfire cycles [137].

Chapter 2

EXPERIMENTAL SETUP & DATA ANALYSIS

This chapter describes the experimental setup used in this study. The testing procedure and operation limits are then described. In addition, definitions of different ignition timing criteria are discussed and the chapter concludes with a brief discussion of the setup. Two different engine experimental setups have been used in this study for data acquisitions and each is described in detail.

2.1 EXPERIMENTAL SETUP

A single cylinder Ricardo Hydra Mark 3 engine fitted with a Rover K-7 head and a single cylinder Ricardo Hydra Mark 3 block fitted with a VVT Mercedes E550 cylinder head are used to carry out HCCI experiments [1]. Table 2.1 lists the geometrical specifications of both the Ricardo with Rover and Mercedes head engines [2]. This engine represents a typical spark ignition engine, outfitted with a piezo-electric pressure transducer mounted between an intake and exhaust valve. A schematic of the test cell is shown in Figure 2.1. The Ricardo engine uses a flat top cast aluminum piston and has a combustion chamber with pent-roof design with a centrally located spark plug. Two intake and two exhaust valves are operated with dual camshafts located in the cylinder head. The fuel is injected into the intake port, when the intake valves are closed, with 3 bar fuel pressure

using a standard automotive fuel injector. In Figure 2.1, one fuel system is used to inject n-Heptane and the other is used to inject iso-Octane. The separate flow rate control of each of these two fuels allows any desired octane number to be obtained. Both n-Heptane and iso-Octane injectors are aimed directly at the back of the intake valves. The fuel injection is done with a dSpace-MicroAutobox ECU (Engine Control Unit), which provides accurate control of the injection timing as well as the duration. The ECU also controls the spark timing, which is used during the engine warm-up in SI mode but is turned off for HCCI combustion. The fresh intake air entering the engine is first passed through a laminar air-flow meter for flow rate measurement. Then, the fresh charge is mixed with recirculated hot exhaust gases (EGR) using an insulated return line controlled with a valve from the exhaust to the intake before the supercharger. Next, a supercharger driven by a variable speed electric motor adjusts the intake manifold pressure and then a 600W electrical band-type heater sets the mixture temperature to a desired value using a closed-loop controller. Finally the exhaust gases exiting the cylinder are sampled for emission analysis. As shown in Figure 2.1, the emission can be sampled from either the intake manifold or from the exhaust manifold. The engine out Air Fuel Ratio (AFR) value is measured by ECM AFRecorder 1200 UEGO with measurement accuracy of 0.01-0.03. Intake temperature is measured with 2 °C resolution using a K-type thermocouple positioned in the intake manifold before the charge entering into the cylinder. The EGR rate is determined by comparing the CO2 concentrations in the intake and exhaust manifolds, and by assuming that all CO2 in the intake manifold is from the exhaust gases. Measurement of the cylinder pressure is done using a Kistler water- cooled ThermoCOMP (model 6043A60) piezoelectric pressure sensor that is flush mounted in the cylinder head. Crank angle measurement with 0.1 ° resolution is done using a BEI optical encoder connected to the crankshaft on the front of the engine.

An emissions test bench is used to collect emissions data. NOx is measured with 1 ppm resolution using Horiba CLA-510SS emission analyzer and Horiba FIZ-510 emission analyzer is used to measure HC with 10 ppm resolution. CO is measured with 0.01% resolution using Siemens ULTRAMAT6 emission analyzer. There are uncertainties associated with measuring each input parameter. Based on the procedure of sequential perturbations, the uncertainty analysis of the inputs necessary in calculating the result is performed to determine the effect of each input error on the output [138]. Table 2.2 lists the estimated uncertainty associated with measured parameters.

Table 2.1: Configuration of the Ricardo single-cylinder engine fitted with Rover and Mercedes cylinder head.

Parameters	Rover	Mercedes
Bore × stroke [mm]	80 × 88.9	97 × 88.9
Compression Ratio	10	12
Connecting Rod Length [mm]	159	159
Displacement [L]	0.447	0.653
Number of Valves	4	4
IVO, IVC [aBDC]	-175 °, 55 °	-
EVO, EVC [aBDC]	-70 °, -175 °	-

Table 2.2: Estimated uncertainty in measured inputs for the Ricardo engine with Rover head. [1]

Parameters	Value	Uncertainty (±)
B [m]	0.080	0.001
S [m]	0.089	0.001
L [m]	0.159	0.001
V_{TDC} $[m^3]$	4.98e-5	0.05e-5
T_{man} [°C]	64 - 141	2
λ []	1.8 - 3.5	1%
N [rpm]	800 - 1200	10
$\dot{m}_{air}$ [g/sec]	3.1 - 4.2	5%
$\dot{m}_{fuel}$ [g/sec]	0.054 - 0.134	3%
T [Nm]	5.2 - 16.9	0.1

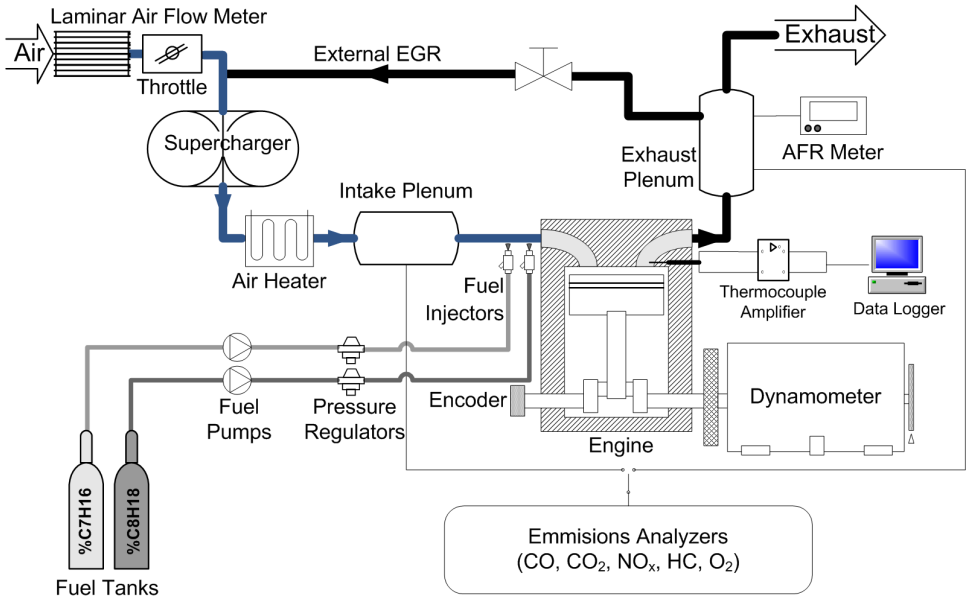

Figure 2.1: Schematic of the experimental setup

The cylinder head used in this study has built in camshaft phasers. In production engine fitted with Mercedes E550 head these phasers are controlled by the engines Electronic Control Unit (ECU) but for this research custom controllers are designed and built. For this study phasers are controlled using the dSPACE MicroAutoBox. The PI controller runs at a 1kHz sample rate and the gains are manually tuned. The timing adjustment of 40 °can individually be set for both the intake and exhaust valves. The timings used in this study can be seen in Table 2.3. The change in valve timing is not instantaneous due to the mechanical inertia of the system. This phaser dynamics is time based, so as the engine speed is increased it will take more engine cycles to complete the same timing change.

Table 2.3: Timing of intake and exhaust valves using Mercedes E550 head. [2]

Parameters	Timing Range
Intake	202-242 aTDC
Exhaust	13-53 bBDC

N-heptane and iso-octane are individually port injected with the fuel scheduling of the two injectors done using a dSpace-MicroAutobox ECU. Realtime combustion analysis is done with A&D Baseline CAS. Using this degree based real time processor the cylinder pressure was recorded 3600 times per crank revolution, this was then analyzed for the pertinent combustion metrics, such as IMEP (Indicated Mean Effective Pressure), ignition timing such as θ_{Pmax}, CA10, CA50, and burn duration. All other parameters are logged on a time basis using the test cell A&D Baseline DAC.

2.2 EXPERIMENTAL SETUP - TEST CONDITIONS

Tables 2.4 to 2.6 details all the experimental engine operating points used for this study. The engines are run for five different PRF blend fuels (PRF0, PRF10, PRF20, PRF30, PRF40)[1]. The relatively low compression ratio of the Ricardo engine does not allow the operation of HCCI for high octane number fuels. The maximum octane number in which the HCCI operation could be maintained is PRF40 for the Ricardo engine.

Table 2.4 list the test operating conditions of 338 operating points with 300 consecutive cycles, of which 9 exclusively consist of 3000 consecutive cycles and are used for the manifold temperature sweep and all are used for the normal distribution analysis. All of the engine operating points are at steady-state operating conditions (inputs to engine and engine speed held constant). All of these operating points are collected using the engine setup fitted with a Rover K7 head.

[1]PRF number is defined as the volume percentage of iso-Octane in the fuel mixture of n-Heptane (PRF0) and iso-Octane (PRF100).

Table 2.4: Ricardo engine operating conditions 1

Parameter	**Range**
Manifold Pressure [kPa]	88-162
Manifold Temperature [°C]	60-161
External EGR [%]	0-30
Fuel Octane Number [PRF]	0,10,20,40
Engine Speed [RPM]	760-1340
Equivalence Ratio [-]	0.29-0.95
Coolant Temperature [°C]	25-84
Oil Temperature [°C]	48-80

Table 2.5 lists the tests operating conditions of 59 operating points with 300 consecutive cycles of which 30 are found at partial burn region, 11 at misfire and 18 at normal operating conditions region. The operating points span the range between normal operating condition to the misfire condition. All of the engine operating points are at steady-state operating conditions (inputs to engine and engine speed held constant). All of these operating points are collected using the engine setup fitted with a Mercedes E550 cylinder head.

Table 2.5: Mercedes engine operating conditions 2

Parameter	**Range**
Manifold Pressure [kPa]	90-120
Manifold Temperature [°C]	85-102
External EGR [%]	0
Fuel Octane Number [PRF]	0,10,20,30,40
Engine Speed [RPM]	1024
Equivalence Ratio [-]	0.30-0.54

Table 2.6 lists the tests operating conditions of 115 operating points with 300 consecutive cycles. The operating points span the range between normal operating condition to the misfire condition. All of the 115 engine operating points are at steady-state operating conditions (inputs to engine and engine speed held constant). All of these operating points are collected using the engine setup fitted with a Mercedes E550 cylinder head.

Table 2.6: Mercedes engine operating conditions 3

Parameter	Range
Manifold Temperature [°C]	85-97
Fuel Octane Number [PRF]	0,10,20,30,40
Manifold Pressure [kPa]	90-120
Equivalence Ratio [-]	0.29-0.55
External EGR [%]	0
Engine Speed [RPM]	1021-1074

2.3 IGNITION TIMING DEFINITION

HCCI combustion of the saturated hydrocarbon compounds known as alkanes including paraffins such as n-Heptane and iso-Octane exhibit a two-stage auto-ignition mechanism attributed to chain branching reactions via alkoxyperoxide dissociation [139, 140]. The two combustion stages as shown for n-Heptane in Figure 2.2 involve Low Temperature Reactions (LTR) for cool flame (1st stage) and High Temperature Reactions (HTR) for the main (2nd stage) combustion. Low Temperature Reactions (LTR), particularly reactions involving n-Heptane control the first combustion stage. The second stage combustion is controlled by High Temperature Reactions (HTR) that starts when the decomposition of H2O2 becomes slower than its production at a temperature around 1000 °K [141]. Timing of the combustion process is important, and there are many different ways that the timing of HCCI can be calculated [142]. The start of the main (2nd stage) combustion, denoted here as SOC, is defined as being the point at which the third derivative of the pressure trace with respect to the crank angle (θ) in CAD (Crank Angle Degree) exceeds a heuristically determined limit [142, 16]:

$$dp3Lim = \frac{d^3P}{d\theta^3} \mid_{ign} = \frac{d^3P}{d\theta^3} \mid_{lim} [\frac{kPa}{CAD^3}] \tag{2.1}$$

where the dp3Lim value is determined from the available experimental data

for each engine. More details about the method to determine SOC is found in section 4.2.

The heat release method [143], that applies the first law analysis on the engine charge assuming ideal gas properties, is used to determine net HRR (the combustion energy release less heat lost to the walls). Fuel Mass Fraction Burnt (MFB) is calculated using the Rassweiler method [144] so that crank angles of the percentage of the fuel burnt can be determined. CA10, CA50, and CA90 are defined as the crank angles for 10%, 50%, and 90% MFB respectively. Burn Duration (BD) is defined as the crank angle rotation between CA10 and CA90 as indicated in Figure 2.2. Definitions of ignition timing are indicated in Figure 2.2 for a sample test point.

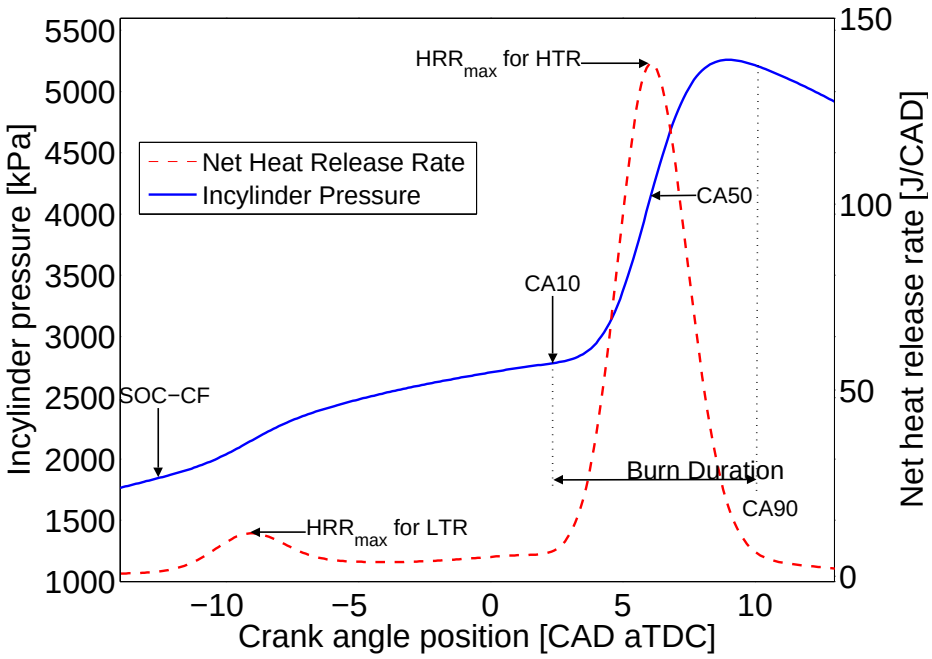

Figure 2.2: Ignition timing definitions – using in-cylinder pressure trace and net heat release rate for PRF10, N= 1000 rpm, Φ= 0.42, EGR= 0%, T_m= 112 ^oC, P_m= 120 kPa

θ_{Pmax} is defined as the crank angle of the maximum in-cylinder pressure during one engine cycle. With early or late combustion, θ_{Pmax} is a representation of the heat release phasing since it is closely coupled to the combustion volume. An example of the location of θ_{Pmax} for HCCI combustion is shown in Figure 2.3 where cylinder pressure is plotted versus crankangle.

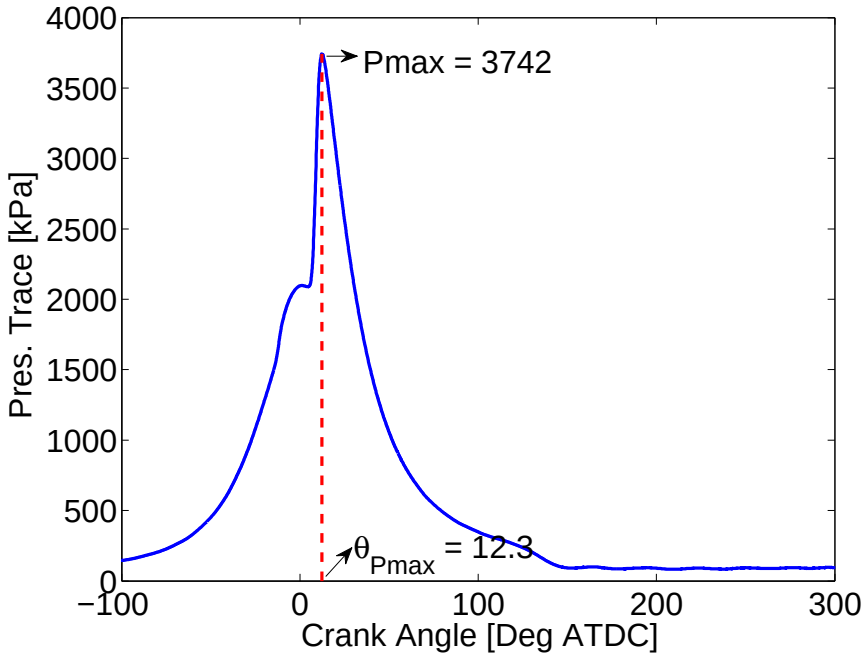

Figure 2.3: Sample operating point for HCCI combustion at point A. Conditions: PRF 0, engine speed n = 800 rpm, T_{man} = 120 °C, P_{man} = 93 kPa, ϕ = 0.51, EGR = 0%, $T_{coolant}$ = 75 °C, T_{oil} = 66.5 °C

In-cylinder pressure traces from 300 or 3000 consecutive engine cycles with 0.1 °resolution are recorded for each experimental point. The experimental pressure signal is filtered with a second order Butterworth low pass filter with cutoff frequency of $f_c = 0 : 556CAD^{-1}$ to remove high frequency noise so that numerically differentiating the pressure trace to get SOC based on equation 2.1 is viable. The pressure signal is filtered in the crank angle domain to avoid having to change the cutoff frequency for different engine speeds and the filtering is done in both forward and reverse directions to avoid any phase shift.

2.4 SUMMARY

The experimental setup used to collect the operating points has been detailed in this chapter. The operating points cover the whole range between knock operating condition to the misfire condition. The combustion behavior characteristics will be examined for these operating conditions in the following chapters in order to detect the unstable region of operation. Then control will be applied in the unstable region in order to stabilize the combustion and extend the HCCI operation region.

Chapter 3

CYCLIC VARIATION CHARACTERIZTION IN HCCI COMBUSTION USING CHAOTIC AND STATISTICAL APPROACH[1]

Under certain operating conditions, HCCI engines can exhibit large cyclic variations in ignition timing. Cyclic variability in an engine can be categorized as ranging from stochastic to deterministic patterns. This chapter focuses on studying how nonlinear scattering patterns of CA50 cyclic variation develop in an HCCI engine.

The return map technique applied in nonlinear dynamics and chaos theory is used in this chapter to observe possible deterministic structures inherent in the experimental data. Transitions from the misfire to knock limit within the HCCI mode are generated by varying intake manifold temperature. Using CA50 return maps, a general trend is observed such that when intake manifold temperature is reduced, the beginning and subsequent development of bifurcation emerges. Dominant deterministic patterns are observed in some of the data which can be caused by nonstationary or transient dynamics of the engine near misfire limit. Return map results for CA50 near the knock limit show an unstructured cluster

[1]The results of this chapter are partially based on [115].

of circular data gathered around a fixed point. The return maps of CA50 start to scatter over the diagonal line as engine conditions are changed towards the misfire limit and fixed points becomes destabilized leading to more structured data points. The structured patterns seen in the data can be attributed to the deterministic coupling between consecutive cycles. These results show that unstable operation of HCCI with higher cyclic variations is observed closer to the misfire region of the engine. The results of this chapter will be used to extend the HCCI limited operating range and controlling the combustion instabilities in subsequent chapters.

3.1 INTRODUCTION

Cyclic variations in SI engines have been experimentally studied for decades [145, 146], but only some experimental studies [117, 83, 147, 148, 149, 150, 37, 151, 152, 127] in recent years partially investigate the cyclic variations in HCCI engines. The transition between spark ignition and HCCI combustion which follows a relatively low-dimensional deterministic dynamics has been documented in [83] where the internal EGR (Exhaust Gas Recirculation) is varied by changing the timing and lift of the intake and exhaust valve. In [117], the connection between past and future combustion events are investigated using experimental nonlinear mapping functions. Their results confirm that the deterministic component of lean combustion variations can be approximated by fitting the data to a low-order nonlinear map. Chaotic behavior in a production internal combustion engine has also been documented in [118]. Different patterns of cyclic variation of combustion patterns have been observed in [119] including normal, periodic and cyclic variations with weak/misfired ignitions. In [149], a single-cylinder engine fueled with different PRF mixtures is run in HCCI mode to study cyclic variations of HCCI combustion. The study shows that when the octane number is decreased

the distribution of combustion parameters is more concentrated around mean values and cyclic variations of performance parameters significantly decrease. In [147], limits of HCCI combustion are investigated on a single-cylinder engine for 19 different gasoline-like fuels with octane numbers higher than 60. An octane index to characterize high HCCI cyclic variation limit and a knock limit is defined. They observe that acceptable HCCI cyclic variation occurs only within a narrow range of ignition timing around TDC. In [37], the variations of cycle resolved gas temperature and unburned hydrocarbons are discussed for a camless gasoline HCCI engine. They find a strong correlation between the combustion phasing and the gas temperature at the beginning of the compression stroke and no correlation is found between the residual (exhaust) gas temperature at the end of the expansion stroke and the combustion phasing of the next cycle. They also report that a high level of hydrocarbons in the residuals is generated by quenching that occurs for late combustion timing. These hydrocarbons auto-ignite during the following gas exchange phase. Experimental results in [151] for a lean burn engine fueled with n-pentane and n-Heptane indicate that HCCI operating conditions are limited by the extent of non-homogeneity of the intake charge – both in mixture quality and temperature. They observe lower HCCI cyclic variations near to the knock limit and for higher compression ratios at a constant equivalence ratio. Stability of late-cycle auto-ignition is studied in [148, 152] for a single-cylinder diesel engine run in HCCI mode. They observe that variations of IMEP increase rapidly after a certain combustion phasing or late limit. Increasing the fueling rate retards the late limit of combustion phasing before the onset of unstable HCCI combustion. This late limit is a function of fuel as iso-Octane (PRF100) fuel tolerates less retarding of combustion phasing compared to a lower PRF blend (i.e. PRF80). Results from [127, 83] on the cyclic combustion variability of a spark-assisted gasoline engine during transition

between SI mode and HCCI mode show that HCCI cyclic variation can follow a repeatable pattern of complex combustion that is not a random process. More deterministic structure is observed in cyclic variation of HCCI ignition timing as the engine operating condition is changed from the knock limit to the misfire limit [115].

Here, cyclic variation of ignition timing in an HCCI engine is investigated using a range of experimental data collected from a single-cylinder Ricardo engine. Two methods, the engine variation and bifurcation plot, to study patterns of CA50 (Crank angle of 50% fuel burnt) cyclic variation is applied in an HCCI engine. Nine points ranging from the misfire to the knock limit within the HCCI mode are experimentally measured by varying the intake manifold temperature. Return maps from chaotic theory are used to check the deterministic structure inherent in the data points as intake manifold temperature decreases. Probability distribution for cyclic combustion timing is the second approach examined. Experimental data of 338 different points over a wide range of operating conditions are examined to find out the conditions where a normal distribution for CA50 is observed. Three common statistical testing methods are used to verify the hypothesis of having a normal distribution for each data point.

The experimental engine setup is explained in Section 2.1 in which the engine fitted with a Rover K-7 head are used for data collection. The tests operating conditions are listed in Table 2.4 and 338 points are analyzed of which 9 are used for the manifold temperature sweep and all are used for the normal distribution analysis.

3.2 TRANSITION ANALYSIS

3.2.1 Stability Analysis

An intake manifold temperature sweep from the knock limit to the misfire limit in HCCI mode where the intake manifold temperature is varied while keeping all the other parameters constant is performed for nine temperatures. The test operating conditions are listed in Table 2.4 for the experimental setup fitted with a Rover K-7 head described in section 2.1. The reason for varying the intake manifold temperature is that HCCI combustion is sensitive to temperature [119]. For these measurements each intake manifold temperature level 3000 consecutive cycles are recorded. To characterize the cyclic HCCI combustion dynamic behavior, several methods are used.

First, the engine stability in terms of Coefficient of Variation (COV) of Indicated Mean Effective Pressure (IMEP) of HCCI combustion during the transition from misfire to knock limit is examined in Figure 3.1. COV is defined as Standard Deviation (STD) divided by the mean value. In Figure 3.1, the point with $T_{man} = 80^oC$ corresponds to the HCCI operation region near the misfire limit where COV of IMEP is high. Near the knock limit region ($T_{man} = 145^oC$), COV of IMEP reaches its minimum value, which indicates the most stable mode of the combustion (in terms of COV of CA50).

Since CA50 is a very good indicator of ignition timing in HCCI [92], it is used here as is the cyclic variation of CA50 during HCCI operation. The Standard Deviation of CA50, which is a good measure of how CA50 variation changes, is shown in the Figure 3.2 for varying intake manifold temperature. Increasing the intake manifold temperature from the misfire limit to the knock limit results in CA50 variation decreasing as shown in Figure 3.2.

A bifurcation diagram is used to reflect the effect of each parameter on the

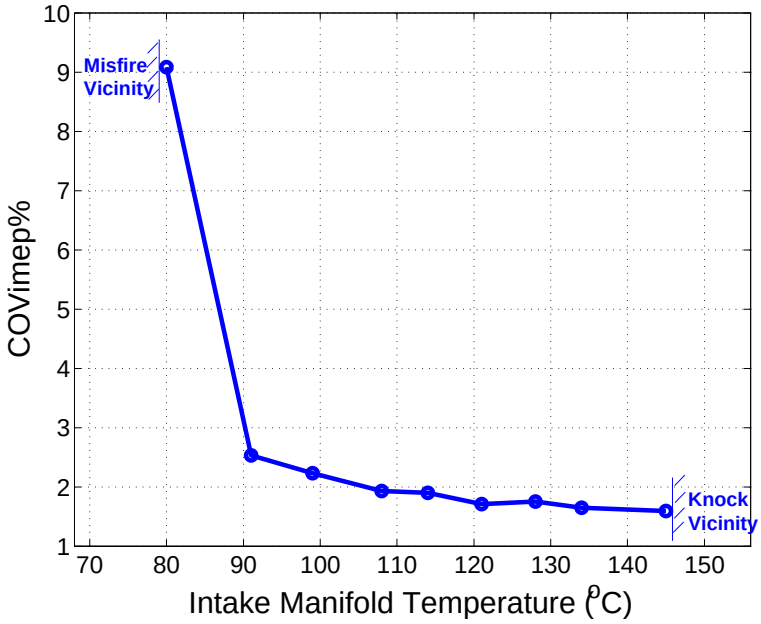

Figure 3.1: The coefficient of variation (COV) in the IMEP for intake manifold temperature sweep

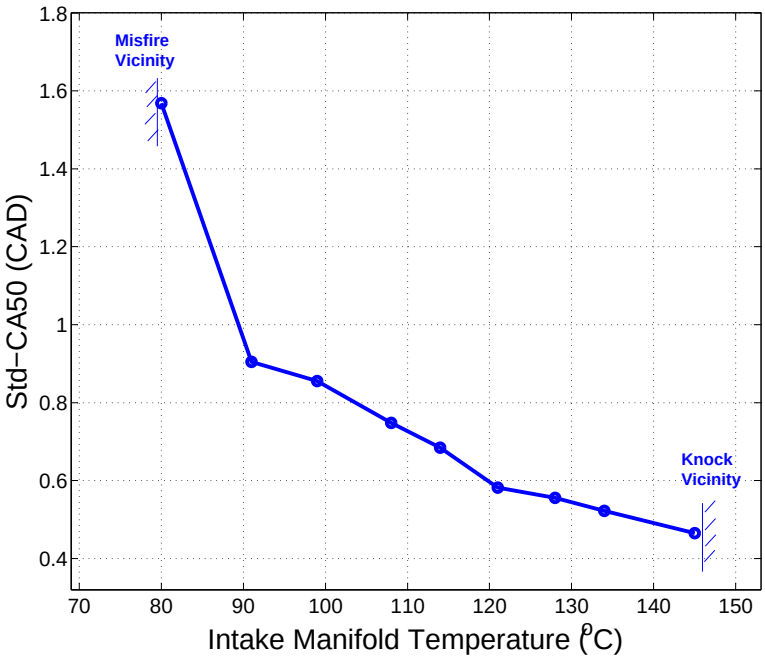

Figure 3.2: Variation in STD of CA50 cyclic ensemble for intake manifold temperature sweep

whole time series [112] and is shown in Figure 3.3 where the variation of the grey scale seen in the plot is indicative of variation in density of CA50 data points. The concentration of data points around their mean point (darker area), increases near the knock limit. In addition, increasing intake manifold temperature advances CA50.

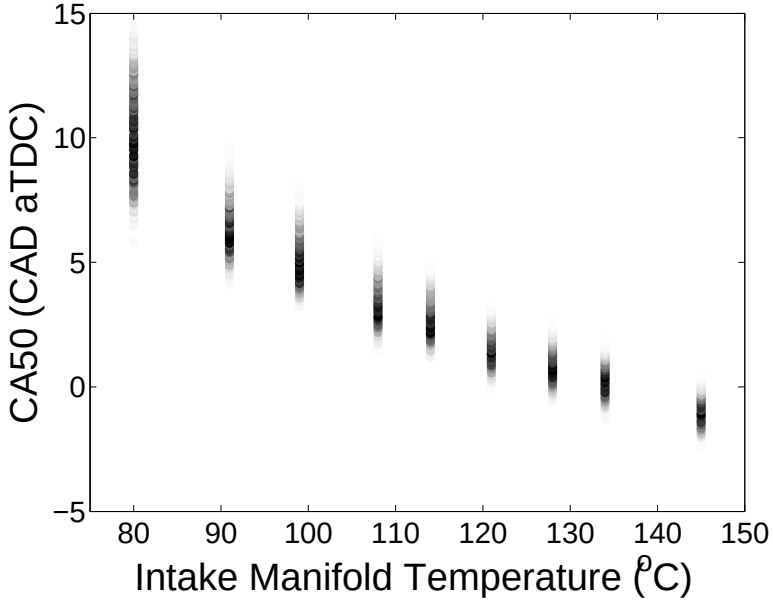

Figure 3.3: CA50 bifurcation diagram for intake manifold temperature sweep

3.2.2 Return Maps

The return maps as a chaotic theory technique is often used to determine the inherent deterministic structure of the data [83, 112, 121]. Return maps plot pairs of successive time series values versus each other (here the CA50 value for cycle i versus cycle i+1 are plotted in a return map). Using return map plots, each cycle point relates to the next cycle through the general statistical picture of the whole cycles interrelation [121] and these maps provide a qualitative tool to check the deterministic structure inherent in the data points [126]. The analysis of CA50 for a HCCI sweep from knock limit to misfire limit during HCCI

combustion in terms of the CA50 return maps is illustrated in Figure 3.4 for the range of intake manifold temperatures previously described. The dispersion of these data points over the diagonal line seem to occur because of nonstationary or transient dynamics of the engine near misfire limit, where oscillations between early and late CA50 occur frequently. Return maps result for CA50 near the knock limit show an unstructured cluster of circular data gathered around a fixed point which indicates the HCCI combustion is getting more stable in the vicinity of the knock limit. These data points start to scatter over the diagonal line as they move towards the misfire limit and fixed points becomes destabilized leading to more structured data points. The structured patterns seen in the data can be attributed to the deterministic coupling between consecutive cycles. Overall, the return maps exhibit more asymmetry as they approach the misfire limit.

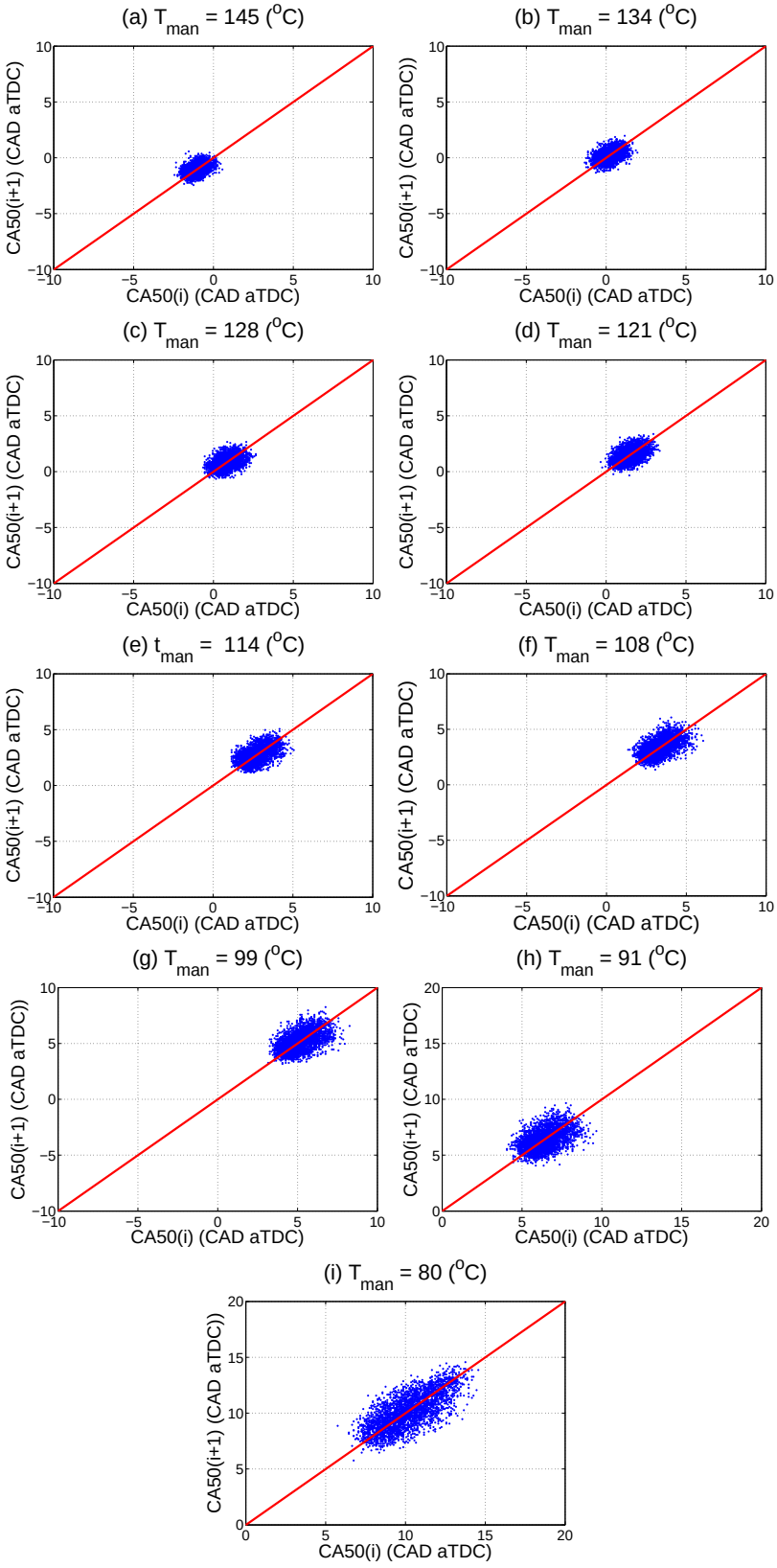

Figure 3.4: CA50 Return maps for HCCI combustion illustrating the transition from (a) knock limit to (i) misfire limit reducing the intake manifold temperature

3.3 NORMAL DISTRIBUTION ANALYSIS

An other common method for analyzing the cycle to cycle combustion timing is using statistical methods. The population of consecutive ignitions at a constant operating point can be used to form a probability distribution for cycle to cycle combustion timing. Normal distribution is the most common probability distribution used to characterize experimental data [153]. Experimental data at 338 different points including the 9 points analyzed previously are analyzed to determine which conditions have a normal distribution for CA50. Two common testing methods for normal distributions are used. The first method is the Lilliefors test that evaluates the input data and returns the result of the hypothesis test for the goodness of fit to the normal distribution [154]. The second method is the Kolmogorov-Smirnov test that compares the values in the data with a standard normal distribution and checks the hypothesis that the data has a standard normal distribution [155, 156]. These two methods are applied on the CA50 data sets from 338 points. Points that successfully pass these two tests are then visually evaluated with normal probability plot. The normal probability plot is a graphical tool to assess whether or not a data set follows a pattern of a normal distribution [153]. Data from the experimental points are plotted against a theoretical normal distribution and if data is normally distributed, it forms an approximate straight line. The level of departures from normality is judged by how far the points vary from the straight line. Figure 3.5 shows a normal probability plot for a sample experimental point that exhibits a normal distribution. CA50 data sets for all experimental points were processed using the procedure mentioned above and 19 points out of 338 points are judged to have a normal distribution. The range of ignition timing parameters for cases with normal distribution are compared with those of the whole data set in Table 3.1.

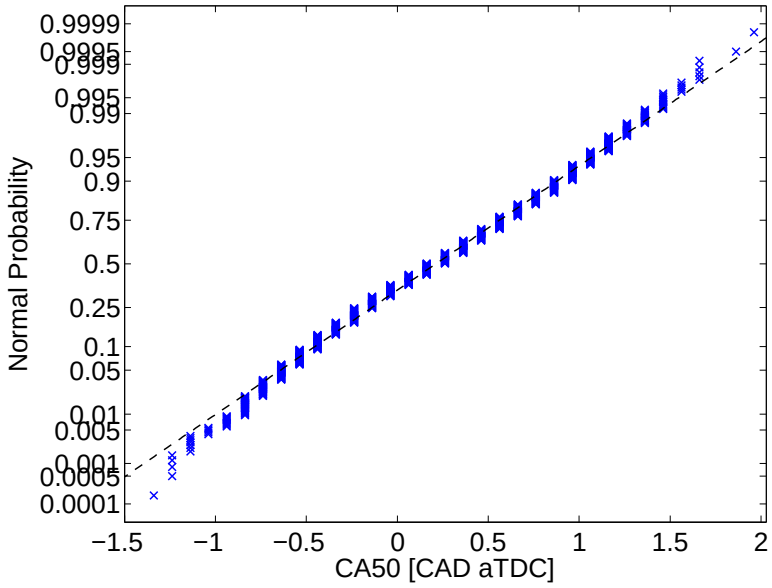

Figure 3.5: Sample normal probability plot for the test point (h) in Figure 3.4.

Table 3.1: Comparing the range of ignition timing parameters for cases with normal distributions with those from the whole 338 HCCI experiments

Parameter	**SOC**	**CA50**	**BD**	**STD$_{CA50}$**
Whole Exp. Data	-4.6 → 21.9	1.8 → 24.9	2.4 → 13.1	0.4 → 4.4
Normal distribution cases	0.8 → 7.7	4.5 → 11.5	2.5 → 4.3	0.5 → 1.4

Table 3.1 shows that normal distribution of CA50 is more likely to occur in HCCI ignitions occurring for a window immediately after TDC (0.8 ≤ SOC ≤7.7 CAD aTDC). In those conditions, cyclic variations of CA50 is typically low (0.4 ≤ STD_{CA50} ≤1.4 CAD) and the burn duration is short (2.5 ≤ BD ≤ 4.3 CAD). A large deviation from the straight line is observed in normal probability plots of the operating points which have mean CA50 occurring after 15 CAD aTDC. Furthermore, all the 19 test points are for fully warmed up conditions and none of the points which have low coolant temperature show a normal distribution for CA50. No direct preference for normal distribution was seen in operating conditions in terms of octane number, engine speed, equivalence ratio and intake

conditions. However, since a combination of these conditions determine the location of SOC, this is expected.

3.4 SUMMARY

Experimental characterization of cyclic variation of HCCI combustion using both chaotic and statistical methods has been performed. The cyclic variations of CA50 increases as manifold temperature decreases.

Using bifurcation diagrams and return maps more structure is observed as the engine operating condition is changed from the knock limit to the misfire limit by using 9 different intake manifold temperatures. This structure is indicative of a coupling between successive CA50 (engine cycle timing) which has the expected sequence of late and early combustion near the misfire limit. This is important since a deterministic structure make prediction and eventual control possible.

A wide range of engine operating conditions (338 points) are analyzed using normal distribution variation statistical tests. As expected, stable HCCI combustion with combustion timing (CA50) near TDC is more likely to have normal distributions since the combustion timing of successive cycles is independent. These results show that unstable operation of HCCI with higher cyclic variations is observed closer to the misfire region of the engine. Thus, misfire region of HCCI will be the main focus of interest in order to extend the HCCI limited operating range and controlling the combustion instabilities for the next chapters.

Chapter 4

RECOGNIZING PARTIAL BURN OPERATION AND PARTIAL BURN CRANKANGLE LIMIT CRITERIA COMPARISON ON AN EXPERIMENTAL HCCI ENGINE [1]

Two challenges of HCCI combustion are: maintaining constant ignition timing despite no direct mechanism to start combustion, and to expand the part load region of HCCI near the misfire limit. In the following section, to accomplish these goals, the accurate on and offline estimates of ignition timing are introduced to recognize a partial burn or misfire.

For offline operating condition ignition timing, a new method is proposed which combines the Coefficient of Variation of Indicated Mean Effective Pressure (COVImep) and percentage of cycles with less than 90 percent heat release of previous cycle. Particularly near the partial burn/misfire limit, this method is more reliable than just COVImep but is an offline method since the COVImep requires all cycles to first be analyzed. For online ignition timing estimates, a new method in which the ratio of the peak of main stage and cool flame stage of heat release curve (HTR to HTRLTR Peak Ratio) is used for each cycle. Using

[1] The results of this chapter are partially based on [46, 133, 132].

this, normal and partial burn engine cycles can be determined in realtime for fuels exhibiting a cool flame.

These two methods are tested on 115 HCCI experimental operating points in which 300 cycles of cylinder pressure data are collected and are found to be more reliable then existing methods in the literature.

4.1 INTRODUCTION

A misfire event is a lack of combustion which results in a momentary lack of torque. Misfire leads to a sudden engine speed decrease [157] and is undesirable since it can lead to speed and torque fluctuations, increased exhaust emissions [158], and unburned fuel in the exhaust that will eventually damage the catalytic converter [159]. In particular, there is a high risk of misfire in HCCI operation, which can have a much more destructive consequence on the engine's performance and emissions than SI combustion [22]. At a fixed fuel octane and engine speed, HCCI operation is limited by two boundaries: partial burn/misfire and knock limit [22]. To reduce HCCI engine knock at high loads, combustion-phasing retard [148, 160] has been used. Combustion-phasing retard can help to reduce knock since the autoignition occurs during the expansion stroke and the effect of the naturally occurring thermal stratification produced by heat transfer are enhanced prolonging the duration of the autoignition event which lowers the peak heat-release rate [160, 161, 162]. To mitigate excessive pressure rise rate, precise control of the combustion phasing is often required [46]. Beyond a certain combustion phasing, if the combustion is retarded too much, CO and HC emissions increase and combustion becomes unstable [163] resulting in partial-burn or misfire cycles. This happens because the charge cooling effect due to piston expansion overcomes the exothermic reactions of the combustion event preventing the charge from undergoing strong combustion. These factors limit the extent of combustion-

phasing retard to reduce the pressure-rise rates but the exact combustion-retard limits and the behavior of the combustion for these conditions are not well known [152].

The acceptable combustion phasing range decreases with increasing fueling. At a sufficiently high fueling rate, the acceptable combustion phasing is highly constrained by the knock and misfire limits, and this operating condition represents the highest possible engine power output for a given intake pressure [164, 165]. On the other hand, as the cylinder charge is made leaner (with excess air) or more dilute (with a higher burned gas fraction from residual gases or exhaust gas recycle) the cycle-by-cycle combustion variations increase until some cycles have partial burning. Further leaning or more charge dilution results in reaching the misfire limit as a portion of the cycles fail to ignite. Such operation is undesirable from the point of efficiency, HC emissions, torque variations and roughness [143].

Increasing dilution rates eventually leads to misfire. Results show that both the start of combustion and burn duration are sensitive to mixture dilution (excess air or EGR). However, only the start of combustion is affected by the fuel octane number [166]. As fuel flow rate is decreased, the net heat release rate decreases resulting in a decrease in the average combustion temperature which results in more unburned products characterized by high CO and unburned HC emissions and by increased cycle-to-cycle variations [22]. Results also show that the position of SOC (Start of Combustion) plays an important role in cyclic variations of HCCI combustion with less variation observed when SOC occurs immediately after top dead centre (TDC) [114]. Higher levels of cyclic variations are observed in the main (second) stage of HCCI combustion compared with that of the first stage for the Primary Reference Fuel (PRF) fuels studied. Cyclic variation of SOC is a function of charge properties and increases with an increase in the EGR rate, but

decreases with an increase in equivalence ratio, intake temperature, and coolant temperature [114].

The combustion phasing is a critical factor in HCCI combustion since it affects the power, fuel combustion and exhaust emissions [167]. The combustion phasing could be defined as when the *SOC* occurs [92]. Main factors that effect the start of combustion for HCCI are investigated in [168]. In [169], the effect of employing different SOC methods on the low temperature combustion (LTC) phase is investigated. Autoignition timing of a mixture in HCCI is very dependant and sensitive to the engine operating condition. To characterize combustion timing, different crank angle dependant methods are used but these methods can exhibit inaccurate results at some operating conditions.

It is difficult to describe the dynamics of HCCI near the misfire operating region and thus to control HCCI effectively to avoid misfires [170]. The understanding of the HCCI engine behavior in case of misfire and delayed combustion is an important first step to provide a control strategy to avoid misfire and expand HCCI operation as close as possible to this region. Some techniques for partial burn recognition use: in-cylinder pressure [171], ionization current [172] and crankshaft angular speed [173].Cost effective methods of misfire detection use existing crankshaft sensors and are based on crankshaft speed fluctuation [174, 175, 176, 177]. Here, equivalent methods to detect misfire in terms of crank-angle based parameters and cylinder pressure are proposed.

4.2 RECOGNIZING PARTIAL BURN OPERATION IN AN HCCI ENGINE

In this section, accurate online and offline estimates of ignition timing are defined to expand the part load region of HCCI near the misfire limit. For offline operating condition ignition timing calculation, a new method is proposed which

combines the Coefficient of Variation of Indicated Mean Effective Pressure (COV-Imep) and percentage of cycles with less than 90 percent heat release of previous cycle. Particularly near the partial burn/misfire limit, this method is more reliable than just COVImep.

In the next following section, SOC (Start of Combustion) is characterized using existing methods in both normal and partial burn regions and a new method is introduced that shows better SOC determination for engine operation with high cyclic variation in partial burn region; The methods for characterizing the start of combustion are: CA50 based on the total heat release; the start of combustion from the third derivative of the pressure trace with respect to crank angle; the start of combustion from the third derivative of the pressure trace with respect to crank angle with two limits; CA10 based on total heat release; CA10 based on peak of main stage of combustion.

For online ignition timing estimates, a new criterion, defined as the ratio between peak of main stage and the sum of peak of main stage and cool flame stage of heat release, is introduced to more accurately identify the operating region of the engine in realtime for fuels exhibiting a cool flame. This criterion is used to understand the performance of each of those crank angle based methods. The performance of each of those methods is investigated for both the low cyclic variation and the high cyclic variation (unstable) region of the engine. Finally, the analysis is extended to all operating points in order to check the performance of the methods over a wide range of operating conditions. The primary aim of this section is to investigate the effect of online method on location of ignition timing for all operating points in order to find an accurate measurement method for HCCI combustion timing that works for both normal and partial burn operating conditions.

The experimental engine setup is explained in 2.1, in which the engine fitted

with a Mercedes E550 cylinder head is used for data collection. The operating points span the range between normal operating condition to the misfire condition. The tests operating conditions are listed in Table 2.6.

4.2.1 Offline method for partial burn region recognition

To recognize the misfire limit using a single parameter, several techniques using IMEP (Indicated Mean Effective Pressure) have been used [22, 152, 2]. The coefficient of variation, is used to measure cyclic variability of engine parameters [114]. In [152] a standard deviation of IMEP more than 2% is deemed unacceptable as this corresponds to the appearance of partial burn and misfire cycles. Applying the same criteria to our 115 operating points, it is found later throughout this section that, *COVImep* (Coefficient of variation of IMEP) is not a single reliable parameter in recognizing high cyclic variation since there exist several operating points having high *COVImep* but have few or zero partial burn cycles.

As shown in Appendix A, a P_{Burn} (partial burn) cycle is defined as when the total heat release is less than 90% of previous cycle. That is, a cycle with 10% reduction in total heat release compared to its previous cycle is considered as a partial burn cycle. An operating point is considered partial burn operating point if it contains more than 15% partial burn cycles [46].

The average total heat release versus *COVImep* for all the 115 operating points are shown in Figure 4.1. As seen from Figure 4.1, there are several operating points with large *COVImep* values $(0.05 < COVImep < 0.15)$ which have high total heat release and therefore do not belong to partial burn operating region. The few operating points with $(0.15 < COVImep)$ are very close to complete misfire and therefore are excluded from partial burn operating region category. Also seen in Figure 4.1 (below the lower line) there is a minimum *COVImep* and there exists no points with low total heat release and low *COVImep*

at the same time. On the other hand, above the higher line, no points with high total heat release and high *COVImep* can be found in Figure 4.1. The operating region is a diagonal band shape, which starts at minimum *COVImep*/maximum total heat release and angles downward to maximum *COVImep*/minimum total heat release. For each total heat release value, the *COVImep* can not be increased above a threshold above the higher line since the operation would not be maintained above the partial burn boundary line. As this threshold for *COVImep* increases, the total heat release decreases. For each *COVImep* value, the total heat release can not be decreased below a ceratin point lower than the lower line since the operation moves towards knocking and the operating point would not be maintained because of large level of heat losses and engine damage due to knocking. Thus, the operating region is a balance of heat release between total heat release and *COVImep*. The operating regions have similar operating boundaries in [178, 179].

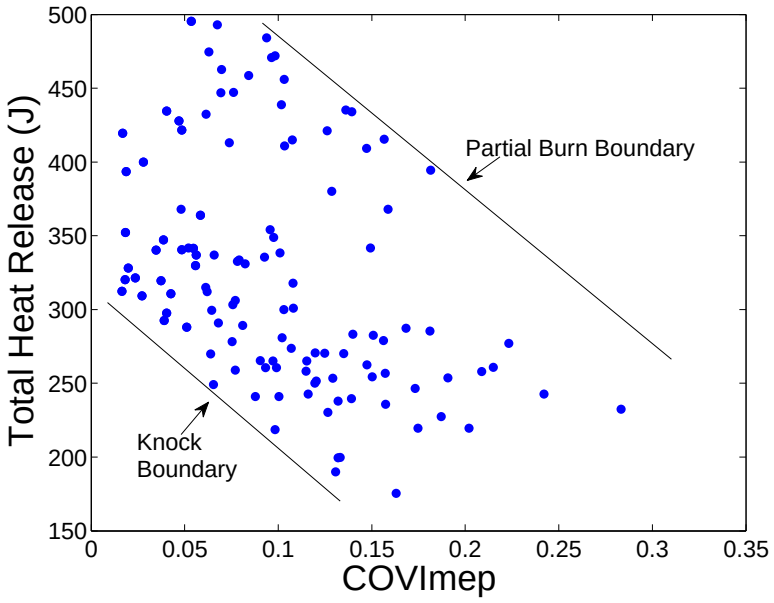

Figure 4.1: Total Heat Release versus COVImep

The total heat release of all operating points versus their number of partial burn cycles is shown in Figure 4.2. The downward trend of heat release is visible for an increase in the number of partial burn cycles in the operating points. Most of the operating points to the right of the dashed line in Figure 4.2 ($0.15 < P_{Burn}Cycles$) have their total heat release less than 300J; however, there are two operating points marked with a circle with high total heat release in the above-defined region. Observing all the operating points, all the operating points with total heat release below 300J have been observed as operating points in partial burn condition. Furthermore, based on the earlier definition of partial burn criteria, all the operating points containing more than 15% partial burn cycles are considered in the partial burn region (regions II and IV in Figure 4.2). If partial burn is defined as points having a total heat release less than 300J and more than 15% partial burn cycles (region IV) then the two points in region II will not be identified as partial burn operating points.

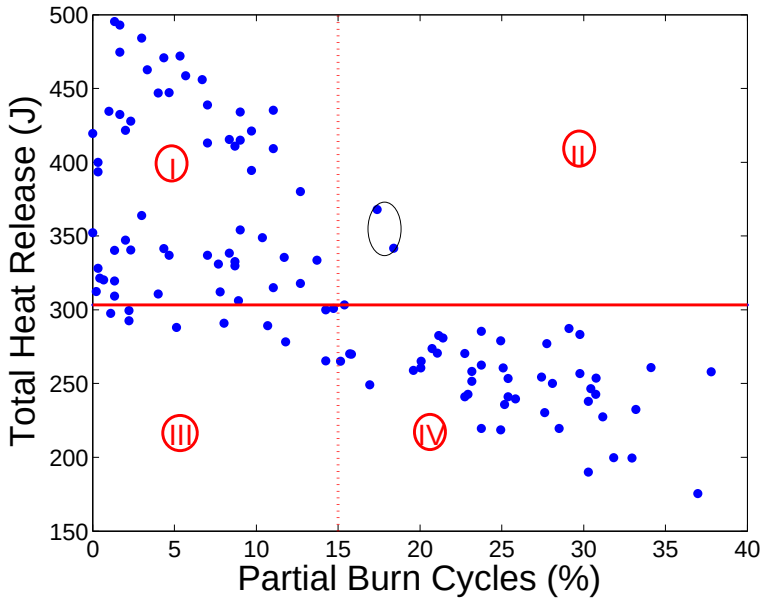

Figure 4.2: Total Heat Release versus Partial Burn Cycles

COVImep versus percent of partial burn cycles for all 115 operating points is shown in Figure 4.3.

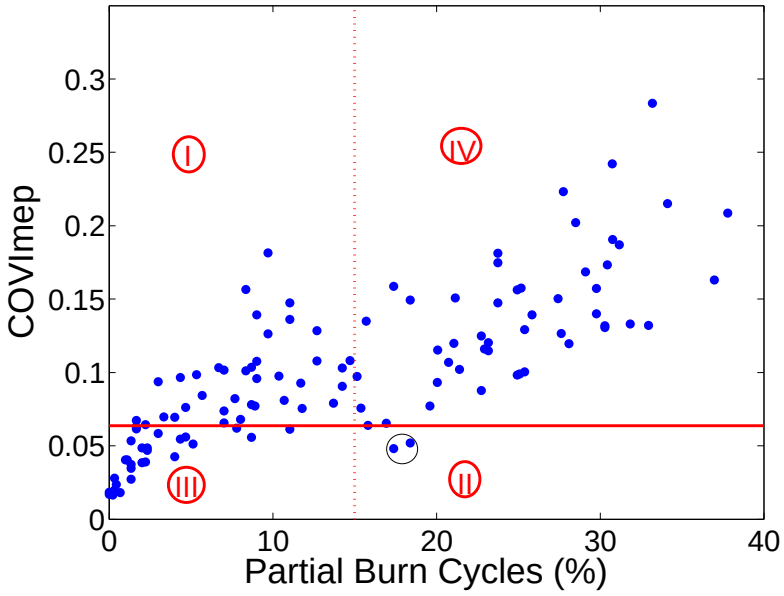

Figure 4.3: Percent of cycles with less than 90 percent of previous cycle versus COVImep

Based on the definition of partial burn operating points having more than 15% partial burn cycles, then the partial burn operating points are specified as the points inside region II and IV in Figure 4.3. The two points in the circle in region II are the same points in region II of Figure 4.2 with conditions in normal operating condition. Figure 4.3 show that the two points in the circle have their *COVImep* less than 6%. Therefore all the operating points with *COVImep* higher than 6% and more than 15% partial burn cycles are considered as the partial burn operating points with no error.

4.2.2 Comparing SOC methods in normal and partial burn region

To compare and understand existing SOC (Start of Combustion) methods and the new SOC method, two representative operating points from the 115 operating

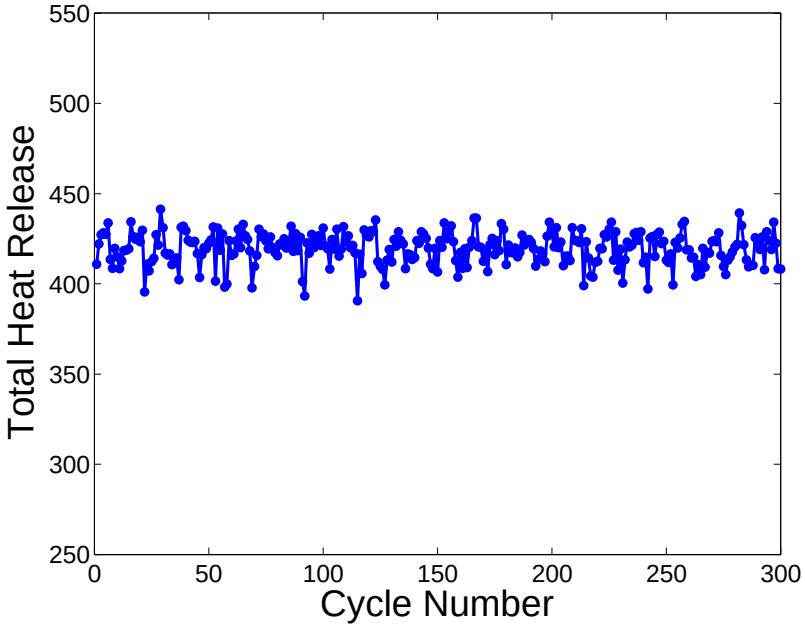

Figure 4.4: Ⓐ - Normal Conditions, low cyclic variations: speed 1025 RPM, Trunner 81 °C, Pman 115 kPa, ON 30, λ 2.28, Total HR 420J, COVImep 1.7percent, Percentage of partial burn cycles 0

points have been selected. These points represent low (Point Ⓐ) and high (Point Ⓑ) cyclic variations (partial burn region). Consecutive cycle total heat release for these two operating points for the 300 engine cycles are shown in Figure 4.4 and Figure 4.5. The number of partial burn cycles are 0% for Ⓐ in Figure 4.4 and 33% for Ⓑ in Figure 4.5 respectively. In these figures the number of cycles with reduction in total heat release is higher in Ⓑ compared to the Ⓐ resulting in considerable reduction in total heat release in Ⓑ. In the next section, different ignition timing methods applied are evaluated for these two cases. Then, methods that work well for these two operating points are evaluated at all 115 operating points.

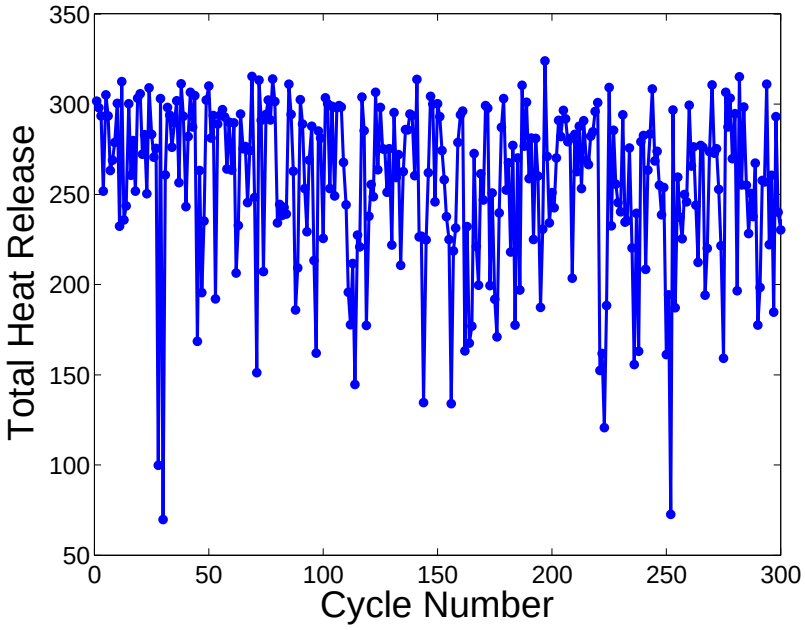

Figure 4.5: Ⓑ - Partial Burn Conditions, high cyclic variations: speed 1025 RPM, Trunner 80 °C, Pman 95 kPa, ON 0, λ 2.61, Total HR 232J, COVImep 28percent, Percentage of partial burn cycles 33.18

4.2.2.1 CA50

This method characterizes ignition timing using CA50 [92, 136, 180, 115]. It is shown later that CA50 combines both the location and duration of combustion making it unsuitable as a single measure of ignition timing. The calculation of CA50 can only occur after the expansion stroke is finished leading to a delay which could be a disadvantage in cycle-to-cycle control applications [180]. Since this study focuses on a method to detect start of combustion, CA50 is excluded as a SOC method to characterize ignition timing.

4.2.2.2 Pressure 3rd derivative

In the crank angle region near TDC during compression, the pressure trace history has a negative concavity, which becomes positive during ignition (i.e. a positive third derivative). This transition from negative to positive concavity is considered as the point of ignition [142, 16]. SOC is defined as being the point at which the third derivative of the pressure trace with respect to the crank angle, θ, exceeds a heuristically determined limit:

$$\frac{d^3P}{d\theta^3} > \frac{d^3P}{d\theta^3}\ |_{lim} = 0.030[\frac{kPa}{CAD^3}] \tag{4.1}$$

The limit is selected such that the point of ignition represents the change in concavity but is not affected by noise in the differential signal. Applying this method to the normal operating point Ⓐ SOC for all 300 cycles is shown in Figure 4.6. This is typical behavior of SOC cyclic variation in most of the operating points without too many partial burn cycles. However, if partial burn cycles appear in the operating point, this criterion does not work, because the transition from negative to positive concavity does not exist clearly anymore. This is shown in Figure 4.7 for Ⓑ where many cycles have weak combustion resulting in unde-

tected SOC. This method identifies 100% SOC of Ⓐ and 8.7% SOC of Ⓑ. Hence this method for determining SOC does not perform well for operating points with partial burn cycles.

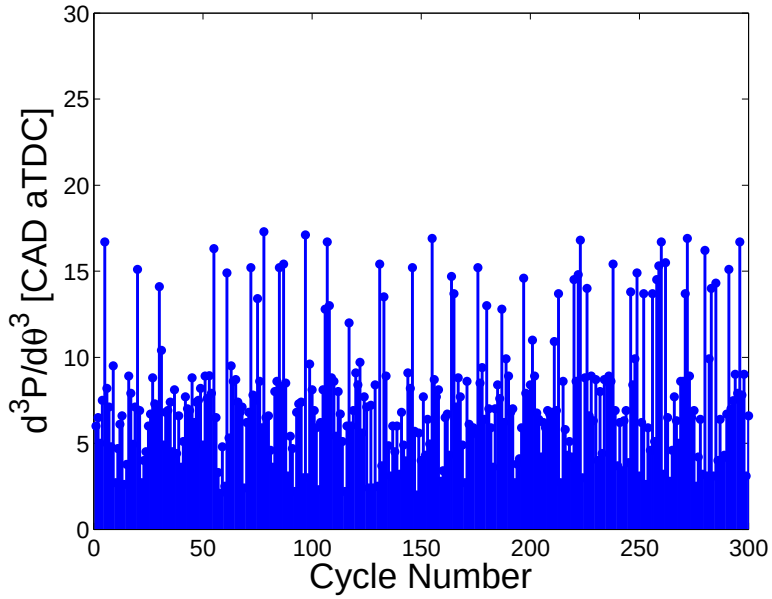

Figure 4.6: Cyclic variation trend of SOC for Ⓐ with Normal Conditions: Same conditions as in Figure 4.4

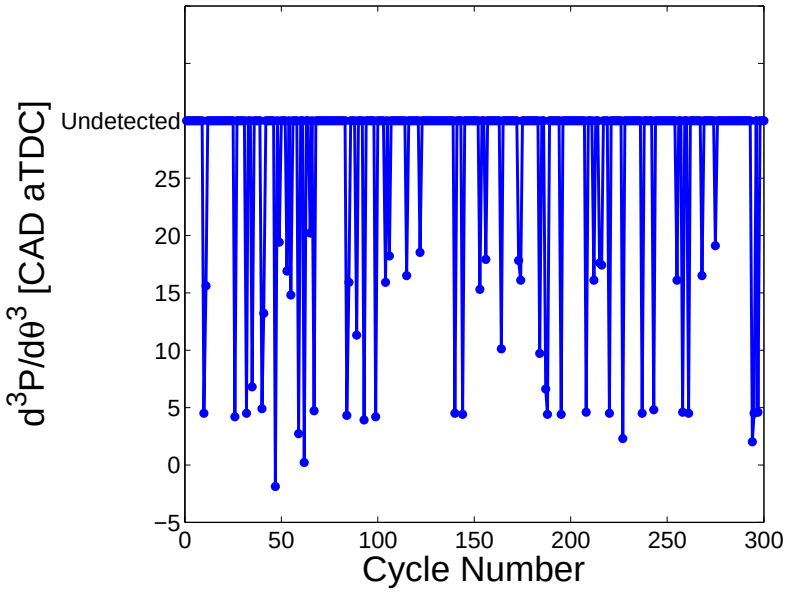

Figure 4.7: Cyclic variation trend of SOC for Ⓑ with Partial Burn Conditions: Same conditions as in Figure 4.5

Having no point (based on 2 rev crank angle data) above the determined limit of Equation 4.1 or having several points above the above-mentioned limit with the same magnitude is considered as the incorrectly detected SOC. To illustrate this, the third derivative of pressure along with the pressure trace is shown in Figure 4.8 for a cycle of normal sample point Ⓐ and is shown in Figure 4.9 for a cycle of partial burn sample point Ⓑ.

It can be seen in Figure 4.9, the choice of an acceptable heuristically determined limit for point Ⓐ is not able to detect any sharp rise in point Ⓑ. This undetected SOC is considered as an erroneous SOC prediction.

Changing the choice of heuristically determined limit for another cycle of same sample partial burn point Ⓑ is shown in Figure 4.10. Although there are many points detected above the limit, there is still no single clear spike in the 3rd derivative of mean pressure regardless of the value of the limit. This is another example of erroneous SOC detection.

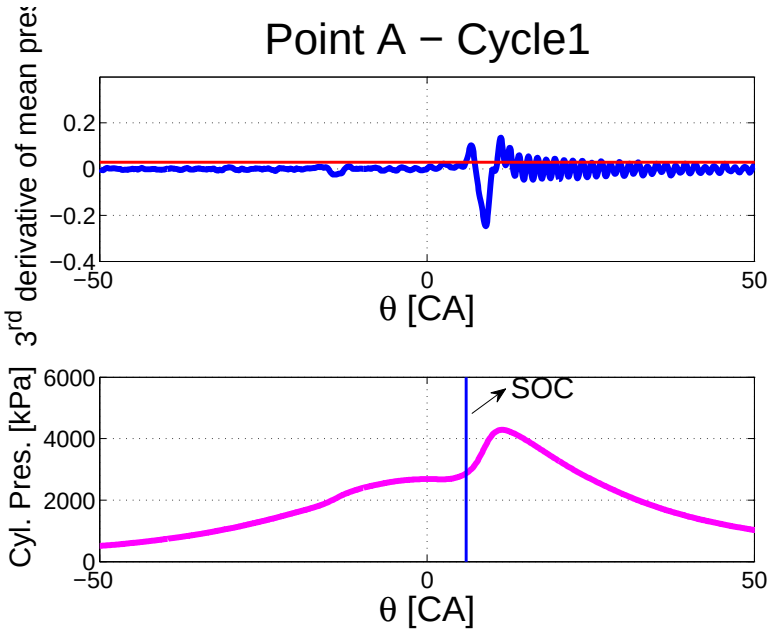

Figure 4.8: Third derivative of pressure with its pressure trace

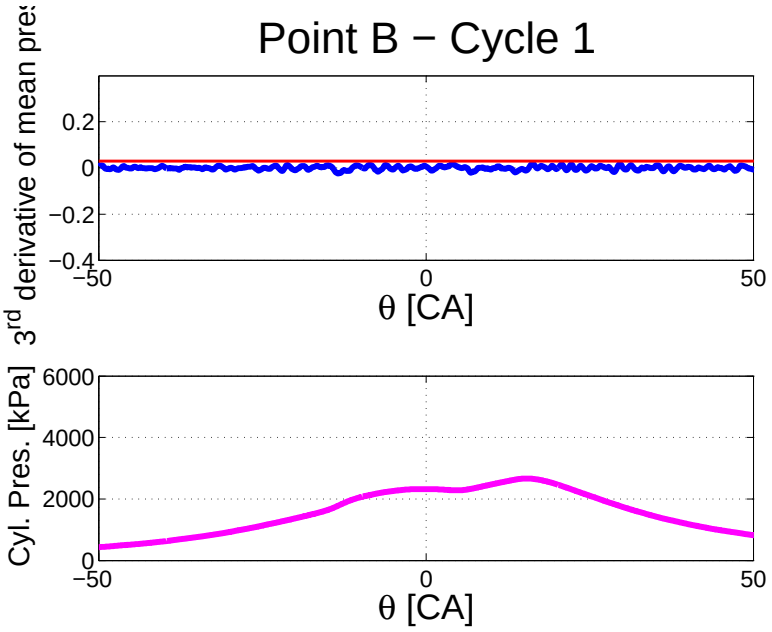

Figure 4.9: Third derivative of pressure with its pressure trace for a partial burn point B for a cycle with undetected SOC

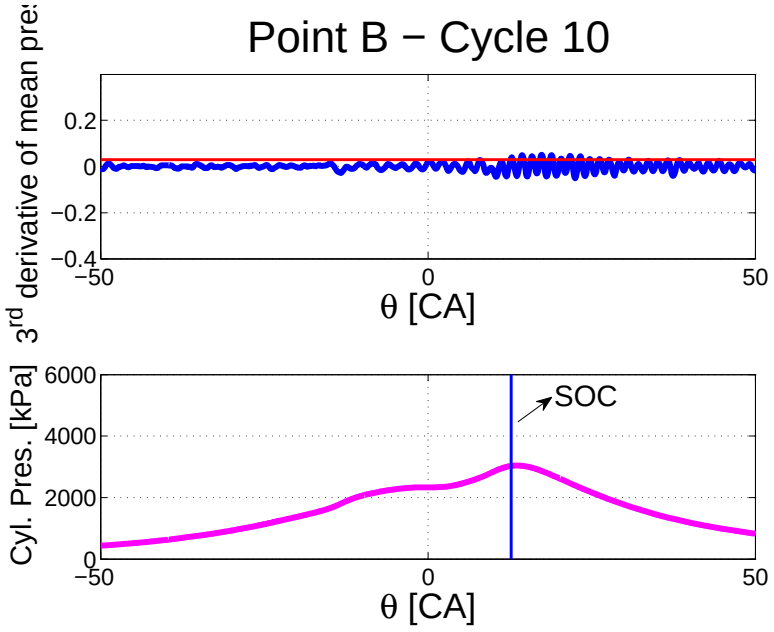

Figure 4.10: Third derivative of pressure with its pressure trace for a partial burn point B for a cycle with detected SOC but no sharp rise from limit

4.2.2.3 Pressure 3rd derivative - 2 limits

In order to improve the performance of Pressure 3rd derivative method, two limits in Equation 4.1 are determined for different loads of the engine. For operating points with an average IMEP of less than 2.91 the third derivative of the pressure trace with respect to the crank angle θ should exceed a heuristically determined limit 0.020 and for the ones with average IMEP higher than 2.91 the limit would be 0.030. Although these new limits increase the percentage of correct detected SOC the lack of concavity for operating points with high number of partial burn cycles still remains. This method correctly identifies 99% SOC of Ⓐ and 50% SOC of Ⓑ. In the case of having no point above the two determined limits for this method or having several points above the above-mentioned limits with the same magnitude, the detected angle is considered as incorrectly detected SOC. Thus this method is not very useful in detecting SOC for engine operation with some misfire cycles.

4.2.2.4 CA10 - total

CA10 is a parameter used in literature as start of combustion indicator. It is defined as the crank angle where 10 percent of total heat release of combustion has occurred. This criterion is widely [169] used but can fail (see next method) for fuels with a low temperature reaction (LTR) and a subsequent poor main stage high temperature reaction (HTR). This method correctly identifies 100% SOC of Ⓐ but only 53% SOC of Ⓑ. The detection of CA10 on the main stage of combustion is regarded as the correctly detected SOC for the CA10 method. Thus this method is not very useful in detecting SOC for engine operation with some misfire cycles.

4.2.2.5 CA10 - main stage

CA10-main is a new method defined as 10 percent of the maximum heat release of only the main stage. This method does not have the disadvantages of CA10-total since it does not jump back to cool flame stage of combustion for same operating conditions.

The heat release percentage as a function of crank angle with their calculated CA10-total and CA10-main are shown in Figure 4.11 and Figure 4.12 for Ⓐ and Ⓑ respectively. All of the calculated CA10-total are on the main stage of combustion for Ⓐ (normal condition) in Figure 4.11. However, for Ⓑ (partial burn case) as shown in Figure 4.12, 47 percent of cycles have CA10-total at the low temperature region of combustion, which gives an erroneous SOC. However, the CA10-main method correctly identifies 100% SOC of Ⓐ and 100% SOC of Ⓑ since it does not jump to the low temperature region. The detection of CA10 on the main stage of combustion is regarded as the correctly detected SOC for the CA10 methods. This method is useful in detecting SOC for engines exhibiting some misfire cycles particularly with fuels that exhibit a cool flame.

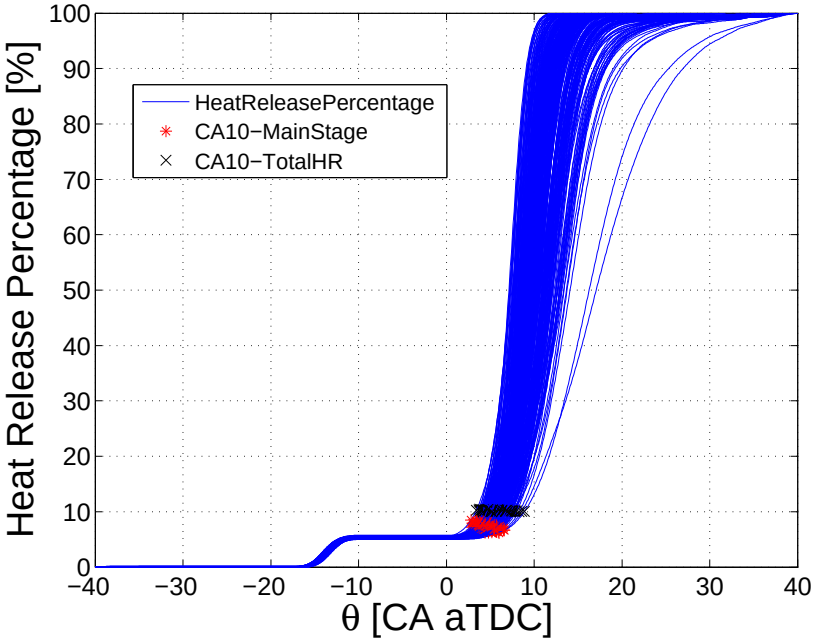

Figure 4.11: Heat Release Ⓐ with Normal Conditions: Same conditions as in Figure 4.4, CA10PercentageMainStage 100

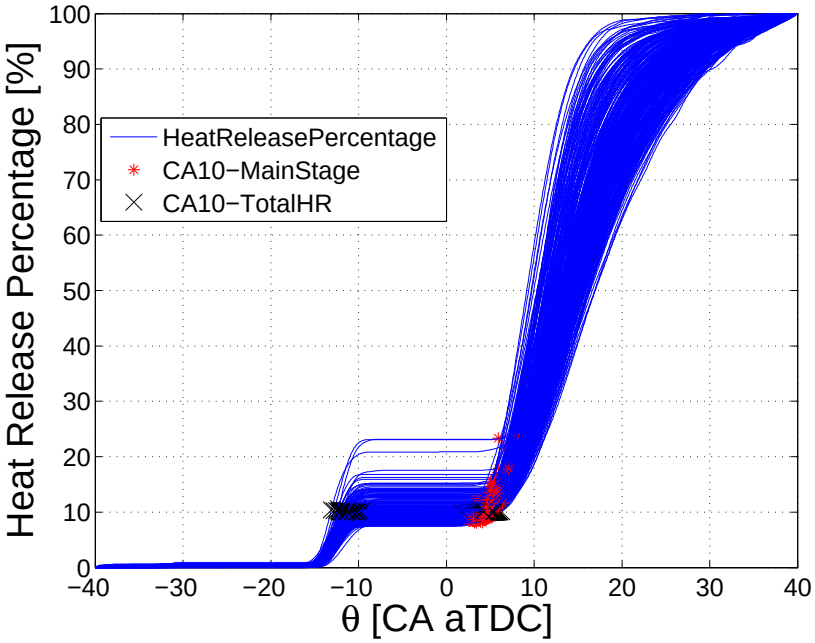

Figure 4.12: Heat Release Ⓑ with Partial Burn Conditions: Same conditions as in Figure A.3, CA10PercentageMainStage 100

4.2.2.6 Summary for Ⓐ and Ⓑ

Table 4.1 summarizes the performance of the five methods applied to Ⓐ and Ⓑ showing what percentage of cycles SOC was correctly identified. This paper focuses on steady-state operating points. The smaller the deviation of SOC would be, the more consistent the ignition timing detection will be for a steady state operating point with no change in operating conditions. Therefore, the smaller the standard deviation of the SOC is, the more robust the method will be.

Table 4.1: Summary of standard deviation of SOC (σ_{SOC}) and percent of correctly detected SOC for methods: ① Pressure 3rd derivative, ② Pressure 3rd derivative with two limits, ③ CA10-total and ④ CA10-main

Methods	SOC (Deg)		σ_{SOC} (Deg)		$SOC_{Correct-det}$	
-	Ⓐ	Ⓑ	Ⓐ	Ⓑ	Ⓐ	Ⓑ
①	8.4	28.3	5.4	5.8	100	8.7
②	5.5	17.3	4.4	13.5	98.7	49.6
③	5.7	-1.9	0.98	7.8	100	53
④	4.6	13.4	0.78	0.83	100	100

Table 4.2 rates the performance of all the methods for both Ⓐ (normal) and Ⓑ (partial burn) operating conditions based on the requirement to correctly detect SOC for all cycles. The only method which satisfy this for both Ⓐ and Ⓑ is CA10-main. Since CA50 combines combustion duration and SOC, CA10-main is the best method for determining SOC for these two cases. Examining combustion criteria in Appendix A, it is found that CA1 and CA50 are not effective metrics for HCCI misfire recognition and thus are excluded from this study. Validating these results on all 115 operating conditions is contained in the next section.

Table 4.2: Method rating for Ⓐ and Ⓑ - ($\surd$) -acceptable, $\times$ -not acceptable)

Methods	Ⓐ	Ⓑ
Pressure 3rd derivative	$\surd$	$\times$
Pressure 3rd derivative - two limits	$\surd$	$\times$
CA10-total	$\surd$	$\times$
CA10-main	$\surd$	$\surd$

4.2.3 Online method for partial burn region recognition

Variation of LTR and HTR peak values is shown in Figure 4.13 for point B. The variations of HTR is much higher compared to LTR peak which does not have very high oscillations.

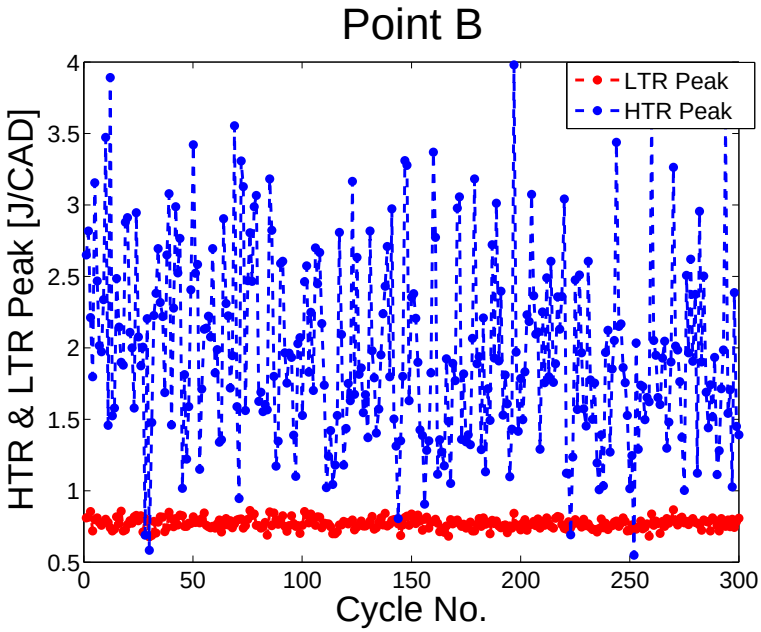

Figure 4.13: HTR and LTR peak variations for point B

A new criterion, called $HTR\,to\,HTR+LTR$ ratio, is defined to quantify the improved performance of CA10-main method compared to CA10-total. This is defined as $R_{HLTR} = \frac{HTR_{max}}{HTR_{max}+LTR_{max}}$ the ratio of peak of main stage to total of

peak of main stage and cool flame stage of heat release rate curve. R_{HLTR} can be used as a real-time criterion to detect the partial burn region for cycle-to-cycle control purposes. For two points Ⓐ and Ⓑ R_{HLTR} is 0.91 and 0.73 respectively as shown in Figure 4.14.

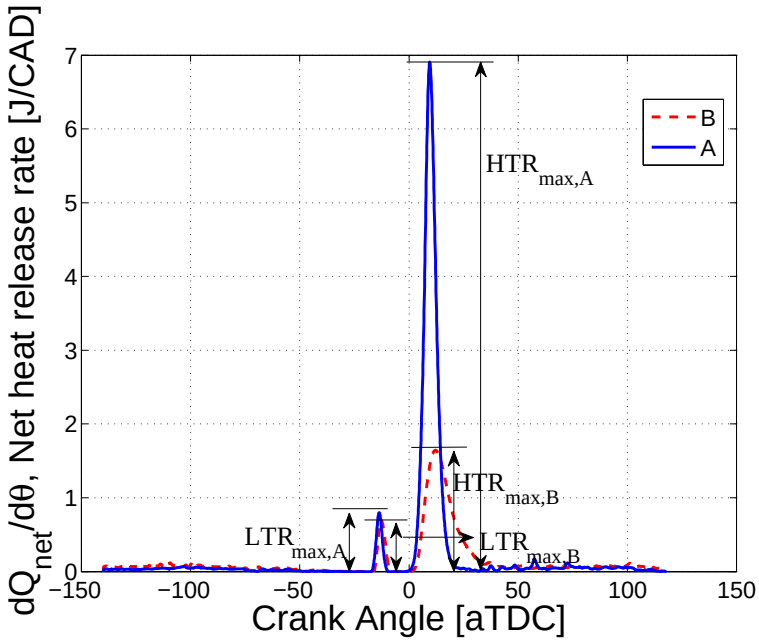

Figure 4.14: Heat release rate and HTR to HTRLTR peak definition for two sample points Ⓐ and Ⓑ

The relation between R_{HLTR} and the location of CA10 for all 300 cycles of point Ⓑ, is shown in Figure 4.15. This figure reflects the effect of R_{HLTR} on the location of CA10. There is a clear boundary between CA10 on main stage and cool flame stage of combustion according to the specific R_{HLTR} of the corresponding cycle. The taller (blue) bars correspond to the R_{HLTR} where CA10 occur on the main stage while the shorter (red) bars correspond to the cool flame stage of combustion. Figure 4.15 shows that for $R_{HLTR} > 0.69$, CA10 always occur on the main stage of combustion.

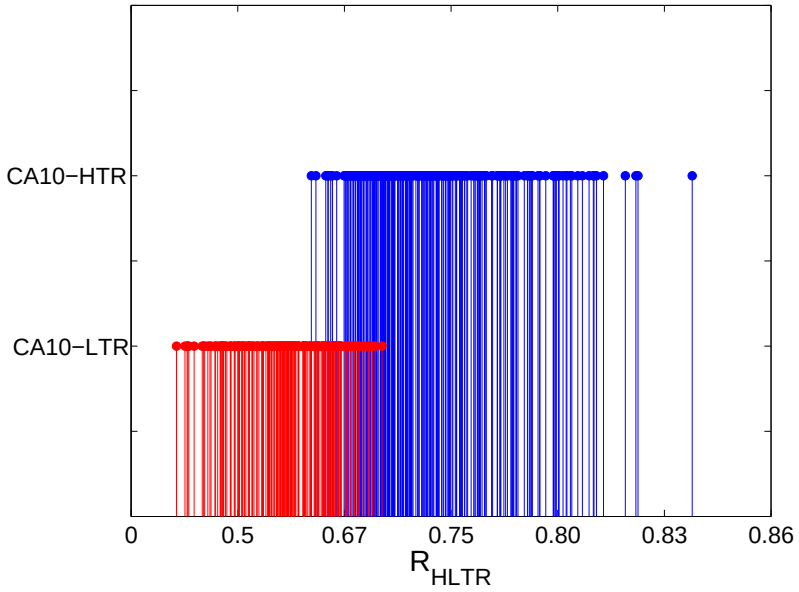

Figure 4.15: Effect of HTR to HTRLTR peak ratio on location of CA10 for Ⓑ

4.2.4 Results for all operating points

Lambda versus the IMEP, for all 115 operating points is shown in Figure 4.16 to provide an overview of the conditions tested. The average values for the 300 cycles for each operating point are plotted. The operating region is a diagonal band shape, which start at minimum IMEP/maximum lambda and angles downward to maximum IMEP/minimum lambda. For each IMEP value, the lambda can not be increased above a threshold above the higher line since the operation would not be maintained above partial burn boundary line. As this threshold for IMEP increases, the lambda threshold decreases.

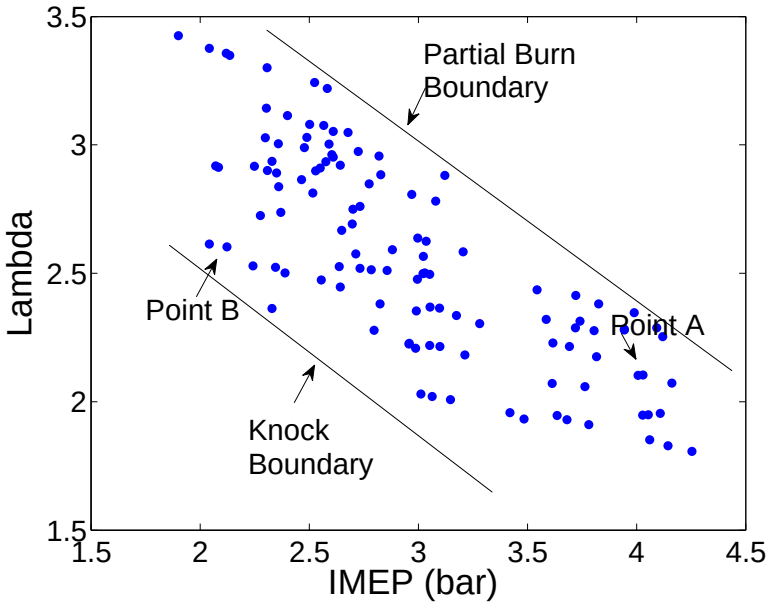

Figure 4.16: Lambda versus engine load

4.2.4.1 Discussion of SOC Methods

CA50 Method Figure 4.17 shows that there is no strong correlation between CA50 and burn duration (CA10-CA90) for 115 operating points.

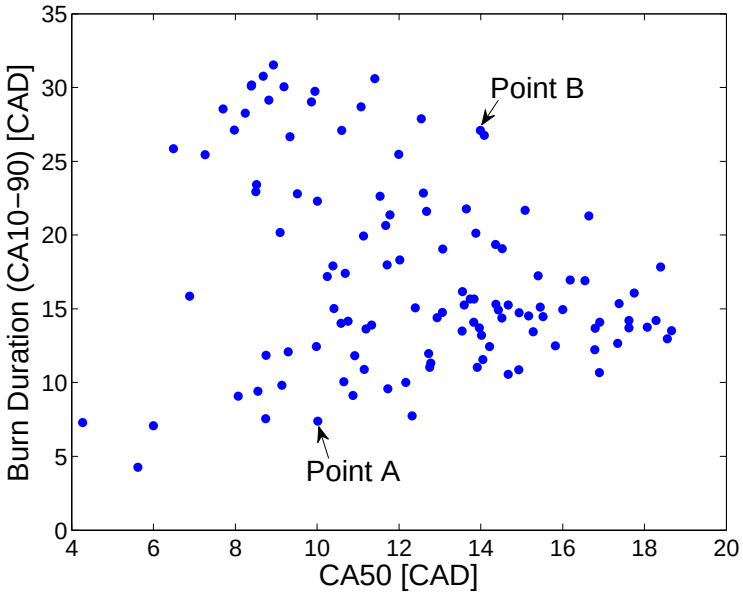

Figure 4.17: Burn duration versus CA50

This is further illustrated in Figure 4.18 which shows how mean (of 300 cycles) of CA50 change as a function of the mean of SOC (determined from 3rd derivative of pressure excluding the cycles which have not been correctly determined). Two different regions can be distinguished in Figure 4.18. An almost linear correlation with deviations from linear trend between mean of CA50 as a function of SOC is observed in region-I so CA50 could be approximately determined from SOC. In region-II, no trend can be observed between CA50 and SOC implying that CA50 does not necessarily provide a good measure of SOC. Only the percentage of correctly detected SOC cycles in each operating point excluding the cycles with incorrect or undetected SOC, is shown in Figure 4.18 with the average value of correctly determined SOC cycles shown on the x-axis.

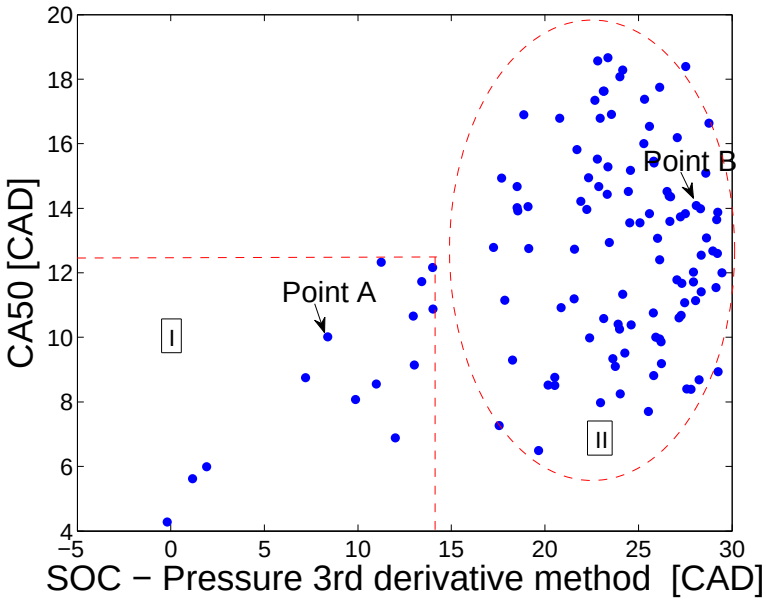

Figure 4.18: Mean of CA50 versus mean of SOC (Pressure 3rd derivative)

Third derivative method The performance of the pressure 3rd derivative method when it is applied to all operating points by plotting the percentage of correct detected SOC versus percentage of partial burn cycles is shown in Figure 4.19. The figure shows that as the percentage of partial burn cycles increases the percentage of correct detected SOC decreases, thus confirming that the 3rd derivative method is not an accurate method for all operating points.

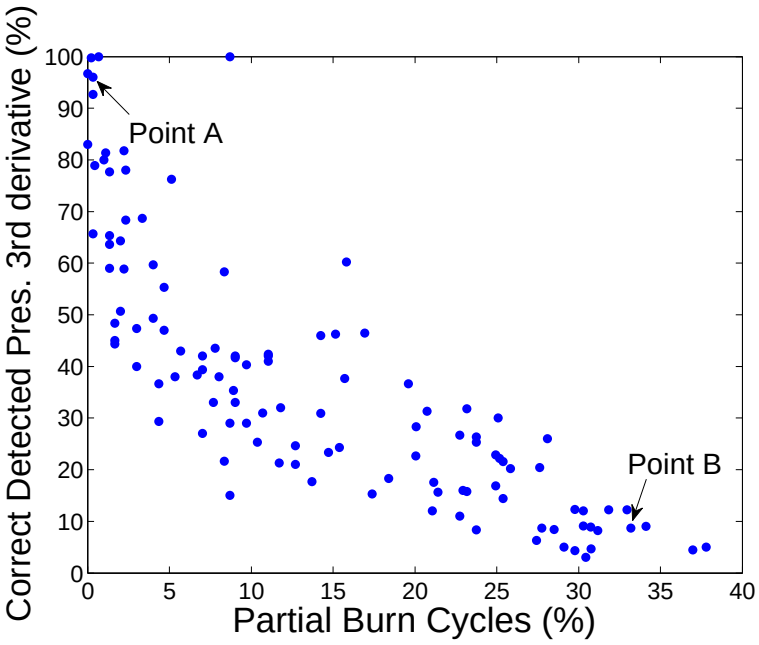

Figure 4.19: Percentage of correctly detected SOC versus percentage of partial burn cycles

Pressure 3rd derivative - 2 limits In Figure 4.20, percentage of correct detected SOC with 2 limits versus R_{HLTR} is shown for all 115 operating points. The figure shows that for most of R_{HLTR} values, there exist several points with incorrect detected SOC with 2 limits that make this method not still precise for all operating points.

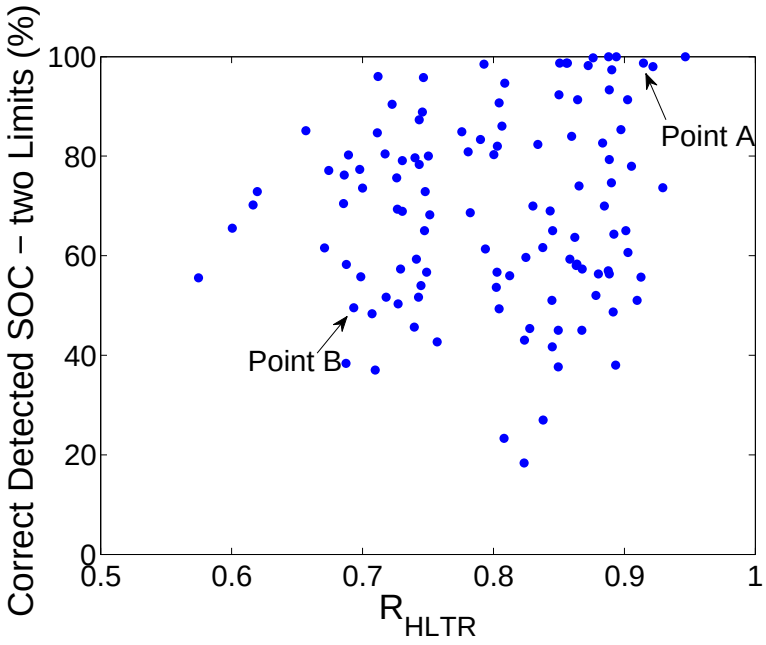

Figure 4.20: R_{HLTR} versus percentage of correct detected SOC with two limits

4.2.4.2 Comparison on crank angle based parameters

To compare the performance of the four crank angle based methods covered in this paper, the percentage of correctly detected cycles of ignition timing versus cumulative percentage of all 115 operating points is shown in Figure 4.21. The cumulative percentage of all operating points is plotted on the x-axis versus the maximum or lower number of correctly detected ignition timing cycles on the y-axis. For example, considering the SOC (red solid) curve, 13% of the operating points have their SOC event correctly determined for 30 cycles or less out of 300. The slope of the curve is relatively low indicating the slow growth of percentage of cycles with correctly detected ignition timing. Thus the pressure 3rd derivative curve is the worst performer when compared to the other methods. The method CA10-main has the best performance (green dot-dashed curve) with a high slope meaning that for almost all the operating points SOC is correctly determined for all 300 out of 300 cycles.

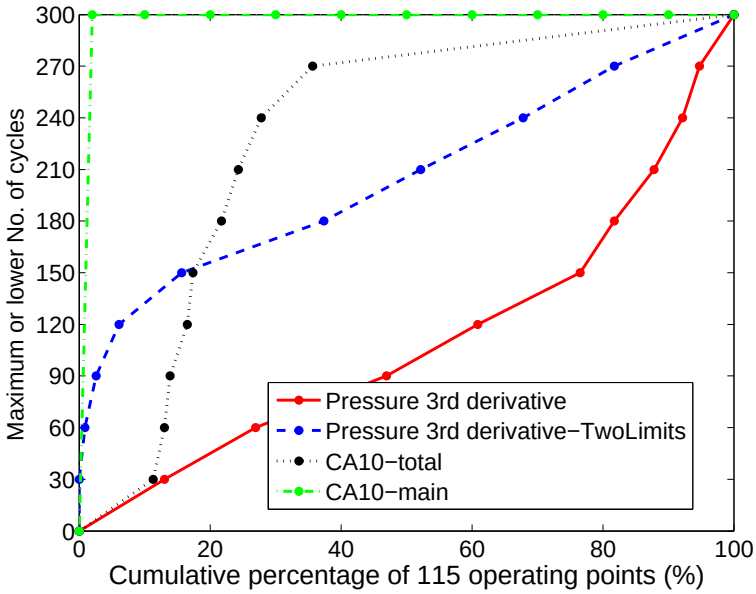

Figure 4.21: Cumulative percentage of operating points versus maximum or lower number of cycles where ignition timing is correctly identified for four different SOC methods based on the pressure 3rd derivative, pressure 3rd derivative - two limits, CA10-total and CA10-main

For each of the 115 operating points SOC is calculated for the 300 cycles (eliminating weak or misfire cycles) and the standard deviation is then calculated. The highest and lowest values of standard deviation for all 115 points is found for four methods and is listed in Table 4.3. The maximum and minimum standard deviation of SOC decreases down the table. The maximum standard deviation of CA10-main is the smallest (1.1 CAD) showing that with this criterion the variation of the location of ignition timing does not vary much at each of the 115 operating points and as such it seems to be the most robust method of determining SOC. Comparing the similar operating conditions, the lower standard deviation of ignition timing indicates the consistency of criteria. Standard deviation of all 115 operating points calculated CA10 based on main stage for all the operating points are shown in Figure 4.22.

Table 4.3: Max/min standard deviation of SOC of 115 operating points by method

Method	**Min (deg)**	**Max (deg)**
Pressure 3rd derivative	1.6	13.5
Pressure 3rd derivative-two limits	1.3	12.0
CA10-total	0.2	7.8
CA10-main	0.5	1.1

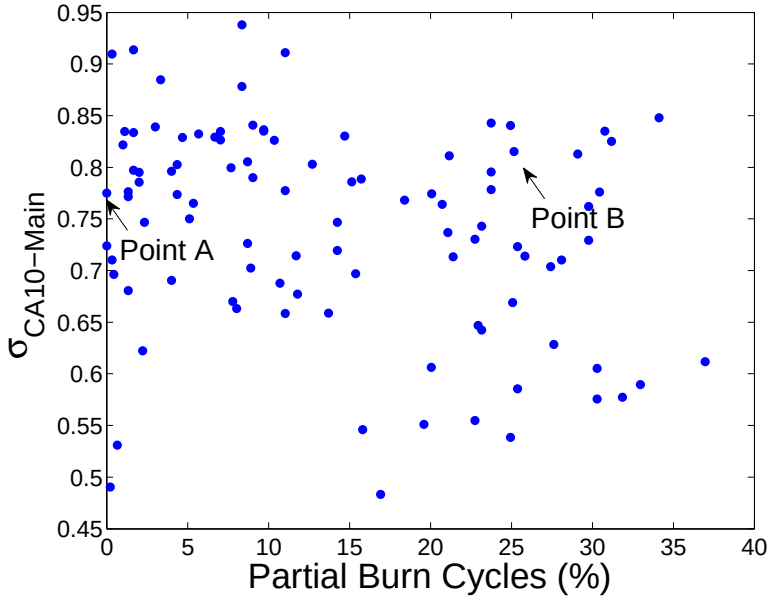

Figure 4.22: R_{HLTR} versus Standard deviation of CA10-main

In Figure 4.23, R_{HLTR} versus Partial Burn Cycles percentage is shown for all 115 operating points with different symbols for different octane numbers. A general trend in Figure 4.23 is that a higher percentage of partial burn cycles in the operating point and hence higher cyclic variations corresponds to a lower R_{HLTR}. Also R_{HLTR} is observed to be generally lower for fuels with lower octane number. This is because the LTR stage has a larger percentage than HTR stage for fuels with lower octane number.

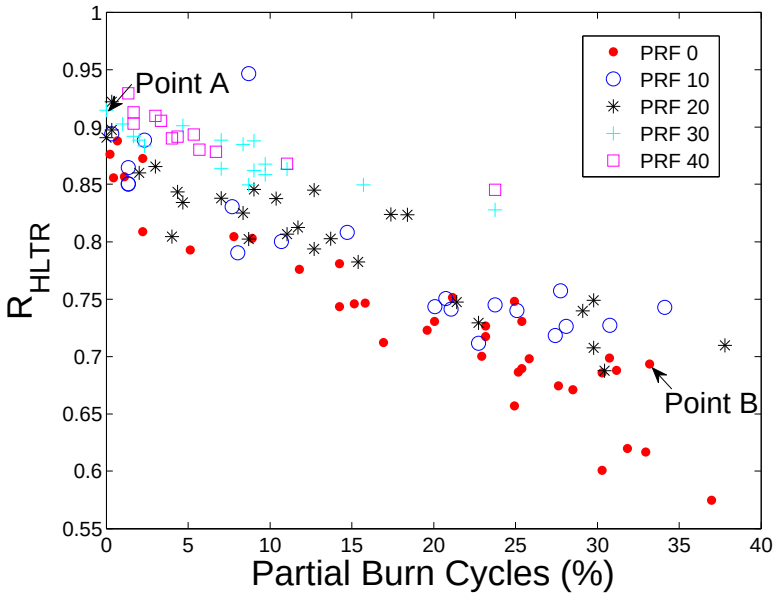

Figure 4.23: R_{HLTR} versus partial burn cycles for all the data points

The percentage of cycles with $R_{HLTR} < X$ for each operating point, representing the cycles with their CA10 occurred on LTR (Low Temperature Region), versus percent of partial burn cycles for that operating point is shown in Figure 4.24. As expected, the value of X changes depending on the octane number and is shown for different octane number values in Figure 4.24. The vertical line at 15% in Figure 4.24 represents the line above which we define a partial burn operating point. The diagonal dotted line indicates a perfect partial burn prediction using R_{HLTR}. For most of the operating points with high percent of partial burn cycles, the percent of cycles with $R_{HLTR} < X$ increase which corresponds to the cycles where the CA10 occur on LTR. This means that for those cycles with $R_{HLTR} < X$ not all the CA10 fall near main stage of combustion which could be problematic since it then does not reflect the start of combustion of the main stage anymore. The closer the percentage of bulk of CA10 gets to the main stage of combustion the higher ratio of R_{HLTR} will be. This shows that as the ratio of R_{HLTR} decrease, tendency of calculated CA10 to move towards the early stage of combustion increases. Also, Figure 4.24 shows that partial burn cycles can be predicted online utilizing the percent of cycles with $R_{HLTR} < X$, where X is a tuned threshold for each octane number.

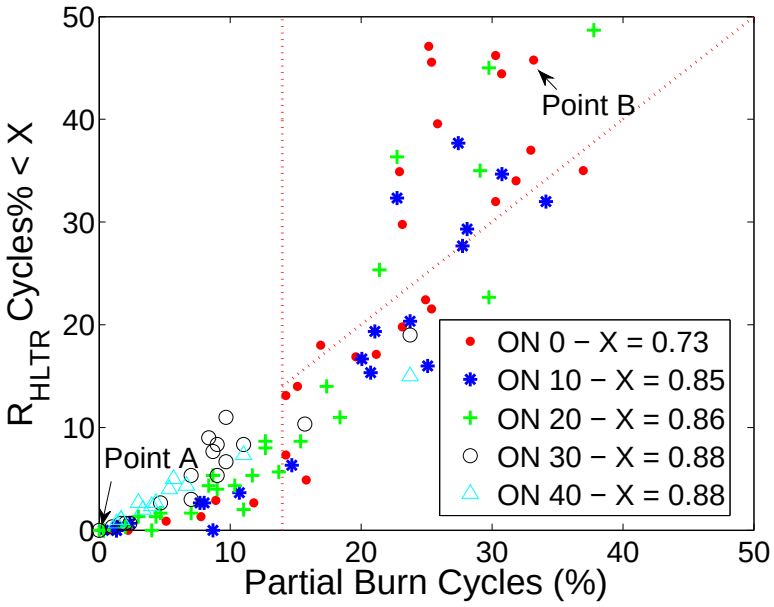

Figure 4.24: HTR to HTRLTR ratio lower than predetermined value versus partial burn cycles for all the data points

4.3 SUMMARY

A partial burn cycle of the engine is identified when the heat release is 90% of the previous cycle. The criterion for characterizing HCCI engine operation as partial burn, when 15 percent of the 300 cycles are partial burn cycles and *COVImep* higher than 6% are used. Based on this criterion, two operating points in the normal and partial burn region of the engine are examined and the performance of five methods for characterizing the combustion timing are investigated and compared. Examining combustion criteria it is found that the four existing methods are not effective during partial burn operation, but a new criterion CA10 based on the main stage of combustion is effective. The results for 115 operating points over a wide range of operating conditions at a fixed engine speed demonstrate that this new criterion is the most effective measure of combustion timing. Also, a new online partial burn criteria R_{HLTR} is defined and is found to achieve a rough correlation with the number of partial burn cycles when the threshold is

adjusted for each octane number. R_{HLTR} threshold is mainly useful to control CA10 as ignition timing criteria since it determines the location of occurrence of CA10 on first or second stage of combustion. This is because R_{HLTR} threshold can determine the occurrence of CA10 on main stage or cool flame stage in the way that if R_{HLTR} drops lower than a threshold, CA10 jumps to cool flame stage which is not necessarily indicative of partial burn cycle. In other words, there can be normal combustion cycles including main stage of combustion while having their CA10 on cool flame stage.

Chapter 5

HCCI ENGINE COMBUSTION PHASING PREDICTION USING A SYMBOLIC-STATISTICS APPROACH [1]

Temporal dynamics of cyclic variation in a Homogeneous Charge Compression Ignition (HCCI) engine near misfire are analyzed using chaotic theory methods. The analysis of variation of consecutive cycles of CA50 (crank angle of 50% mass fraction fuel burnt) for an n-heptane fueled engine is performed for a test point near the misfire condition. The return map of the time series of CA50 cycle values reveals the deterministic and random portions of dynamics near misfire occurring in an HCCI engine. A symbol-statistic approach is also used to find the occurrence of possible probabilities of the data points under the same operating conditions. These techniques are then used to predict CA50 one cycle-ahead. Simulated data points in phase space have similar dynamical structure to the experimental measurements. CA50 is used in this chapter as an ignition timing criteria in order to validate the predictive model that will be used later in Chapter 7 to control the instabilities in partial burn region. The data that have been recorded to be analyzed in this chapter did not contain CA10 and θ_{Pmax}

[1] The results of this chapter are partially based on [135, 136].

and just included of CA50 as the ignition timing, but since the functionality of the predictive method is the purpose of this chapter, CA50 analysis is sufficient as the ignition timing criteria.

5.1 INTRODUCTION

HCCI operating range is limited by the knock limit at high load and high cyclic variation at low load [147, 119]. High cyclic variations are responsible for unstable combustion and limited operating range of engine [111]. Reasons for cyclic variations are grouped in linear random, and deterministic coupling between consecutive cycles both of which have been analyzed using nonlinear and chaotic theory [116, 109, 82]. In this chapter the term deterministic is used when future states for some horizon of the system can be calculated from the past values [181].

Understanding the dynamics of HCCI combustion during the high cyclic variation operating conditions can potentially be used to extend the operating range, if there is deterministic structure inherent between engine cycles. This structure can then be used to predict future cycles which can be incorporated in a control algorithm to influence ignition timing of HCCI engines [126].

Cyclic variation of HCCI is highly dependent on the timing of start of combustion [114]. Early combustion timing right after Top Dead Center (TDC) tends to have low cyclic variations of Start of Combustion (SOC) while late HCCI combustion tends to have high cyclic variations [114]. The development of period-doubling and bifurcation in the experimental measurements of spark ignition engines are investigated as the mixture is made leaner [112]. Their results indicate that there is a transition from stochastic behavior to a relatively deterministic structure as λ increases to very lean conditions. This seems to indicate that for a lean mixture conditions, cycles are related. In [120, 121], a method is proposed based on a symbolic approach to measure temporal irre-

versibility in time series and a new method is introduced to detect and quantify the time irreversibility. In [123], the symbolic method is analyzed in such a way that the symbolization is used to enhance the signal-to-noise ratio. Onset of combustion instabilities under lean mixture conditions have been studied using symbolic methods for observed in-cylinder pressure measurements in SI engines [120, 124, 125]. In [122], the recent developments for applying a time-series analysis technique called symbolic time series analysis is summarized. The observation of time irreversibility in cycle-resolved combustion measurements of SI engines is discussed in [126] and the advantage of their model compared to linear gaussian random processes is presented. The sequential unstable cyclic combustion measurements in the SI-HCCI transition are used to obtain the global kinetic parameters [150]. This aids in discriminating between the multiple combustion states and to provide qualitative insight into the SI-HCCI mode transition.

The main objective of this chapter is to investigate the cyclic variation of CA50 near the misfire limit to predict the following cycles using the identified dynamics. The results have specific implications for the control design used to stabilizing unstable HCCI operation near the misfire condition. Since the parameter CA50 is a widely used indicator of ignition timing [92] it is used here. Nonlinear and chaotic theory tools are used to identify the inherent deterministic patterns of cyclic variation during HCCI combustion. The return maps are a useful tool to recognize the dependency of the current combustion cycle on previous ones. Then the deterministic structure inherent in the data points is captured using a symbol-sequence approach. Joint probability distributions are calculated using the frequency histograms obtained in previous sections. Finally, those joint probability estimators are used to predict the next cycle ahead combustion timings in the experimental data points. Adding appropriate noise to the predicted values results in simulation results with similar statistics to the

experimental data.

The experimental engine setup is explained in 2.1 in which the engine fitted with a Rover K-7 head are used for data collection.

5.2 CYCLE-AHEAD PREDICTION

To predict CA50 one cycle ahead using past and present values of CA50 for the engine operating near misfire is the goal. To do this a variety of techniques are used. First a chaotic analysis is performed on a steady test point with the (COV_{IMEP}) of 35% for 6000 consecutive engine cycles. Then, the first half of the data (Cycles 1 to 3000) is analyzed to find the probabilistic histogram while the second portion of data (Cycles 3001 to 6000) is kept for validation. The test point is very close to complete misfire with many misfire combustion events and has only slightly larger engine torque than the motoring condition. The severity of misfire is recognized by looking at power or output torque which is too low (5Nm in this case). A flowchart of cycle-ahead prediction based on chaotic analysis results is illustrated in Figure 7.1. This figure outlines the analysis procedure in the next part of the chapter.

5.2.1 Return Maps

A return map can be used to observe the structures inherent in a time series [127]. Here they provide a tool to check the probable interaction between a cycle parameter and its next consecutive cycle. For a random time series, consecutive cycles are uncorrelated and the return map shows an unstructured cloud of data points gathered around a fixed point. With deterministic coupling between consecutive points the return map shows more structure such as dispersed data points about a diagonal line [182]. In this chapter the analysis of HCCI engine data at an engine speed of 1000 rpm, a manifold temperature of 44 °C and a

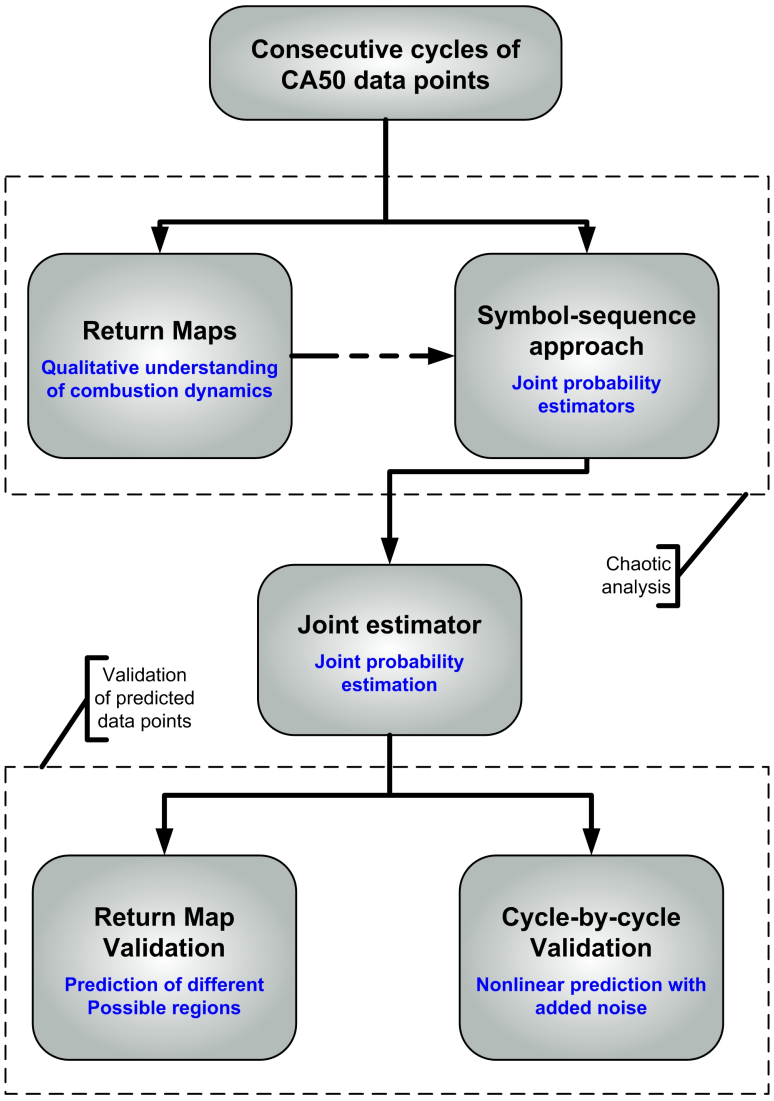

Figure 5.1: Flowchart: Using chaotic tools for analysis and nonlinear prediction

manifold pressure of 94.5 kPa is performed. The return map of all 6000 points of CA50 for this engine operating point is shown in Figure 5.2. A relationship of combustion phasing between the current cycle and the next cycle is shown in Figure 5.2 as this return map appears to show a possible deterministic dependency on previous cycles. Thus to predict future cycles (for some prediction horizon) previous combustion cycles are needed. However, the detailed relationship between cycles is not apparent in the Figure 5.2 and it will be further discussed in

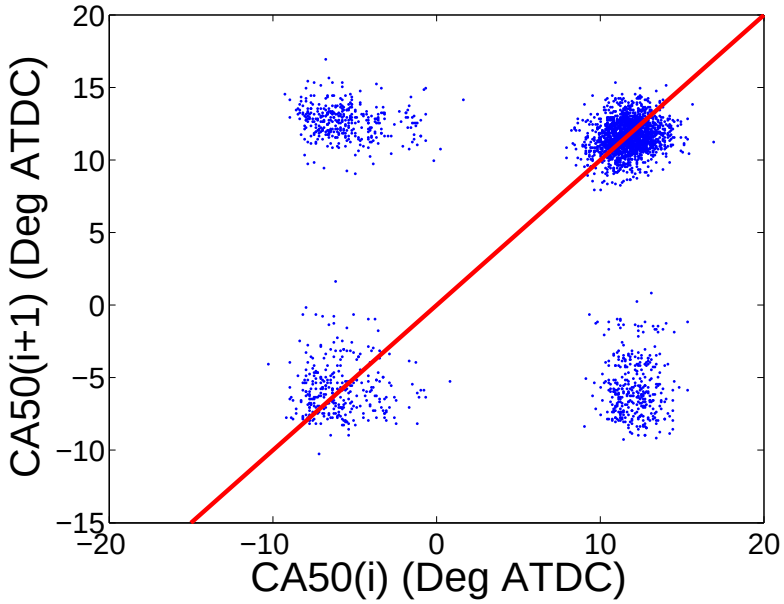

Figure 5.2: CA50 Return map for HCCI combustion under these conditions: engine speed 1000 rpm, Tman 44 °C, Pman 94.5kPa, λ 2.34

the following sections. To characterize the combustion dynamics behavior, the following functional form for CA50 (at cycle i) using previous cycles is used:

$$CA50(i) = f(CA50(i-1), CA50(i-2), ..., CA50(i-L))$$

Chaotic tools such as return maps and symbol-sequence techniques are employed to find the approximate function f and value of L. Since a random time series with an unstructured cluster of data points tends to produce a high dimensional function f, the return map of Figure 5.2 shows a relative low value of L. It can also be inferred from Figure 5.2 that the function f is a nonlinear function [127].

5.2.2 Symbol-sequence Analysis

In this section the symbol-sequence method is used to extract information from the experimental measurements of CA50. This method is used to detect the patterns occurring in the data points and is useful when dealing with data with high measurement error or dynamic noise [112]. Using symbol-sequence statistics requires converting the continuous phase space plots into discrete partitions [183]. Symbolization includes generating discretized symbols from raw experimental analog signals. The symbolization method is based on partitioning the original data points into finite discrete regions and each region is then attributed to a particular symbolic value. The number of possible symbols is called symbol-set size n [122, 183, 184]. After symbolization, each group of symbols forms a finite-length template called the symbol sequence L. These symbol sequences consist of consecutive symbols stepping through the whole data set point by point forming a new sequence. The sequence of symbols carries some important information about the experimental measurement dynamics [120]. The total possible number of sequences N is a combination of symbol-set size n and symbol sequence length L as follows: $N = n^L$ [120].

The symbol-sequence approach also has tools to find inherent structure in experimental data points despite random-like appearance. This is performed by observing if some patterns dominant the time series, since any Gaussian process, on average, would result in a flat histogram of the N symbol-set [112].

For the HCCI data near misfire $n=8$, eight equidistant partitioning, are used which transforms the CA50 data to symbol series from 0 to 7. The data points, below the first bottom partition are assigned to symbol 0 and those higher than first bottom partition are assigned to symbol 1 and so on. The relatively high number of eight partitions selected is used to obtain detailed information out of the original data set despite that the observed dynamics is obscured with noise

[183, 185].

Using the symbol-sequence approach, much of the deterministic structure inherent in the data can be captured [184]. To determine L, a joint probability distribution to predict the next cycle occurrence using previous cycles from information is useful. These frequency histograms give the maximum likelihood probability of next cycle given the occurrence of previous cycles in the whole time series. Then by comparing the one-cycle ahead predictions for different values of L, the optimal value of L can be determined. These histograms also give the probabilistic function for different data series. For the engine test point with return map of Figure 5.2, the optimal one-step ahead prediction is found using three previous cycles ($L = 3$).

Symbol-sequence histogram for the first 3000 consecutive cycles of CA50 data of Figure 5.2 is shown in Figure 5.3. The vertical axis corresponds to normalized frequency of occurrence of this symbol sequence; and the horizontal axis indicates the symbol-sequence equivalent binary code. The symbol set size $n = 8$ and sequence length $L = 3$, so there are $8^3 = 512$ possible sequences.

A large normalized frequency peak accompanied by some smaller peaks in the sequence code histogram is apparent in Figure 5.3, which indicates non-random sequences. The large peak occurs at sequence 438 (symbol series 666) which is three consecutive late timing of ignition. Pattern number 433 and 118, which correspond to sequence 661 and 166 respectively, are two of main local peaks in the diagram. These cases indicate that CA50 does not stay in the late regions but oscillates between relatively early and late CA50 angle regions. In addition sequence codes 661 and 166 are among the possible sequences that the dynamics would pass through before entering or leaving three consecutive symbols of 6. These local peaks indicate relative deterministic behavior of CA50 combustion timing for the experimental case studied.

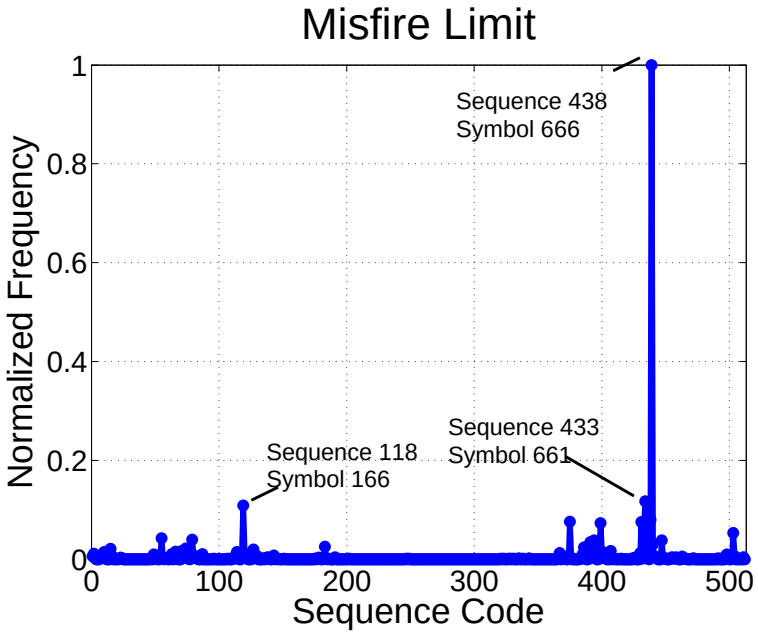

Figure 5.3: CA50 Symbol sequence histogram with (n=8, L=3) for HCCI combustion cycles 1 to 3000 (conditions as in Figure 5.2)

5.2.3 Nonlinear Prediction

Using the joint probability estimator for the first half of the CA50 data (Cycles 1 to 3000), the simulated behavior of consecutive cycles of CA50 is constructed using the deterministic part of the data captured by the model. To obtain the predicted return map, the two previous CA50 values are used to predict the CA50 of the following cycle. The predicted return map uses the validation data (CA50 Cycles 3001 to 6000) and the resulting prediction is shown as large round symbols in Figure 5.4. The experimental CA50 data points are also plotted in Figure 5.4 using small dot symbols in order to compare the prediction to experiment. The prediction seems to capture the nonlinear dynamics of the real data without the random variation as shown in Figure 5.4.

To simulate CA50 with statistics similar to the measured CA50, a random

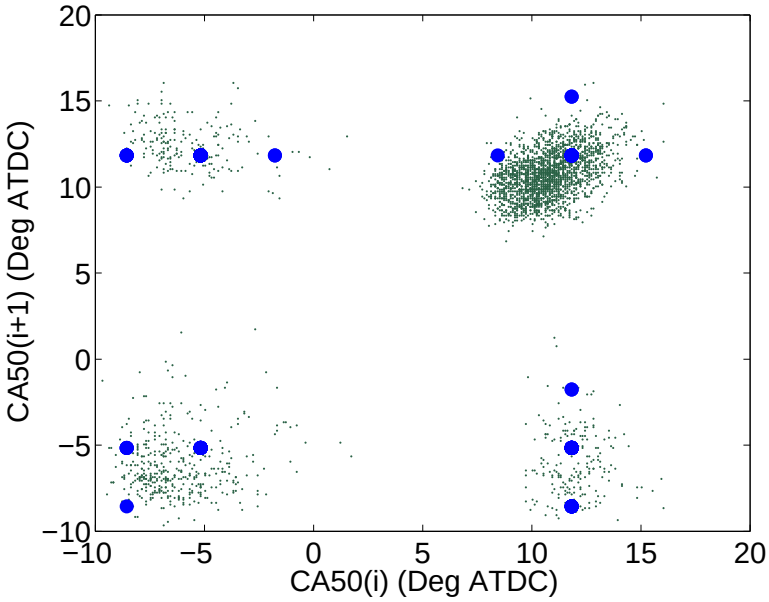

Figure 5.4: Comparing predicted CA50 return map to experiment (for validation data - cycles 3001 to 6000 for conditions as in Figure 5.2)

component is added to the simulated data points as:

$$CA50(i) = f(CA50(i-1), CA50(i-2), ..., CA50(i-k)) + rand(i) \qquad (5.1)$$

where *rand(i)* is a gaussian random variable with zero mean and a variance of $\sigma \cong 4\%$ of maximum function *f*. The experimental data for cycles 3001 to 6001 in Figure 5.5(a) is compared to the simulation with noise for the same cycles in Figure 5.5(b).

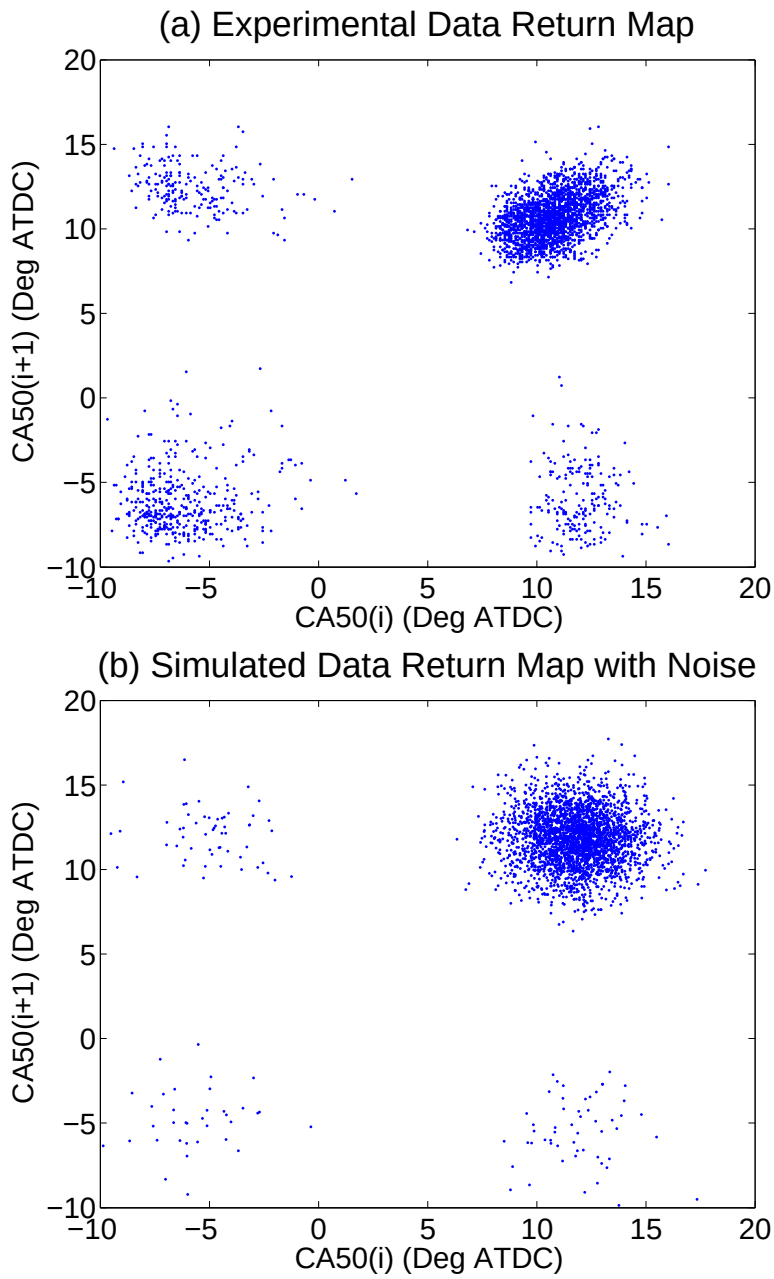

Figure 5.5: Simulated CA50 return map including noise compared to experimental measurements for HCCI combustion cycles 3001 to 6000 - conditions as in Figure 5.2

The simulated return map in Figure 5.5(b) has the general appearance of the experimental data in Figure 5.5(a).

5.2.4 Validation

An 800 point portion of the validation data is used to check the prediction quality. The corresponding residuals and autocorrelation function are shown in Figure 5.6 and Figure 5.7 respectively.

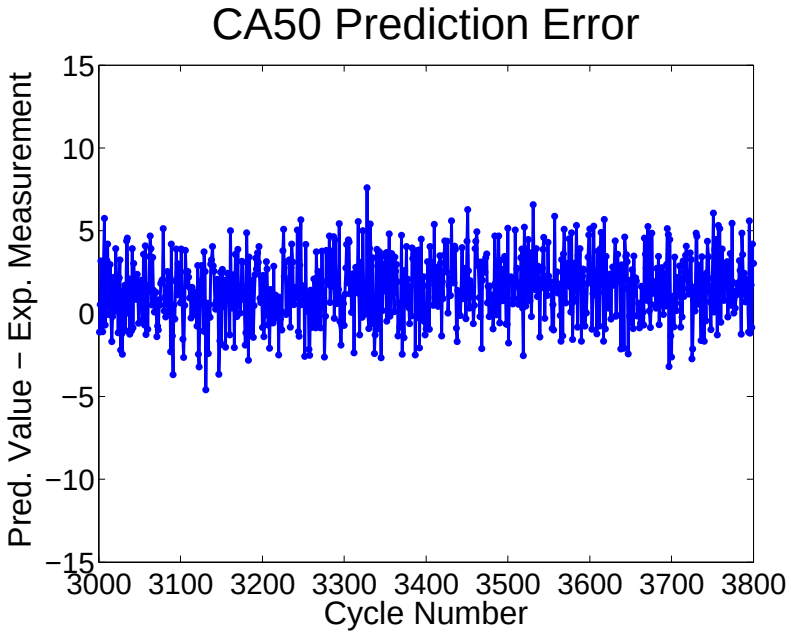

Figure 5.6: Prediction error between predicted CA50 values and experimental measurements for HCCI combustion - conditions as in Figure 5.2

There is no obvious visible pattern in residuals error values in Figure 5.6. This indicates no dependency between consecutive error values, thus the model used to predict seems to capture the dynamics. To confirm that there is no dependency between consecutive error values, the autocorrelation function for the residuals (prediction errors) are computed and shown in Figure 5.7 for all the 3000 CA50 validation data points. The confidence interval for these functions is shown by dashed lines. Ideally for an acceptable model the correlation curves should fall between these lines [153] which is the case in Figure 5.7.

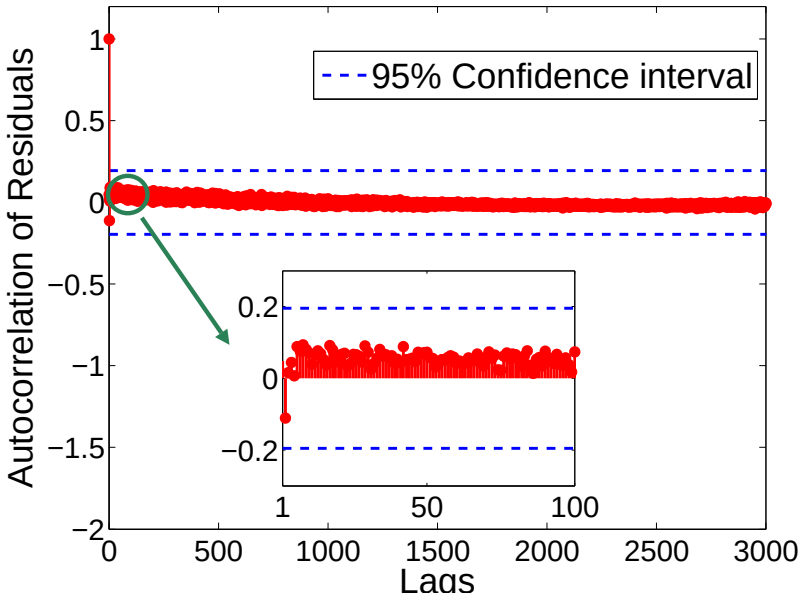

Figure 5.7: Autocorrelation of residuals for predicted CA50 consecutive cycles for HCCI combustion - conditions as in Figure 5.2

5.3 SUMMARY

Deterministic patterns in cyclic variation of ignition timing (CA50) at one operating point near the misfire limit operation of an HCCI engine are observed. The nonlinear cluster of consecutive CA50 values near the misfire limit is illustrated in the return map consisting of multiple different regions which indicates non-constant combustion timing near the misfire limit. Considerable fluctuations in late ignition timings (CA50) occur since prior cycles affect the current cycle. Non-random patterns of cyclic variation of ignition timing under this specific operating conditions emerge in symbol sequence analysis as large peaks in the symbol-sequence histogram. A joint probability estimator to predict one cycle ahead using two previous values is developed and on validation data predicts combustion timing well. Adding random noise with the appropriate magnitude results in a simulation that looks similar to experimental measurements on a return map. An autocorrelation of predicted-actual CA50 residual shows un-

correlated residuals (with 95% confidence) which indicates the joint probability model is acceptable.

Chapter 6

IGNITION TIMING CRITERIA FOR FEEDBACK CONTROL OF AN EXPERIMENTAL HCCI ENGINE [1]

Understanding the variations of ignition timing with changing engine operating conditions is an essential step to be able to control HCCI engines for achieving fuel consumption and vehicle's emissions targets. The first step is to come up with a comprehensive ignition timing which covers a wide range of operating conditions particularly partial burn region of HCCI engines. The crank angle where the maximum pressure occurs (θ_{Pmax}) is proposed as a robust criterion for distinguishing between normal and misfire HCCI combustion modes. Particularly near the partial burn/misfire limit, this method is found to be more reliable than the existing methods of $CA50$ (Crank angle of 50 percent mass fraction burned). Using θ_{Pmax}, normal and partial burn engine cycles can be determined cycle by cycle for fuels exhibiting a cool flame. The performance of this new criterion is then analyzed for different engine loads at both constant fueling and constant equivalence ratio at 329 HCCI experimental operating points, each with 300 cycles of cylinder pressure data. For operating points with high cyclic

[1] The results of this chapter are partially based on [134].

variation θ_{Pmax} is found to be more reliable than $CA50$. Thus θ_{Pmax} could be used in feedback algorithms to help control to stabilize ignition timing in these regions extending the useful operating range of HCCI.

6.1 INTRODUCTION

The primary aim of this section is to investigate the effect of online method on location of ignition timing for all operating points in order to find an accurate measurement method for HCCI combustion timing that works for both normal and partial burn operating conditions. In the next section, the crank angle where the maximum pressure occurs θ_{Pmax} is proposed, as a new ignition timing criteria. The performance of θ_{Pmax} for a specific partial burn operating condition is compared to $CA50$ (common ignition timing method) for this case. The performance of θ_{Pmax} is then analyzed for different engine loads at both constant fueling and constant equivalence ratio at 329 HCCI experimental operating points, each with 300 cycles of cylinder pressure data. For operating points with high cyclic variation θ_{Pmax} is found to be more reliable than CA50. The cyclic variation correlation of θ_{Pmax} with maximum cylinder pressure and $CA50$ is discussed and the effect of θ_{Pmax} on $IMEP$ in two different scenarios in order to evaluate the θ_{Pmax} criteria as HCCI engine load changes is investigated for several operating points. These two scenarios are: constant, and varying fueling rate. Thus, θ_{Pmax} is proposed as a robust criteria for distinguishing between normal and misfire HCCI combustion modes. Particularly near the partial burn/misfire limit, this method is found to be more reliable than the existing methods of CA50 (Crank angle of 50 percent mass fraction burned). Using θ_{Pmax}, normal and partial burn engine cycles can be determined cycle by cycle for fuels exhibiting a cool flame. The experimental engine setup is explained in 2.1 in which the engine fitted with a Rover K-7 head are used for data collection. Out of 338 operating points de-

tailed in Table 2.4 only 329 points with 300 consecutive cycles are considered for this study.

6.2 RESULTS & DISCUSSION

6.2.1 Ignition Timing

θ_{Pmax} is defined as the crank angle of the maximum in-cylinder pressure during one engine cycle. θ_{Pmax} is used as ignition timing parameter as it is simple and requires minimum computational resources [186] and using heat release analysis the cyclic variability in ignition timing, θ_{Pmax}, compared to other common criteria is found to be robust [143, 187, 132]. θ_{Pmax} also depends predominantly on the phasing of combustion and is independent of charge variations which makes it a useful measure of variability in combustion phasing [187]. With early or late combustion, θ_{Pmax} is a representation of the heat release phasing since it is closely coupled to the combustion volume. An example of the location of $\theta_{Pmax} = 12.30$ for HCCI combustion is shown in Figure 6.1 where cylinder pressure is plotted versus crankangle. The location of $CA50 = 8.9$ is also shown in Figure 6.1 and, in this case, closely matches θ_{Pmax}.

6.2.2 Comparison of Ignition Timing Criteria

The cyclic variation of ignition timing for two criteria of θ_{Pmax} and $CA50$ are shown in Figure 6.2 for a portion of consecutive engine combustion cycles for an operating point, denoted A, and shows that the cyclic variation of θ_{Pmax} is higher than $CA50$ indicating higher sensitivity of θ_{Pmax}. In particular θ_{Pmax} captures the one cycle of early ignition timing when misfire occurs at cycle 44 while CA50 does not.

The pressure trace for the consecutive misfire and normal engine cycles for

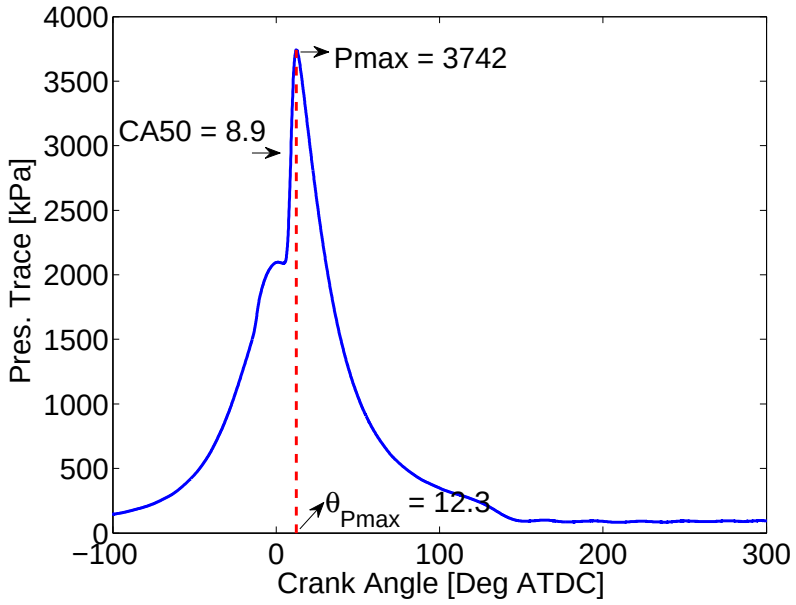

Figure 6.1: Sample operating point for HCCI combustion at point A. Conditions: PRF 0, engine speed n = 800 rpm, T_{man} = 120 °C, P_{man} = 93 kPa, ϕ = 0.51, EGR = 0%, $T_{coolant}$ = 75 °C, T_{oil} = 66.5 °C

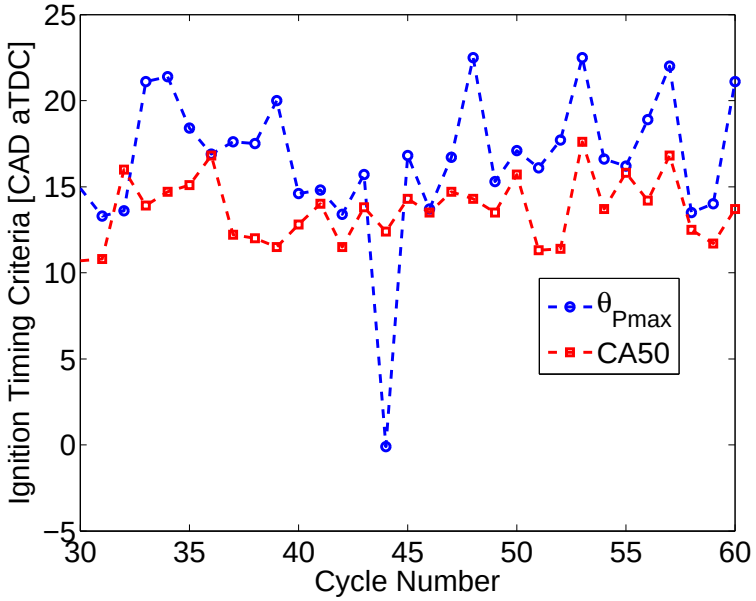

Figure 6.2: θ_{Pmax} and $CA50$ of consecutive cycles for HCCI combustion for operating point A: PRF 0, n = 1000 rpm, T_{man} = 100 °C, P_{man} = 93 kPa, ϕ = 0.57, EGR = 0%, $T_{coolant}$ = 75 °C, T_{oil} = 66.2 °C

the operating point A is plotted in Figure 6.3. The upper plot has only one stage of combustion representing a misfire cycle with $\theta_{Pmax} = -0.1$ [Deg ATDC] while the second plot shows the next cycle indicating a normal cycle with $\theta_{Pmax} = 16.8$ [Deg ATDC]. The large difference of $\Delta\theta_{Pmax} = 16.9°$ values for normal and misfire cycles can be used to distinguish between these different combustion modes particularly near the partial burn and misfire region of the engine. Conversely, $CA50$ (a common ignition timing criteria) differs by only $\Delta CA50 = 1.9°$ for these two cycles making it difficult to detect the misfire cycle.

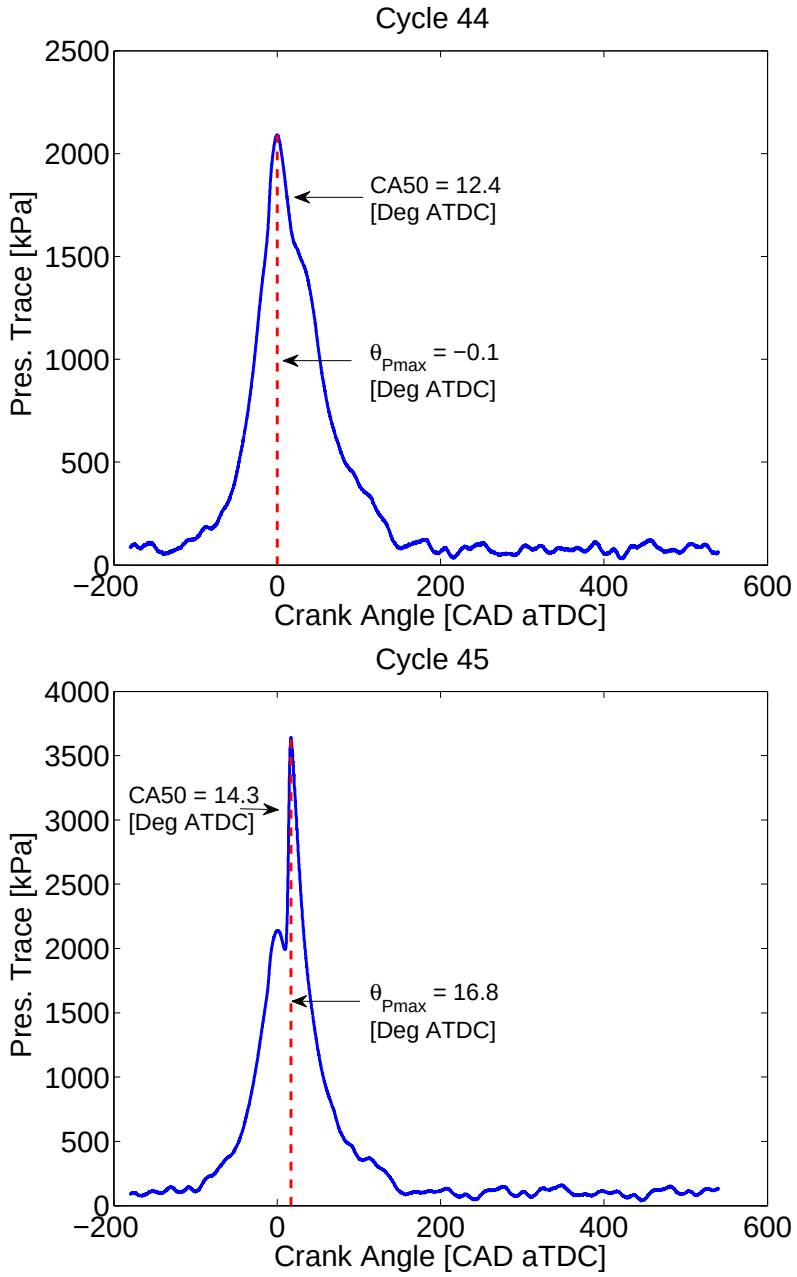

Figure 6.3: Cylinder pressure trace of two consecutive cycles for HCCI combustion at point A. Misfire (left) and normal combustion (right) (conditions as Figure 6.2)

Cyclic Variation of Ignition Timing

For all 329 operating points, 300 engine cycles are collected and the combustion metrics of P_{max}, θ_{Pmax} and $CA50$ are calculated for each of the 300 cycles. A measure of the cyclic variation of P_{max}, θ_{Pmax} and $CA50$ are determined by tak-

ing the standard deviation of the 300 cycle values of each and are denoted σ_{Pmax}, $\sigma_{\theta_{Pmax}}$ and σ_{CA50} respectively and used to represent combustion cyclic variability at each operating point. Cyclic variations of P_{max} (σ_{Pmax}) as a function of $\sigma_{\theta_{Pmax}}$ and σ_{CA50} for each of the 329 operating points are shown in Figure 6.4. In this plot, a correlation is observed between the σ_{Pmax} with those of $\sigma_{\theta_{Pmax}}$ which makes this ignition timing criteria a predictor for the variation in strength of combustion. However, for cases with high cyclic variations ($\sigma_{CA50} > 2CAD$), this correlation is not apparent between $\sigma_{P_{max}}$ and σ_{CA50}.

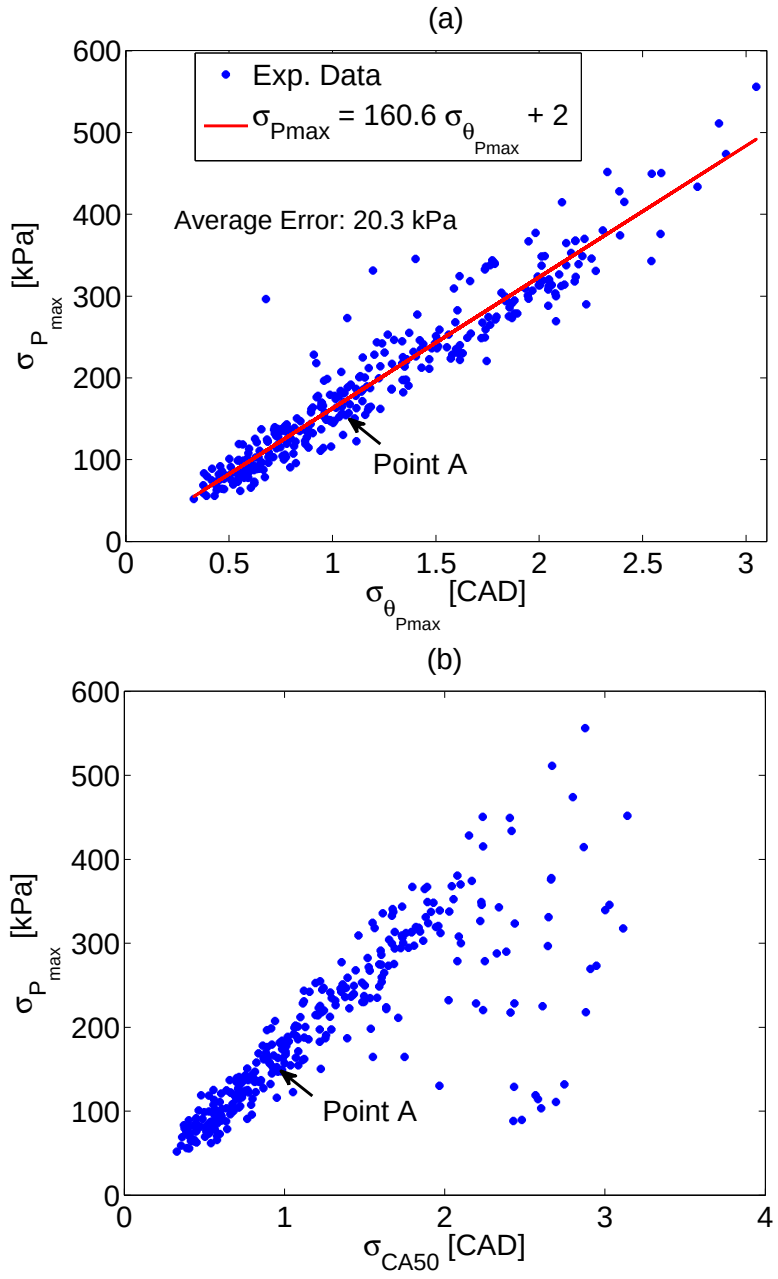

Figure 6.4: Cyclic variations of P_{max} versus cyclic variations of θ_{Pmax} and CA50

The 300 cycle mean of the combustion metrics θ_{Pmax} and $CA50$ for each of the 329 operating points is calculated and plotted in Figure 6.5(a). θ_{Pmax} correlates linearly with $CA50$ with an average error of 0.3, as shown in Figure 6.5(a). The cyclic variations of $\sigma_{\theta_{Pmax}}$ correlate with σ_{CA50} only when cyclic variations of $CA50$ are low ($STD_{CA50} \leq 2CAD$), as shown in Figure 6.5(b). For the cases with

high cyclic variations ($STD_{CA50} > 2CAD$), different ranges of cyclic variations for $\sigma_{\theta_{Pmax}}$ are visible forming various standard deviations of θ_{Pmax}. This will then correspond to different combustion modes of normal and misfire while having a fixed same standard deviation for $CA50$. Thus θ_{Pmax} is a better indicator for distinguishing cyclic variation and thus the different regimes of misfire/normal in those cases.

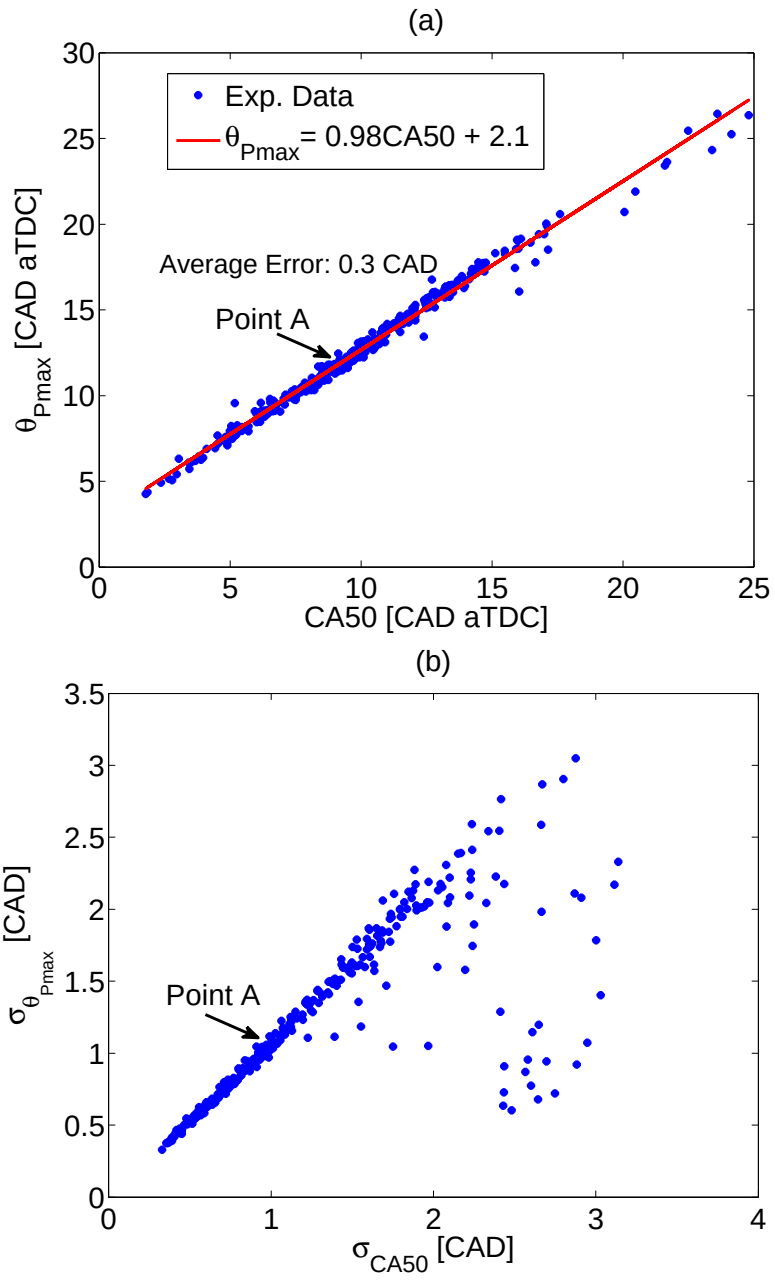

Figure 6.5: θ_{Pmax} versus location of CA50 and STD of θ_{Pmax} versus STD of CA50

IMEP values for changing θ_{Pmax} are plotted in Figure 6.6 for two different scenarios: (a) constant fueling rate (variable λ) and (b) variable fueling rate (constant λ). In Figure 6.6(a), combustion timing (θ_{Pmax}) advances from 19.9 to 9.1 [Deg ATDC] by increasing the intake pressure from 96 to 138 kPa at a constant fueling rate. Increasing the intake pressure results in a large air change

in the cylinder, which due to constant injected fuel, causes a leaner mixture (ϕ of 0.61 $\longrightarrow$ 0.38). IMEP increases in Figure 6.6(a) as the combustion timing advances towards TDC. By varying combustion timing in Figure 6.6(a) IMEP changes about 0.5 bar or 10% change in the engine thermal efficiency at this base condition of 5 bar IMEP. As expected the combustion timing directly influences engine thermal efficiency. In Figure 6.6(b), an opposite trend to Figure 6.6(a) is shown. Here IMEP decreases when advancing the combustion timing to TDC. In Figure 6.6(b) θ_{Pmax} advances from 15.9 to 8.3 [Deg ATDC] by increasing the intake temperature from 73 to 112 °C and keeping (ϕ) constant by increasing the fueling rate from 0.357 kg/h to 0.379 kg/h. IMEP in Figure 6.6(b) follows the same trend as that of the fuel mass flowrate and increases when the fuel rate is increased. A comparison between Figure 6.6(a) and (b) indicates that IMEP is more strongly influenced by fueling rate rather than the ignition timing.

A linear normalized sensitivity function ($S_x = \frac{\partial \theta_{Pmax}}{\partial X} \times \frac{X}{\theta_{Pmax}} \times 100$) is used to analyze the sensitivity of θ_{Pmax} to the variations to each of two different parameters (X). The two parameters are: ϕ and $\dot{m}_{fuel}$. Sensitivity analysis is done around two operating points with conditions outlined in Table 6.1.

Table 6.1: Base conditions used for the sensitivity analysis

	PRF	N [rpm]	T_{man} [°C]	P_{man} [kPa]	ϕ	EGR %	$T_{coolant}$ [°C]
Fig. 6.6(a)	40	810	15	96.2	0.606	0	73
Fig. 6.6(b)	10	1000	81	119.7	0.42	0	74

The sensitivity of θ_{Pmax} to ϕ at constant fueling (Figure 6.6(a)) is $S_\phi = 144\%$ while the sensitivity of θ_{Pmax} to $\dot{m}_{fuel}$ at constant ϕ (Figure 6.6(b)) is $S_{\dot{m}_{fuel}} = 828\%$. The sensitivity of HCCI combustion timing helps to understand how to control HCCI timing effectively. For the controller of HCCI combustion timing, it is essential to know the effect from which charge variables are more significant

than the others and which charge variable is more dominant in a competition to affect the combustion timing.

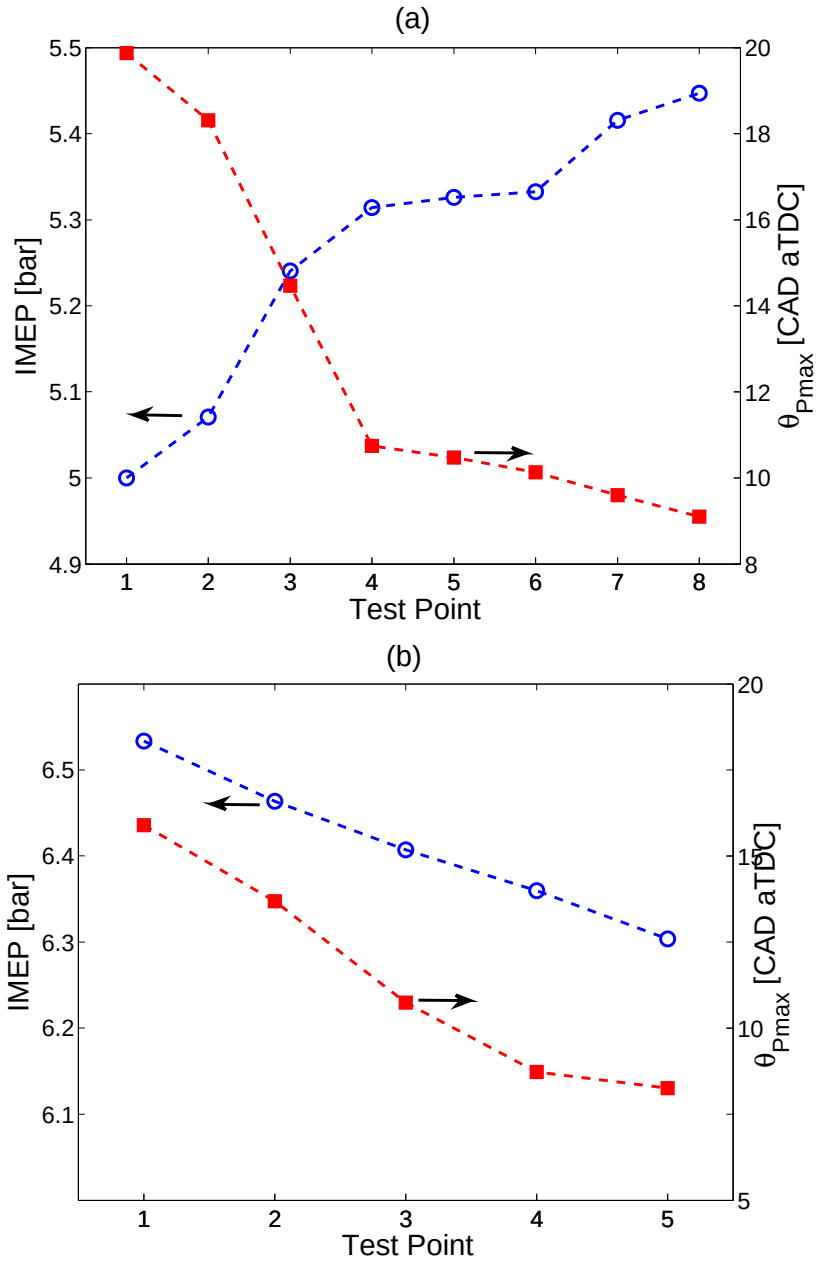

Figure 6.6: IMEP versus θ_{Pmax} for (a) variable ϕ, constant fueling rate (0.31 $\pm$ 0.003 kg/h), PRF40, N = 810r/min, EGR = 0 %, T_m = 15 °C; (b) variable fueling rate and intake temperature, PRF10, ϕ = 0.42, N = 1000r/min, EGR = 0 %, P_m = 119.8 $\pm$ 0.2 kPa

6.3 SUMMARY

Experimental data from HCCI engine collected at 329 operating points is used to evaluate the performance of an ignition timing criteria θ_{Pmax} over a wide range of operating conditions. θ_{Pmax} is better able to distinguish between the normal and misfire combustion cycles than $CA50$, particularly near partial burn region. Finally, the correlations between θ_{Pmax} and P_{max}, $CA50$ and $IMEP$ are investigated at different conditions in order to confirm the validity of this new ignition timing criteria. Although several crank angle based parameters as indicators of ignition timing have been studied, the θ_{Pmax} is used as the final ignition timing criteria for feedback control because of its characteristics in distinguishing the different modes of combustion as well as its simplicity compared to other criteria. One other reason to prefer θ_{Pmax} for feedback control parameter versus other ignition timing criteria such as CA10, which has been shown as a good criteria in Chapter 4, is simplicity of its calculation compared to CA10 since its calculation does not require heat release and mass fraction analysis. In addition, θ_{Pmax} is closely coupled to the volume of combustion as the early/late θ_{Pmax} corresponds to the normal and partial burn cycles while this distinction is not as clear using CA10.

Chapter 7

CONTROLLING CYCLIC COMBUSTION TIMING VARIATIONS USING A SYMBOL-STATISTICS PREDICTIVE APPROACH IN AN HCCI ENGINE [1]

Cyclic variation of a HCCI engine near misfire is analyzed using chaotic theory methods and feedback control is used to stabilize high cyclic variations. Variation of consecutive cycles of θ_{Pmax} for a primary reference fuel engine is analyzed near misfire operation for five test points with similar conditions but different octane numbers. The return map of the time series of θ_{Pmax} at each combustion cycle reveals the deterministic and random portions of the dynamics near misfire for this HCCI engine. A symbol-statistic approach is used to predict θ_{Pmax} one cycle-ahead. Predicted θ_{Pmax} has similar dynamical behavior to the experimental measurements. Based on this cycle ahead prediction, and using fuel octane as the input, feedback control is used to stabilize the instability of θ_{Pmax} variations at this engine condition near misfire.

[1] The results of this chapter are partially based on [137].

7.1 INTRODUCTION

HCCI engines are of interest due to certain advantages over conventional Spark Ignition (SI) and Compression Ignition (CI) engines. In particular, low emission levels in terms of NOx and particulate matter and high thermal efficiency of these engines are beneficial [7, 188]. Two main concerns about this engine technology are: limited operation range, and lack of any direct control on ignition timing [17, 189, 81]. Typically the HCCI operating range is limited by engine damaging knock at high load, and by undesirable high cyclic variation at low load [147, 119]. This paper focuses on understanding how to extending the low load range of HCCI where high cyclic variations are responsible for unstable combustion which limits the operating range of the engine [114]. The combustion stability of a SI engine has been investigated by means of both experimental tests and numerical analysis [190]. Cyclic variations are classified as linear random or having deterministic coupling between consecutive cycles, both of which have been analyzed using nonlinear and chaotic theory [116, 109, 191, 82]. The term deterministic is used when future states, for some horizon of the system, can be calculated from the past values [181]. Temporal dynamics of the combustion process in a lean-burn natural gas engine was studied by the analysis of time series of consecutive experimental in-cylinder pressure data [192, 193]. This structure is then used to predict future cycles and incorporated in a control algorithm to influence the HCCI ignition timing [126, 194]. Thus, understanding the dynamics of HCCI combustion during high cyclic variation operating conditions, could be used to extend the operating range if there is deterministic structure inherent between engine cycles. The combustion process in a SI engine is analyzed and shows that the system can be driven to chaotic behavior [195]. Temporal dynamics of the variation of consecutive cycles of crank angle of 50% mass fraction

of fuel burnt (CA50) are analyzed using chaotic theory tools in [135]. CA50 is predicted one cycle ahead using a symbol-statistics approach in [136].

The main objective of this chapter is to investigate and control the cyclic variation of combustion timing near the misfire limit by using the identified dynamics to predict one cycle ahead and use this prediction in feedback control to stabilize unstable HCCI operation near misfire. Nonlinear and chaotic theory tools are used to identify the inherent deterministic patterns of cyclic variation during HCCI combustion. The return maps are used to qualitatively observe the dynamical patterns near engine misfire. The return maps are a useful tool to recognize the dependency of the current combustion cycle on previous ones. Then the deterministic structure inherent in the cyclic engine data at 5 octane numbers is captured using a symbol-sequence approach. Joint probability distributions are calculated from the frequency histograms. Then, a joint probability estimator is used to predict combustion timing one cycle ahead for each octane number. Finally, the cycle ahead prediction at all 5 octane numbers is combined with feedback control that modulates the octane number to control ignition timing and extending the HCCI operating range of the engine.

The experimental engine setup is explained in 2.1 in which the engine fitted with a Mercedes E550 cylinder head is used for data collection. Five engine operating points are collected at steady-state operating conditions and 3000 engine cycles of cylinder pressure data are recorded for each. Cylinder pressure is recorded 3600 times per crank revolution and processed with an NI-Labview and A&D Baseline CAS using a degree based real time processor. The operating points span the range between stable operating condition to the unstable condition. The details of the base engine experimental conditions used in this chapter are listed in Table 7.1.

Table 7.1: Base test operating conditions4

Parameters	Values
Engine Speed [RPM]	1000
Manifold Temperature [°C]	38
Oil Temperature [°C]	60
Manifold Pressure [kPa]	93-95
IVC [aBDC]	200
EVC [aBDC]	-26
PRF	3, 4, 5, 6 , 7

7.2 CYCLE-AHEAD PREDICTION

θ_{Pmax} is considered as the feedback parameter in this work as it is a simple ignition timing parameter requiring minimum computational resources [186]. Using heat release analysis the cyclic variability in ignition timing, θ_{Pmax}, is found to be a robust criteria of ignition timing [143, 187] since θ_{Pmax} depends predominantly on the timing of combustion and is independent of charge variations. This makes it a useful measure of variability in combustion timing [187]. An example of the location of θ_{Pmax} for HCCI combustion is shown in Figure 2.3 in section 2.3 where cylinder pressure is plotted versus crankangle.

A one step ahead prediction of θ_{Pmax}, using previous and current values of θ_{Pmax} is used in subsequent feedback control. To obtain an accurate prediction several techniques are evaluated. First a chaotic analysis is performed on 5 test points with 5 different octane numbers at steady-state for 3000 consecutive engine cycles. Then the data is analyzed at each of these operating points to find the probabilistic histogram. At those 5 operating points the data is used for analysis while one operating point within the similar conditions is kept for validation. A test point with varying octane number, close to misfire with many partial burn combustion events and with engine torque only slightly above the motoring condition, is used as a final validation and is not used to parameterize the model.

This is also the condition where feedback control is used to stabilize ignition timing. A flowchart of cycle-ahead prediction based on chaotic analysis results is illustrated in Figure 7.1. This figure outlines the analysis procedure that is described next.

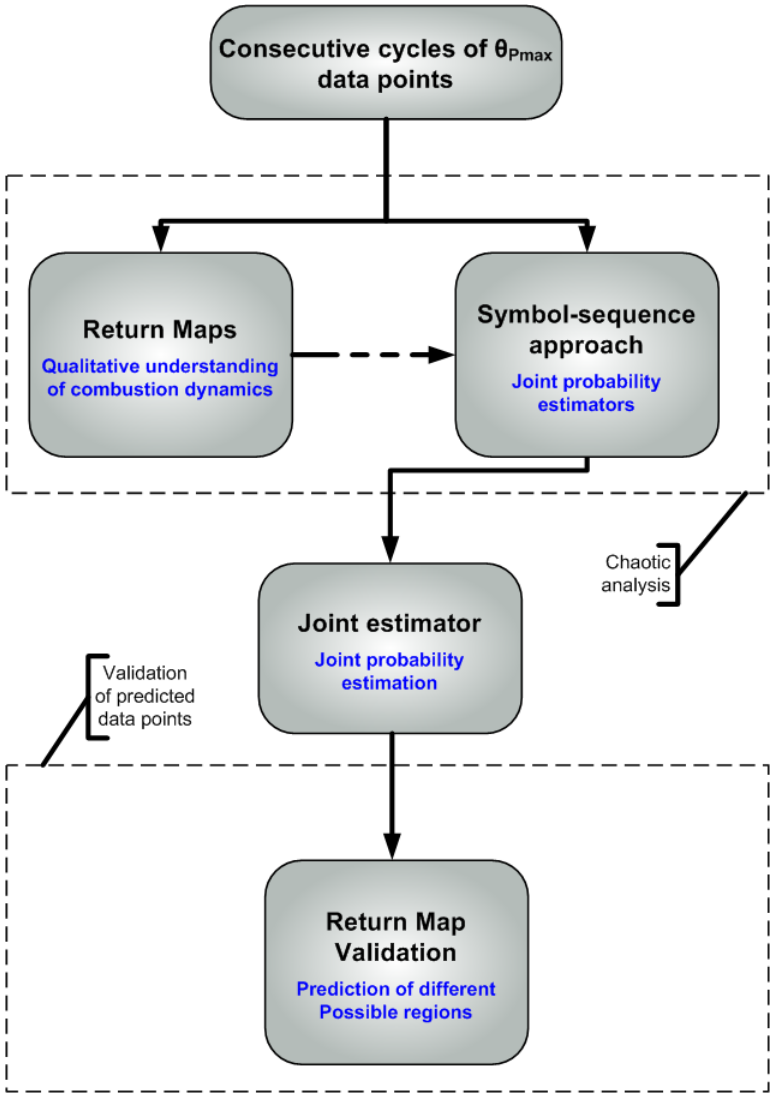

Figure 7.1: Flowchart: Use of chaotic tools for nonlinear prediction

7.2.1 Return Maps

A return map is used to observe the structure inherent in the time series. Here they provide a tool to check the probable interaction between the combustion timing at the current cycle (θ_{Pmax_i}) with the next consecutive cycle ($\theta_{Pmax_{i+1}}$). As previously mentioned, for a random time series, consecutive cycles are uncorrelated and the return map shows an unstructured cloud of data points gathered around a fixed point. With deterministic coupling between consecutive points, the return map shows more structure such as dispersed data points about a diagonal line [182]. In this chapter analysis of HCCI engine data at condition listed in Table 7.1 is performed. The octane number is varied from 3 to 7 in steps of 1 by changing the ratio of fuels injected by two fuel injectors and the return maps of all 3000 engine cycles of θ_{Pmax} for these 5 engine operating conditions are shown in Figure 7.2. The combustion timing return map is a phase plane and plots θ_{Pmax} at cycle $i+1$ on the y-axis and θ_{Pmax} at cycle i on the x-axis where i represents the engine cycle (time). The relationship between combustion timing of the current cycle and the next cycle indicates that for some of the cases shown in Figure 7.2 there is a deterministic dependency on previous cycles. In these cases, predicting future cycles (for some prediction horizon) using previous combustion cycles is possible. However, the detailed relationship between cycles is not apparent in Figure 7.2 and further analysis is needed. To characterize the combustion timing dynamics, the following functional form defined in the previous chapter but now with θ_{Pmax} (at cycle i) using previous cycles is used:

$$\theta_{Pmax}(i) = f(\theta_{Pmax}(i-1), \theta_{Pmax}(i-2), ..., \theta_{Pmax}(i-(L-1)))$$

Return maps and symbol-sequence techniques are used to find the approximate function f and value of L. The return maps of ON 5 through 7 in Figure 7.2

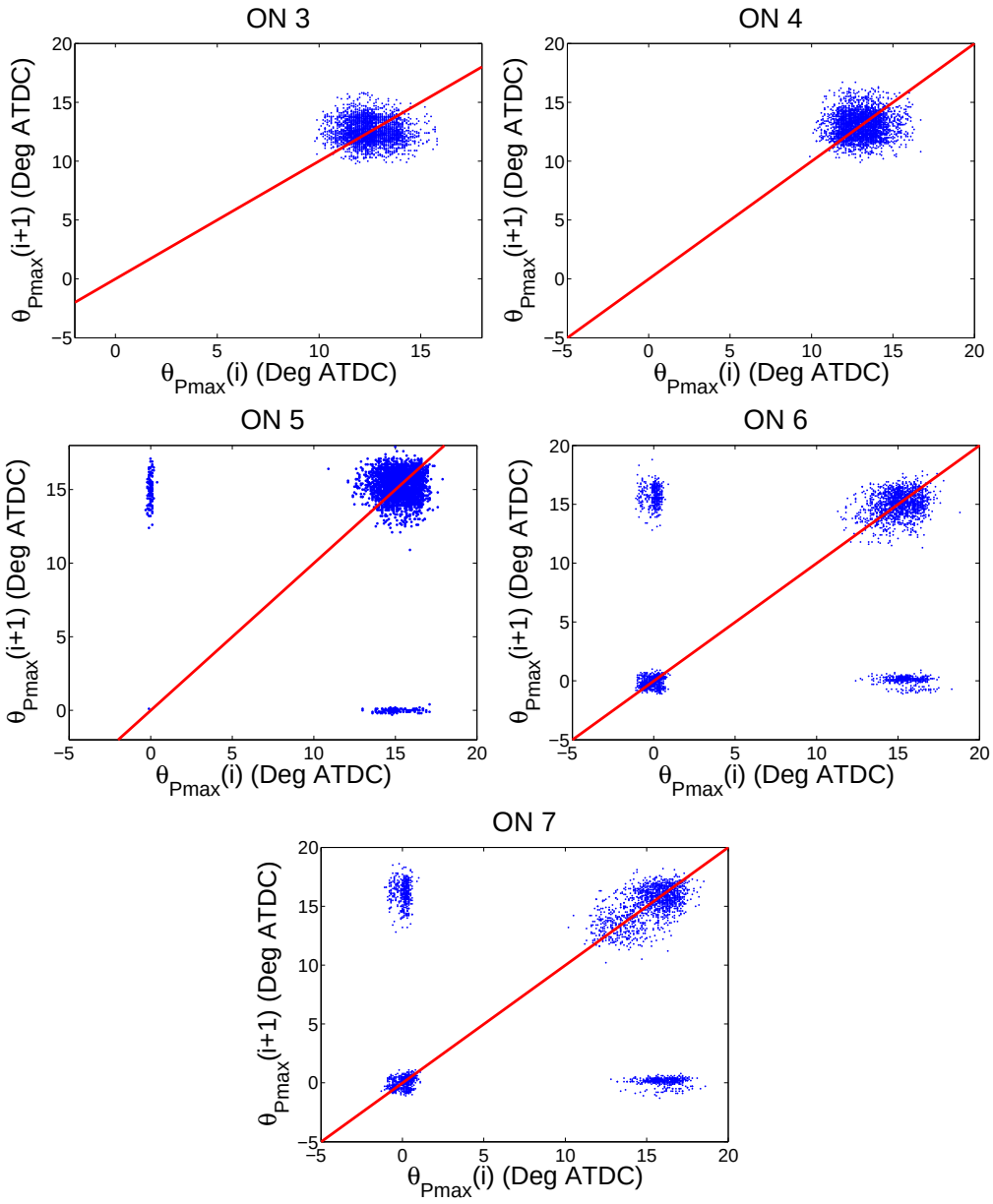

Figure 7.2: Return map of combustion timing,θ_{Pmax}, for 5 octane numbers. conditions listed in Table 7.1

seem to indicate a relatively low value of L.

7.2.2 Symbol-sequence Analysis

The symbol-sequence method is used to extract information from the experimental measurements of θ_{Pmax}. This conversion has the practical effect of producing low-resolution data from high resolution data and reducing the effect of dynamic and measurement noise. In a practical sense for combustion timing prediction and control purposes in this work, the more qualitative description such as early or late combustion timing is desired.

For the HCCI combustion data near misfire, θ_{Pmax} is partitioned equally in eight partitions, n=8, in a symbol series from 0 to 7. The data points, below the first bottom partition are assigned to symbol 0 and those between the first and second partition are assigned to symbol 1 and so on. The relatively high number of eight partitions is selected to extract detailed information from the original data set despite that the observed dynamics are obscured with noise [183, 185].

A joint probability distribution to predict the next cycle occurrence using previous cycle information is used to determine L. These joint probability histograms give the maximum likelihood probability of next cycle given the occurrence of previous cycles in the whole time series. Then by comparing the one-cycle ahead predictions for different values of L, an optimal value of L can be determined. These histograms also give the probabilistic function for different data series. For the engine test points (with return maps in Figure 7.2), the optimal one-step ahead prediction is found using two previous cycles ($L = 2 + 1 = 3$).

Another important way to choose the optimum value of L is to employ Shannon entropy. Shannon entropy is a quantitative measure of nonrandom structure in time series measurements based on information theory. Because Shannon entropy provides an unambiguous indicator of temporal patterns, it is useful in determining the optimum sequence length L [184]. Shannon entropy is defined as:

$$H_S(L) = -\frac{1}{log(N)} \sum p_L log(p_L)$$

where N is the total number of symbol sequences with nonzero frequency, p_L is the probability of observing a sequence L. For the defined quantity, a value of one indicates the measured data are random, while a value of less than one indicates the presence of temporal correlation [82]. In the current context, lower H_S implies more deterministic structure. The value of H_S varies as the sequence length L changes. In this work, it is found that H_S typically reaches a minimum value as L is increased from 1. This trend is shown in Figure 7.3 for the five operating points listed in Table 7.1. The minimum H_S occurs at a sequence length of 3 which is optimal for these cases and also reflects the symbol-sequence transformation which best distinguishes the data from a random sequence.

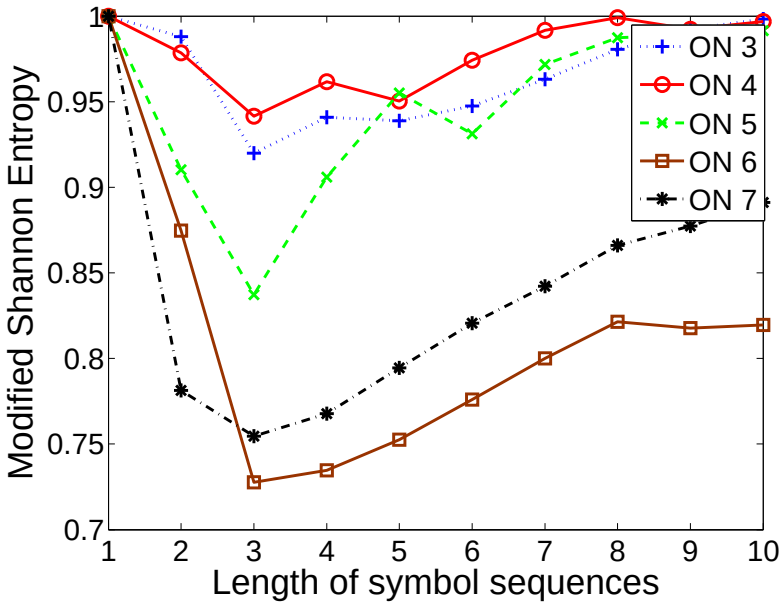

Figure 7.3: Modified Shannon entropy vs. symbol sequence length for 5 octane numbers. conditions listed in Table 7.1

The symbol-sequence histogram for consecutive cycles of θ_{Pmax} corresponding to the data in Figure 7.2 is shown in Figure 7.4. In Figure 7.4, the vertical axis corresponds to the normalized frequency of occurrence of a symbol sequence and

the horizontal axis is the symbol-sequence equivalent binary code. The symbol set size is $n = 8$ and sequence length is $L = 3$, resulting in $N = 8^3 = 512$ possible sequence codes.

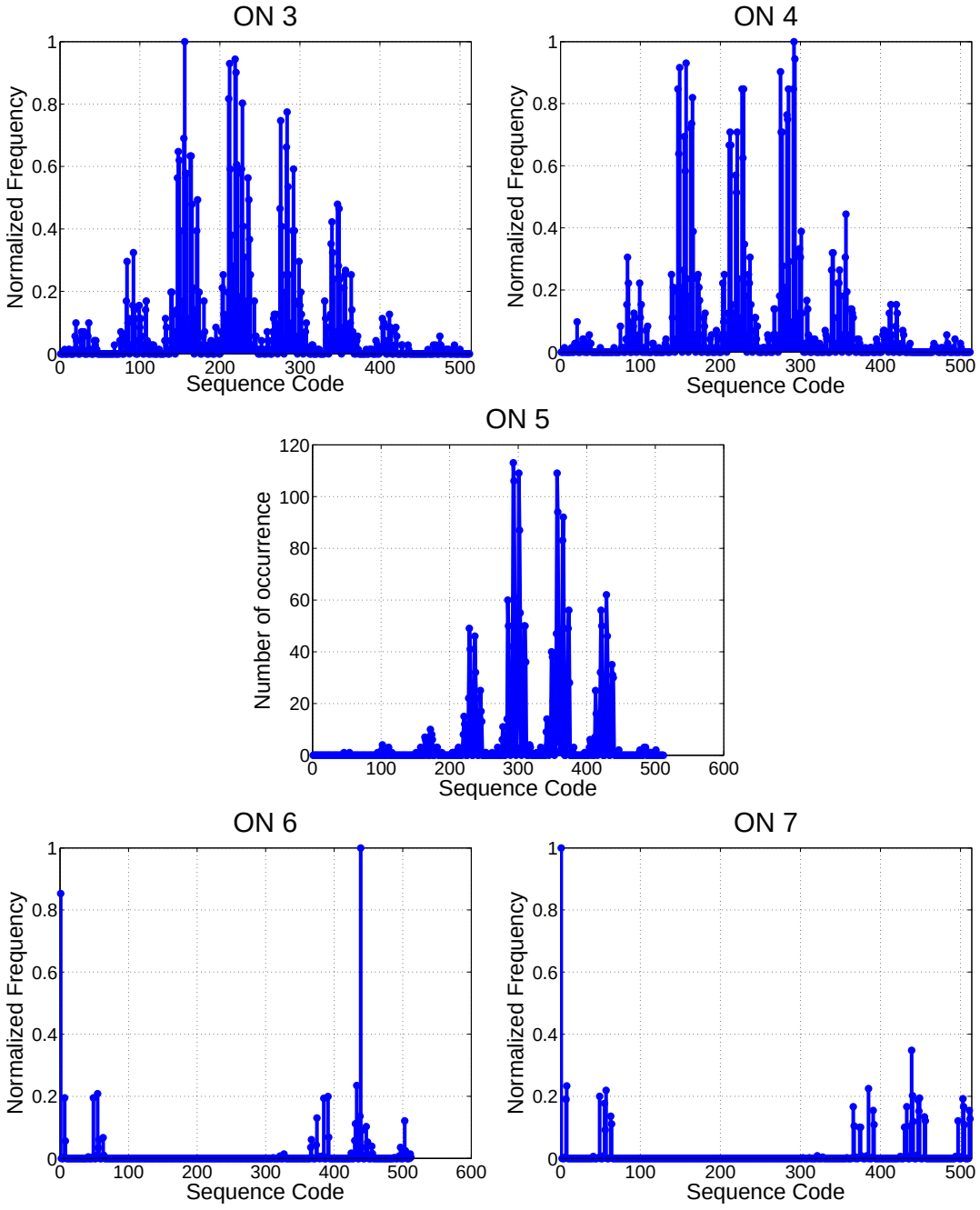

Figure 7.4: θ_{Pmax} Symbol sequence histogram with (n=8, L=3) for HCCI combustion cycles 1 to 3000 (conditions as in Figure 7.2)

A large normalized frequency peak accompanied by some smaller peaks in the sequence code histogram is apparent in the ON 7 plot of Figure 7.4 indicating a non-random sequence. The large peak occurs at sequence 0 (symbol series 000) which is three consecutive early values of θ_{Pmax} and physically corresponds to a weak combustion (most probably not having a main stage of combustion). Pattern number 438, which correspond to sequence 666, is also one of main local peaks for plots with ON 6 and ON 7. In addition, sequence codes 007 and 700, corresponding to pattern numbers 7 and 448 respectively, are among the possible sequences that the dynamics would pass through before entering or leaving three consecutive symbols of 0. For these cases, θ_{Pmax} does not stay in the late regions but oscillates between relatively early and late θ_{Pmax} angles. These local peaks indicate relative deterministic behavior of θ_{Pmax} combustion timing for the experimental cases with ON 6 and ON 7.

7.2.3 Time-Irreversibility

The use of symbol-sequence histograms for determining the time irreversibility is used since the relative frequencies will shift when they will be observed with time reversed. It has been shown that one of most important features to discriminate the gaussian random processes from deterministic prior-cycle effects is time irreversibility [196]. Particularly, processes with non-random structure between consecutive cycles show an arrow of time which increases as the nonlinear memory between cycles increase. On the other hand, processes with random inherent structure are symmetric in time(i.e. the behavior of forward and reverse time series are the same) [126].

Time irreversibility versus the five cases is plotted in Figure 7.5 and shows that increasing the octane number results in higher time irreversibility. The details of time irreversibility for the operating points studied in this work are listed in the Appendix. The higher time irreversibility close to the engine misfire region at higher octane numbers is also an indication of having more deterministic patterns in that region. These deterministic patterns can be captured in a chaotic predictive model and is detailed next.

For the case when a process is time symmetric, there should not be a major difference between forward and backward time histogram. The observed relative frequency of the pattern numbers of a specific time series are compared with their reverse counterparts and the comparison is quantified with the following Euclidean-norm:

$$T_{irr} = \sqrt{\sum (F_i - R_i)^2} \tag{7.1}$$

where i is indexed over all possible sequence codes. F and R in the above

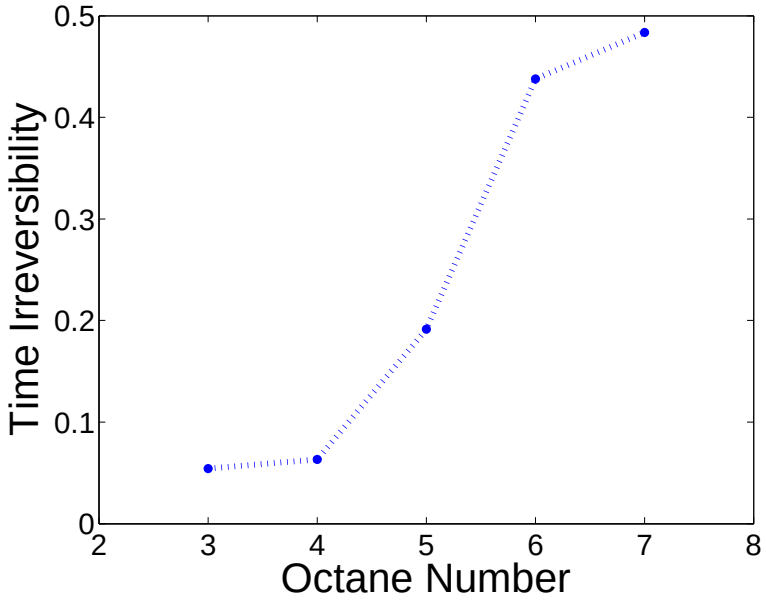

Figure 7.5: Time irreversibility versus octane number (conditions as in Figure 7.2)

equation are the histogram frequencies for the forward and reverse-time. The magnitude of T_{irr} is a quantitative measure of the level of time irreversibility. Figure 7.6 illustrates symbol-sequence histograms for the forward and reverse time of the HCCI θ_{Pmax} data corresponding to Figure 7.2. Reverse time series of the data points is generated by reversing the order of forward flow of data points.

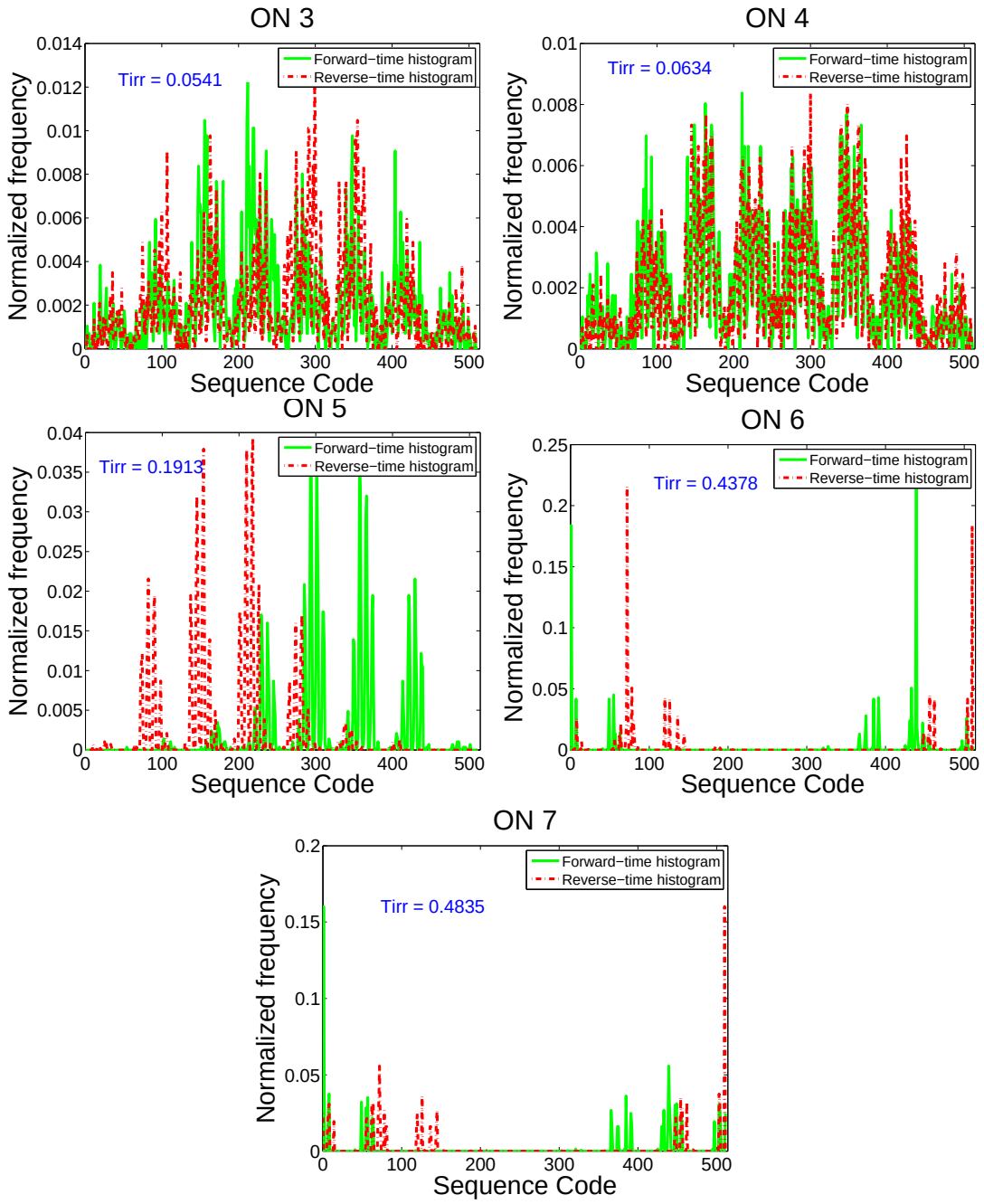

Figure 7.6: Forward and reverse θ_{Pmax} Symbol sequence histogram with (n=8, L=3) for HCCI combustion cycles 1 to 3000 (conditions as in Figure 7.2)

In Figure 7.6 for ON 7, there are large peaks at sequence codes 0 (symbol sequence 000) and sequence code 438 (symbol sequence 666) for the forward direction which are very different in the reverse time realizations. This is attributed

to the nonstationary or transient dynamics of the engine near the misfire limit, where the sequences of 0 or 6 occur often. The Euclidean-norm increases with octane number indicating that time irreversibility increases with increasing octane number as the engine operation approaches the misfire limit. As the engine is operated away from misfire (eventually knock could occur) the forward and reverse time symbol sequence histograms appear more similar to each other implying no major time irreversibility.

7.2.4 Chaotic Predictive Model with Added Fuel Octane Number Dynamics

HCCI combustion timing is not only dependant on the temperature and pressure of the compression stroke, but also on the fuel chemistry and burnt gas residual from previous cycles [80]. The cycle-by-cycle combustion timing is strongly dependant on the octane number [93] which can be changed cycle-by-cycle in this experiment by injecting two fuels (n-heptane and iso-octane) using two fuel injectors. The fuel octane number is then used to increase the load range of the HCCI engine [166].

The range of HCCI combustion timing over 3000 cycles for each of the five octane numbers is shown in Figure 7.7. All other inputs are kept constant but the variation of θ_{Pmax} increases with increasing octane number as the engine has more misfire cycles. The combustion timing angle increases as expected with an increase in fuel octane number for octane numbers ranging between 3 to 5. By increasing the octane number further, the average θ_{Pmax} advances primarily due to θ_{Pmax} occurring early due to partial burn or misfire. The variation of θ_{Pmax} also increases with octane number due to the combustion instability.

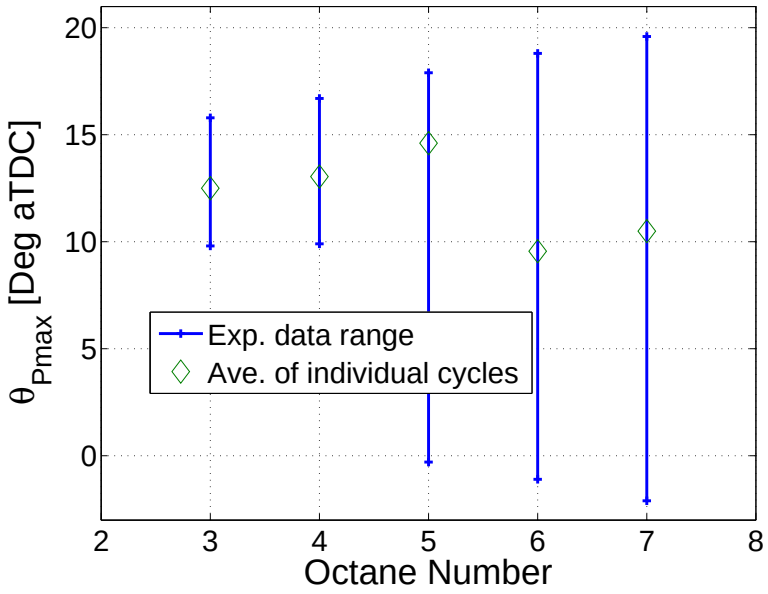

Figure 7.7: Combustion timing range of engine for 5 octane numbers used for HCCI combustion operating points near misfire (conditions as in Figure 7.2)

7.2.4.1 Nonlinear Prediction

A schematic of the real-time chaotic prediction for all five octane numbers is shown in Figure 7.8. To predict θ_{Pmax} with varying octane number, the interpolated deterministic part of the data captured by each of the five models is used. To obtain the predicted return map, the octane number and two previous θ_{Pmax} values are used to predict θ_{Pmax} of the next cycle such that the pattern of two previous inputs for each of the five octane numbers and the input octane number determines the most probable one step ahead θ_{Pmax}.

Using the joint probability estimator of θ_{Pmax} for each of the five operating points and the measured octane number in the test where the octane number varies between 3 to 7, the simulated behavior of consecutive cycles of θ_{Pmax} is constructed. To predict θ_{Pmax}, the following form is used:

$$\theta_{Pmax}(i) = f(ON(i), \theta_{Pmax}(i-1), \theta_{Pmax}(i-2), ..., \theta_{Pmax}(i-(L-1))) \quad (7.2)$$

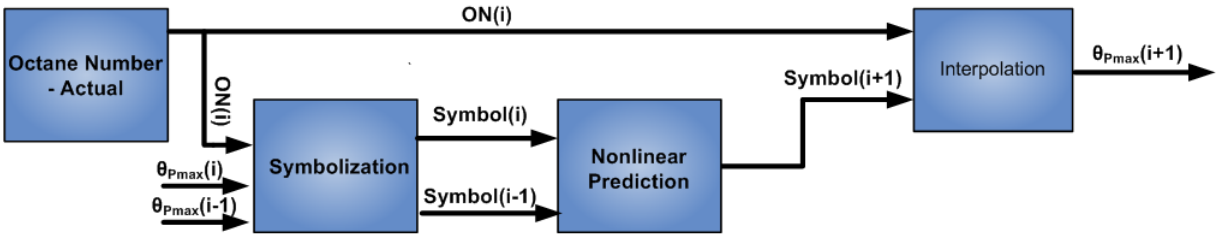

Figure 7.8: Schematic of the chaotic prediction used in Figure 7.12 for prediction of θ_{Pmax} for HCCI combustion operating points near misfire (conditions - Figure 7.2)

The experimental data for θ_{Pmax} in Figure 7.9(a) is compared to the prediction for the same cycles in Figure 7.9(b). The direction of arrows in Figure 7.9(b) illustrates transitions between different θ_{Pmax} phase plane locations and gives an indication of the complexity of the dynamics.

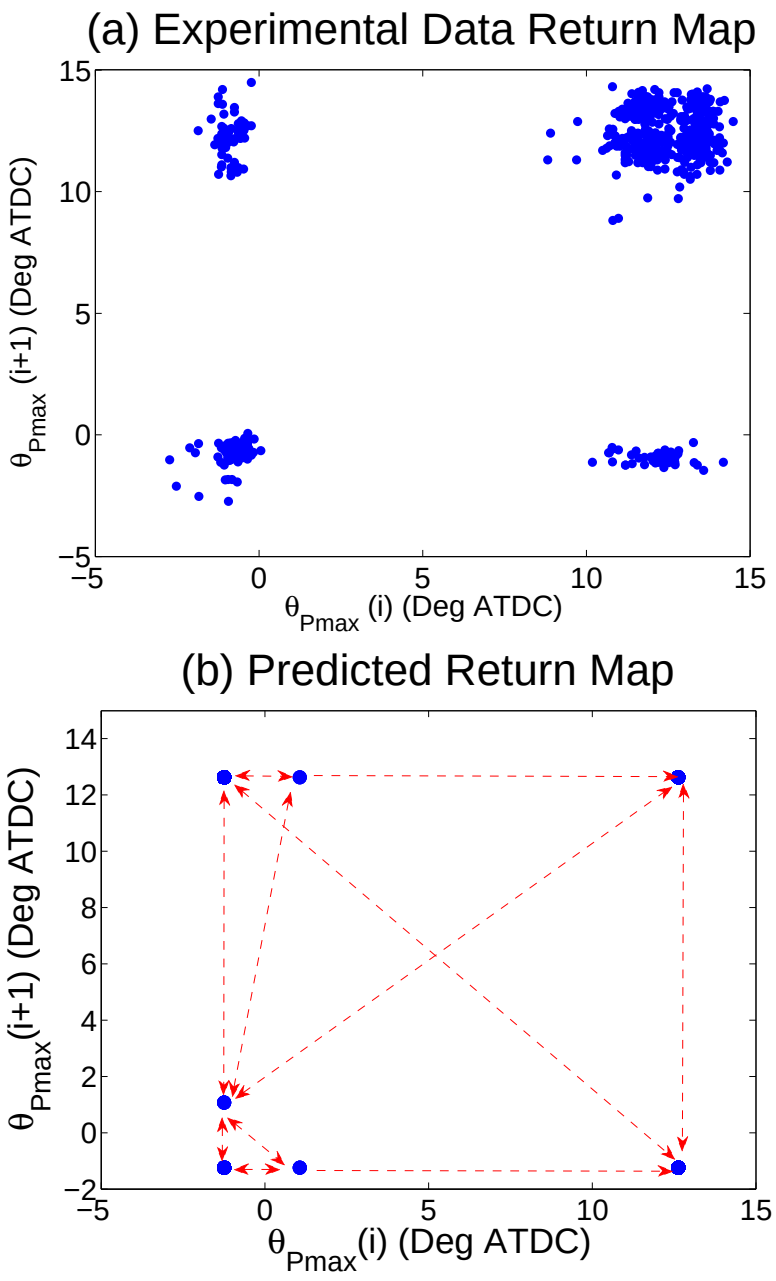

Figure 7.9: Comparison of experiment and prediction of θ_{Pmax} for HCCI combustion with varying octane number and different P_{man}

The predicted return map in Figure 7.9(b) has the general appearance of the experimental data in Figure 7.9(a).

7.2.4.2 Prediction Validation

Cycles 900 to 1250, a 350 cycle portion of the test point with varying octane number, is used to check the prediction quality. The residual ($\Delta\theta_{Pmax} = \theta_{Pmax}(pred) - \theta_{Pmax}(measured)$) is shown in Figure 7.10 and autocorrelation of the residual is shown Figure 7.11. No obvious visible pattern in the residual

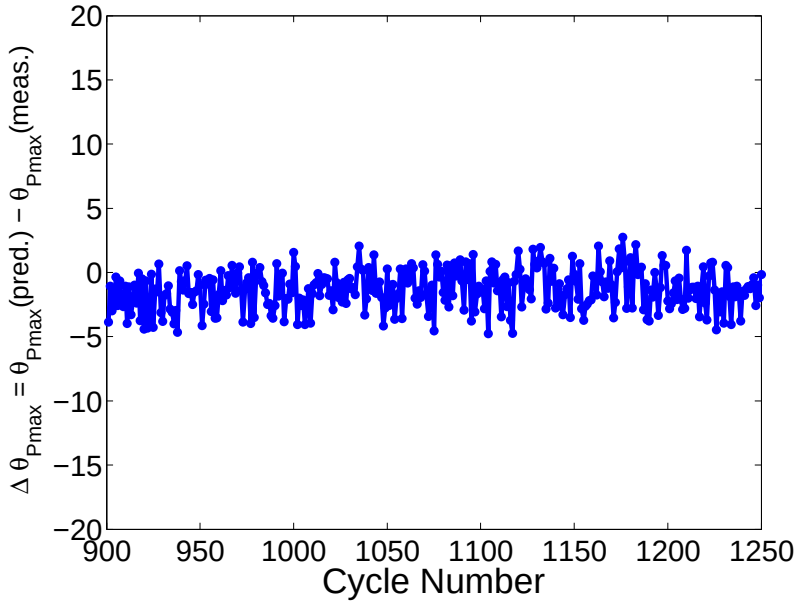

Figure 7.10: Prediction error ($\Delta theta_{Pmax}$) between predicted values and experimental measurements for HCCI combustion (same condition as in Figure 7.9)

error values in Figure 7.10 indicate, as a simple first check, that there is no dependency between consecutive error values and the model seems to capture the dynamics. The autocorrelation function for the residuals ($\Delta\theta_{Pmax}$) is shown in Figure 7.11 for all the 3000 $\Delta\theta_{Pmax}$ residuals with the 99% confidence interval is shown by dashed lines. The correlation curves indicating an acceptable model fall between these lines [153].

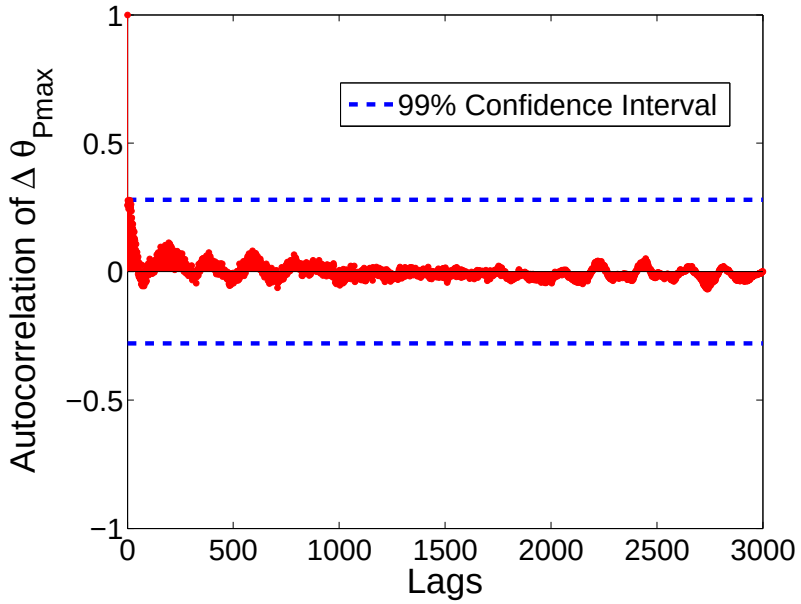

Figure 7.11: Autocorrelation of residuals $\Delta theta_{Pmax}$) for predicted consecutive cycles for HCCI combustion (same condition as in Figure 7.9)

7.3 CONTROLLER

7.3.1 θ_{Pmax} control based on a chaotic predictive model using fuel octane changes

To control the unstable HCCI operating region, the fuel octane number is varied using two injectors. Iso-octane is injected by one injector while n-heptane is injected by the other and by varying the volumetric ratio the octane number in the engine can be changed cycle by cycle.

A proportional-integral (PI) controller using combustion timing for the next cycle as determined by the chaotic predictive model, regulates combustion timing (θ_{Pmax}) by varying the ratio of iso-octane and n-heptane. A block diagram of the control system is shown in Figure 7.12. A single-input single-output controller is used since other inputs are kept constant. Since the engine combustion timing θ_{Pmax} can have a chaotic pattern, i.e. for an early/late θ_{Pmax} the next cycle

could have late/early combustion timing, the chaotic predictive model described previously, is used to predict the next cycle combustion timing. This prediction is used as the feedback signal to stabilize the combustion timing.

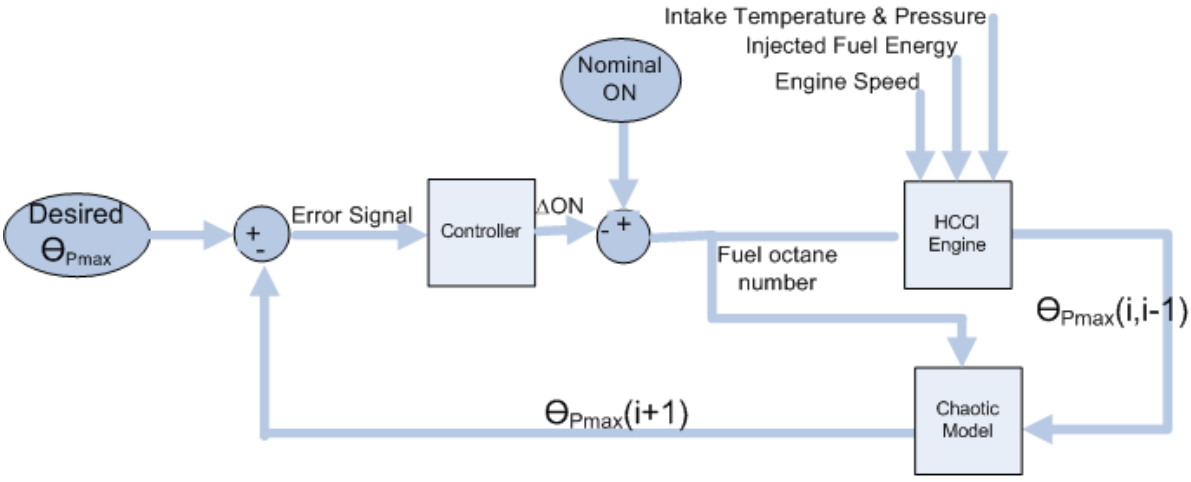

Figure 7.12: Schematic of the Controller of HCCI combustion timing for θ_{Pmax} in unstable region using fuel octane

To implement the control in real time, θ_{Pmax} is calculated (on the NI computer) at each cycle using 0.1 degree cylinder pressure data. This value θ_{Pmax}(i, i-1) in Figure 7.12 is output to the MicroAutobox via an analog signal once per engine cycle and well before the next combustion. The engine controller is combustion event based with a sampling rate of once every two engine revolutions and modulates the two fuels to command the injector pulse widths to set the fuel octane (wall wetting is ignored) while maintaining a constant injected fuel energy despite changing the octane number. A schematic of the control structure can be seen in Figure 7.13.

To tune the controller the proportional gain is increased until unstable operation of the engine. The proportional gain is then decreased to half and the integral term is then increased until the desired behavior of the engine is observed. The PI controller is tuned using simulation and then manually adjusted

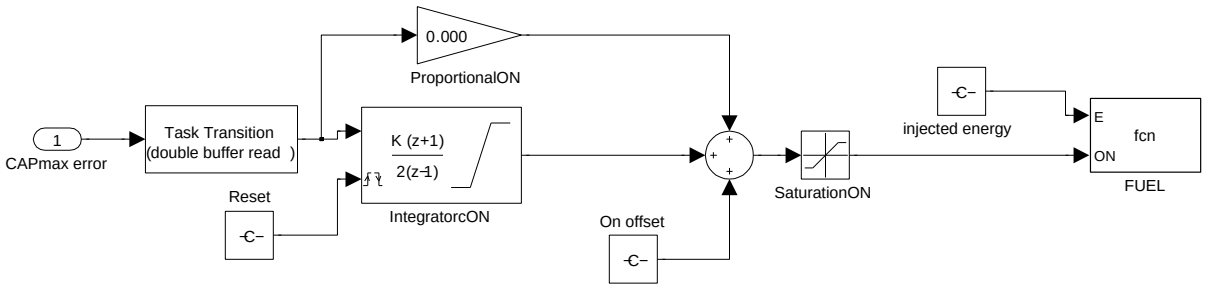

Figure 7.13: Simulink diagram of the implemented controller for CA_{Pmax} using fuel octane

on the real engine. The controller implementation is $u_i = k_P e_i + k_I \sum e_j$ where $e = \Delta\theta_{Pmax}$ is the difference between the desired and predicted θ_{Pmax}, and u is the controller output ΔON as shown in Figure 7.12.

7.3.2 Experimental Results

With PI control, the fuel octane number (input) and θ_{Pmax} (output) are recorded and shown in Figure 7.14. For this case θ_{Pmax} is about 10 °aTDC for normal combustion and 0 °for misfire. Cycles 800 to 900 show uncontrolled engine operation with the controller off and the octane number manually set to 5. At cycle 901, the PI controller is activated and modulates the octane number to stabilize θ_{Pmax} to the desired value. As seen in Figure 7.14, the controller reduces θ_{Pmax} variation resulting in a more stable engine operation with fewer misfire cycles. The average octane number is about 4 for the controlled portion of cycles 901 to 1260. The uncontrolled operation of the engine with the same conditions and octane number 4 exhibits unstable operation with misfire cycles as shown in Figure 7.15. The minor change in operating conditions (specifically intake manifold pressure) results in unstable operation of Figure 7.15 compared to conditions of Figure 7.2. The standard deviation of θ_{Pmax} decreases from 6.2 °(for cycles 800 to 900 without control) to 2.5 ° for the next 360 cycles with control. Most θ_{Pmax} values are within the normal operating condition of the engine after the

controller is turned on although the control is not perfect with some cycles near misfire. This can be quantified by counting the percentage of misfire cycles for the region with the controller on (3%) versus percentage of misfire cycles for the uncontrolled operation (79%).

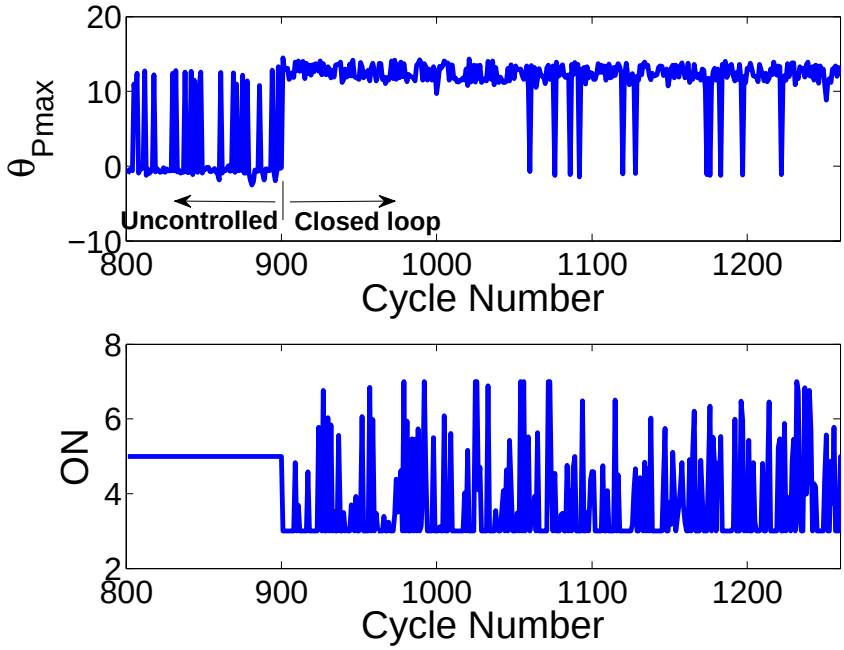

Figure 7.14: Combustion timing θ_{Pmax} using fuel octane input. Controller is turned on at cycle 901; $k_P = 1.7$;$k_I = 0.1$

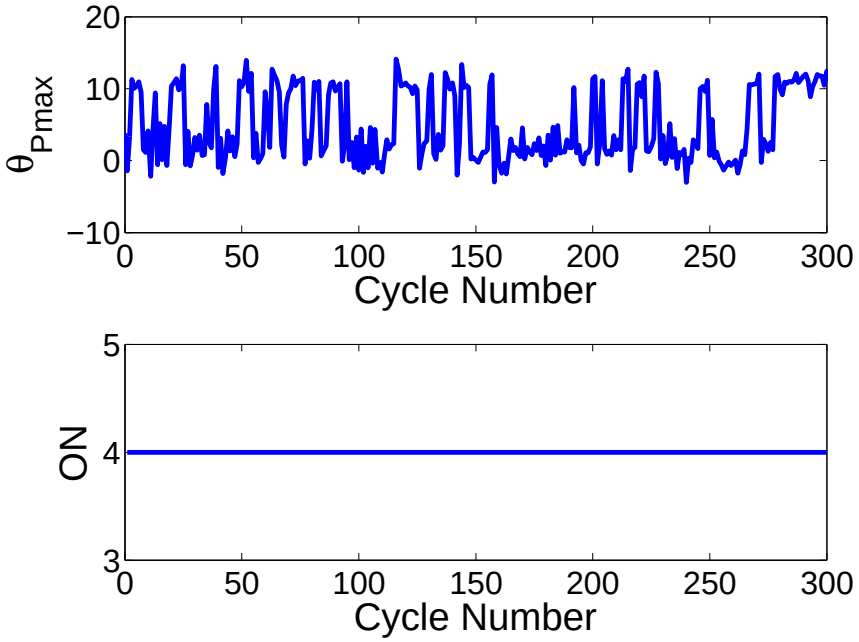

Figure 7.15: Combustion timing θ_{Pmax} using fuel octane input. Uncontrolled Operation

The pressure trace for the last two cycles of the uncontrolled operation (cycle 899 and 900) and the first two cycles of the controlled operation condition (cycle 901 and 902) of Figure 7.14 are shown in Figure 7.16. Cycle 899 and 900 have the characteristics of misfire cycles while 901 and 902 have the characteristics of HCCI combustion indicating that the controller is effective in this case.

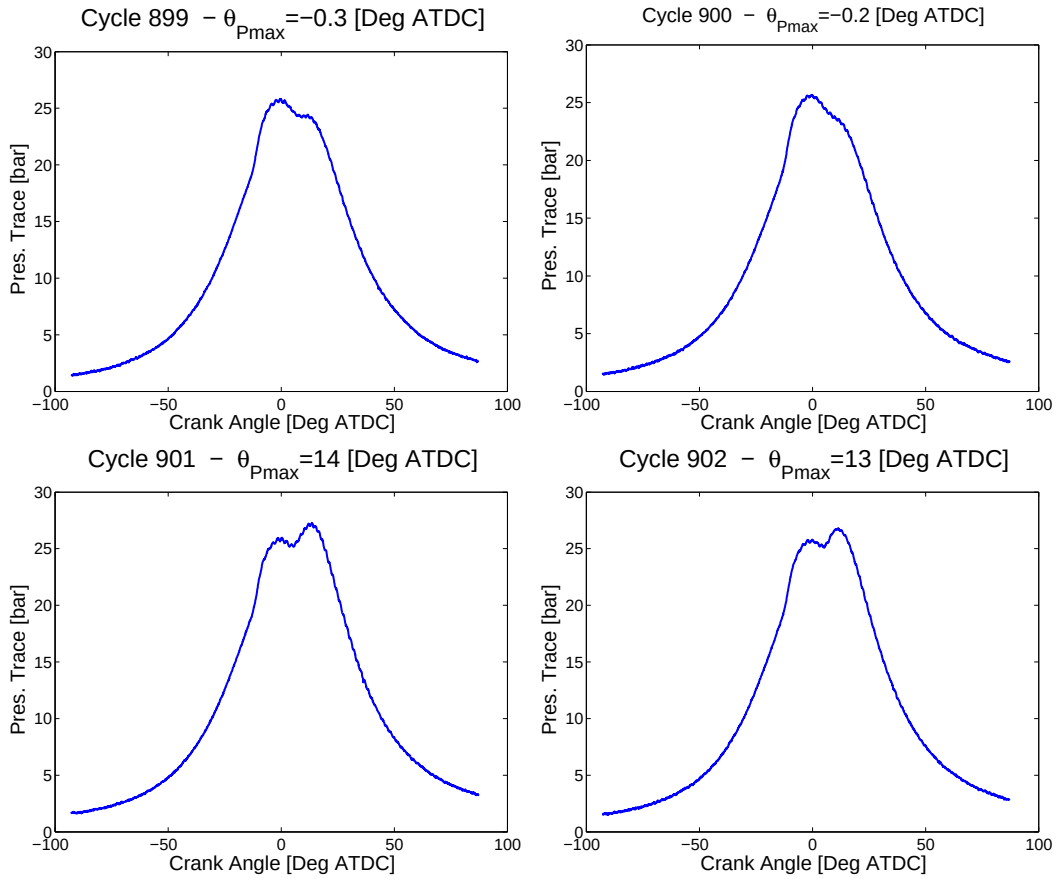

Figure 7.16: Cylinder pressure trace of cycles 899-902 of Figure 7.9

7.4 SUMMARY

Deterministic patterns in cyclic variation of ignition timing (θ_{Pmax}) at operating points near the misfire limit of an HCCI engine are observed. Near the misfire limit the return map of θ_{Pmax} consists of multiple different regions, indicating non-constant nonlinear combustion timing. Non-random patterns of cyclic variation of ignition timing θ_{Pmax} under specific operating conditions emerge in symbol sequence analysis as large peaks in the symbol-sequence histogram and indicate a coupling between consecutive cycles. A joint probability estimator to predict one cycle ahead using the two previous cycles is developed and is used to predict combustion timing. An autocorrelation of predicted-actual θ_{Pmax} residual shows uncorrelated residuals which indicates that the joint probability model

is acceptable. For the one base engine operating condition tested, θ_{Pmax} one cycle prediction is used to command fuel octane number (and thus modify combustion timing θ_{Pmax}) and results in a significantly lower number of misfires. The θ_{Pmax} prediction is combined with feedback control and demonstrates lower HCCI combustion variation and misfire rates in an experimental engine at one operating point for the same average octane number. This indicates that this method could potentially be used to extend into the misfire region of the HCCI engine range.

Chapter 8

Summary and Conclusions

An experimental and simulation study has been conducted to characterize HCCI operation in the normal and partial burn region. In addition, an ignition timing criterion that is more robust than existing methods in the partial burn region is used as the control input for unstable high cyclic variations engine operation. A chaotic predictive model useful for control applications is also developed. Then, the cyclic combustion phasing variations is combined with varying octane number control input and the chaotic predictive model to stabilize the combustion. Major results and contributions from this thesis are summarized in this chapter and recommendations for further work are outlined.

8.1 CONCLUSIONS

The analysis of the results in this study leads to the following findings and conclusions:

8.1.1 Experimental Study of HCCI

- Under certain operating conditions, HCCI engines can exhibit large cyclic variations in ignition timing. Experimental characterization of cyclic variation of HCCI combustion using both chaotic and statistical methods has

been performed. Cyclic variability can be categorized ranging from stochastic to deterministic patterns. The development of nonlinear scattering patterns of CA50 cyclic variation in an HCCI engine is studied.

The return map techniques applied in nonlinear dynamics and chaos theory are used to observe possible deterministic structures inherent in the experimental data. Transitions from the misfire to knock limit within the HCCI mode is done by varying intake manifold temperature. Using bifurcation diagrams and return maps more structure is observed as the engine operating condition is changed from the knock limit to the misfire limit by using 9 different intake manifold temperatures. This structure is indicative of a coupling between successive CA50 (engine cycle timing) which has the expected sequence of late and early combustion near the misfire limit. Dominant deterministic patterns are observed in some of the data near misfire limit. Return map results for CA50 near the knock limit show an unstructured cluster of circular data gathered around a fixed point. These data points start to scatter over the diagonal line as they move towards the misfire limit and fixed points becomes destabilized leading to more structured data points. The structured patterns seen in the data is attributed to the deterministic coupling between consecutive cycles. The results show that unstable operation of HCCI with higher cyclic variations is observed closer to the misfire region of the engine.

- A wide range of engine operating conditions (338 points) is analyzed to determine which conditions have a normal distribution for ignition timing (CA50). Two common testing methods for normal distributions are used. These two methods are applied on the data sets from 338 points. Points that successfully pass these two tests are then visually evaluated with normal

probability plot. Ignition timing (CA50) data sets for all experimental points were processed using the procedure mentioned above and 19 points out of 338 points are judged to have a normal distribution. Results show that normal distribution of ignition timing (CA50) is more likely to occur in HCCI ignitions occurring for a window immediately after TDC ($0.8 \leq$ SOC $\leq$7.7 CAD aTDC). In those conditions, cyclic variations of ignition timing (CA50) is typically low ($0.4 \leq STD_{CA50} \leq$1.4 CAD) and the burn duration is short ($2.5 \leq$ BD $\leq$ 4.3 CAD). A large deviation from the straight line is observed in normal probability plots of the operating points which have mean ignition timing (CA50) occurring after 15 CAD aTDC. Generally, results show that unstable operation of HCCI with higher cyclic variations is observed closer to the misfire region of the engine. Thus, misfire region of HCCI will be the main focus of interest in order to extend the HCCI limited operating range and controlling the combustion instabilities in this work. No direct preference for normal distribution was seen in operating conditions in terms of octane number, engine speed, equivalence ratio and intake conditions. However, a combination of these conditions determine the location of SOC.

- Experimental data from HCCI engine collected at 115 operating points are used to define two criteria for partial burn operation, one used as offline criteria after collecting all the cycles and one online method by comparing the cyclic peak of main and cool flame stage of heat release curve. In order to control the ignition timing in the partial burn region of the engine, accurate offline and online estimates of ignition timing are introduced. For offline operating condition ignition timing, a new method is proposed which combines the Coefficient of Variation of Indicated Mean Effective Pressure (COVImep) and percentage of cycles with less than 90 percent heat release

of previous cycle. Particularly near the partial burn/misfire limit, this method is more reliable than just COVImep. For online ignition timing estimates, a new method in which the ratio of the peak of main stage and cool flame stage of heat release curve (HTR to HTRLTR Peak Ratio) is used for each cycle. Using this, normal and partial burn engine cycles can be determined in realtime for fuels exhibiting a cool flame. This ratio is found to achieve a rough correlation with the number of partial burn cycles when the threshold is adjusted for each octane number. This threshold is mainly useful to control CA10 as ignition timing criteria since it determines the location of occurrence of CA10 on first or second stage of combustion. The effect of online method on location of ignition timing is investigated for all operating points in order to find an accurate measurement method for HCCI combustion timing that works for both normal and partial burn operating conditions. Based on this criterion, the performance of five methods for characterizing the combustion timing are investigated and compared. The methods for characterizing the start of combustion are: CA50 based on the total heat release; the start of combustion from the third derivative of the pressure trace with respect to crank angle; the start of combustion from the third derivative of the pressure trace with respect to crank angle with two limits; CA10 based on total heat release; CA10 based on peak of main stage of combustion. Examining combustion criterion it is found that the four existing methods are not effective during partial burn operation but a new criterion CA10 based on the main stage of combustion is effective. CA10-main is a new method defined as 10 percent of the maximum heat release of only the main stage.

A P_{Burn} (partial burn) cycle is defined as when the total heat release is less than 90% of previous cycle. That is, a cycle with 10% reduction in total

heat release compared to its previous cycle is considered as a partial burn cycle. An operating point is considered partial burn operating point if it contains more than 15% partial burn cycles and *COVImep* higher than 6%.

- Understanding the variations of ignition timing with changing engine operating conditions is an essential step to be able to control HCCI engines for achieving fuel consumption and vehicle's emissions targets. The effect of online method on location of ignition timing is investigated for all operating points in order to find an accurate measurement method for HCCI combustion timing that works for both normal and partial burn operating conditions. The first step is to come up with a comprehensive ignition timing which covers a wide range of operating conditions particularly partial burn region of HCCI engines. The crank angle where the maximum pressure occurs (θ_{Pmax}) is proposed as a robust criteria for distinguishing between normal and misfire HCCI combustion modes. Particularly near the partial burn/misfire limit, this method is found to be more reliable than the existing method of $CA50$ and is better able to distinguish between the normal and misfire combustion cycles than $CA50$. Using (θ_{Pmax}), normal and partial burn engine cycles can be determined cycle by cycle for fuels exhibiting a cool flame. The performance of this new criteria is then analyzed for different engine loads at both constant fueling and constant equivalence ratio at 329 HCCI experimental operating points. For operating points with high cyclic variation θ_{Pmax} is found to be more reliable than $CA50$. Thus θ_{Pmax} could be used in feedback algorithms to help control to stabilize ignition timing in these regions extending the useful operating range of HCCI.

  Although several crank angle based parameters as indicators of ignition timing have been studied, the θ_{Pmax} is used as the final ignition timing

criteria for feedback control because of its characteristics in distinguishing the different modes of combustion as well as its simplicity compared to other criteria. One other reason to prefer θ_{Pmax} for feedback control parameter versus other ignition timing criteria such as CA10, which has already been shown as a good criteria, is simplicity of its calculation compared to CA10 since its calculation does not require heat release and mass fraction analysis.

8.1.2 Chaotic Modeling and Control of HCCI Ignition Timing

- The analysis of variation of consecutive cycles of ignition timing (CA50) for an n-heptane fueled engine is performed near the misfire condition in order to predict the following cycles using the identified dynamics. The results have specific implications for the control design used to stabilizing unstable HCCI operation near the misfire condition. Nonlinear and chaotic theory tools are used to identify the inherent deterministic patterns of cyclic variation during HCCI combustion. Then the deterministic structure inherent in the data points is captured using a symbol-sequence approach. Joint probability distributions are calculated using the frequency histograms obtained in previous sections. Finally, those joint probability estimators are used to predict the next cycle ahead combustion timings in the experimental data points. Adding appropriate noise to the predicted values results in simulation results with similar statistics to the experimental data. These techniques are then used to predict ignition timing (CA50) one cycle-ahead. Simulated data points in phase space have similar dynamical structure to the experimental measurements. An autocorrelation of predicted-actual ignition timing residual shows uncorrelated residuals which indicates the joint probability model is acceptable.

- Cyclic variation of a HCCI engine near misfire is analyzed using chaotic the-

ory methods and a feedback control has been developed to stabilize high cyclic variations. Variation of consecutive cycles of θ_{Pmax} for a primary reference fuel engine is analyzed near misfire operation for five test points with similar conditions but different octane numbers. The return map of the time series of θ_{Pmax} at each combustion cycle reveals the deterministic and random portions of the dynamics near misfire for this HCCI engine. A symbol-statistic approach is used to predict θ_{Pmax} one cycle-ahead. Based on this cycle ahead prediction, and using fuel octane as the input, feedback control is used to stabilize the instability of θ_{Pmax} variations at this engine condition near misfire. The cycle ahead prediction at all 5 octane numbers is combined with feedback control that modulates the octane number to control ignition timing and extending the HCCI operating range of the engine. A proportional-integral (PI) controller using combustion timing for the next cycle as determined by the chaotic predictive model, regulates combustion timing (θ_{Pmax}) by varying the ration of iso-octane and n-heptane. A single-input single-output controller is used since other inputs are kept constant. Since the engine combustion timing θ_{Pmax} can have a chaotic pattern, i.e. for an early/late θ_{Pmax} the next cycle could have late/early combustion timing, the chaotic predictive model described previously, is used to predict the next cycle combustion timing. This prediction is used as the feedback signal to stabilize the combustion timing. For the one base engine operating condition tested, θ_{Pmax} one cycle prediction is used to command fuel octane number (and thus modify combustion timing θ_{Pmax}) and results in a significantly lower number of misfires. The θ_{Pmax} prediction is combined with feedback control and demonstrates lower HCCI combustion variation and misfire rates in an experimental engine at one operating point for the same average octane number. The controller reduces θ_{Pmax} varia-

tion resulting in a more stable engine operation with fewer misfire cycles. The uncontrolled operation of the engine with the same conditions exhibits unstable operation with misfire cycles. Implementing this control on the engine, a single operating point near the misfire condition is controlled by changing the octane number over a limited range.

8.2 MAJOR THESIS CONTRIBUTIONS

The major contributions of this thesis with published results referred are outlined below:

- Investigated cyclic variation of HCCI combustion using both chaotic and statistical methods such as return maps, bifurcation diagram; Categorized range of cyclic variability from stochastic to deterministic patterns in engine experimental data points.

- Determined conditions having a normal distribution for ignition timing in a wide range of operating conditions (338 points) using common testing methods; Observed unstable operation of HCCI with higher cyclic variations closer to the misfire region of the engine; Focused on the misfire as the region of the interest in order to extend the HCCI limited operating range and controlling the combustion instabilities.

- Defined two criteria for partial burn operation; used COVImep and percent of partial burn cycles to define offline estimate of ignition timing; determined normal and partial burn engine cycles in realtime using online ignition timing estimate for fuels exhibiting a cool flame; studied the effect of online method on location of ignition timing for all operating points in order to find an accurate measurement method for HCCI combustion timing

that works for both normal and partial burn operating conditions; defined partial burn cycle and partial burn operating point.

- Proposed a robust ignition timing criteria as the feedback control parameter for distinguishing between normal and partial burn HCCI combustion modes; Analyzed the performance of this criteria for different engine loads at both constant fueling and constant equivalence ratio at 329 HCCI operating points.

- Performed an analysis of variation of consecutive cycles of ignition timing for an n-heptane fueled engine near the misfire condition in order to predict the following cycles using the identified dynamics; Captured the deterministic structure inherent in the data points using a symbol-sequence approach; Calculated joint probability distributions using the frequency histograms; predicted ignition timing one cycle-ahead.

- Developed and validated a feedback control to stabilize high cyclic variations; regulated the combustion timing by varying the ration of iso-octane and n-heptane using a proportional-integral (PI) controller for the next cycle as determined by the chaotic predictive model; reduced combustion timing variations resulting in a more stable engine operation with fewer misfire cycles.

8.3 FUTURE WORK

The HCCI predictive model and feedback controller in this work are useful tools to understand the combustion behavior near partial burn region of HCCI and its control application. More experimental data and analysis are needed to extend the predictive control to a wide range of engine operation that is near misfire.

8.3.1 HCCI Control Using the Cycle ahead prediction

- The feedback control of HCCI ignition timing cyclic variation in this work can be extended to use the variable valve timing instead of fuel type as the control actuator for future HCCI control applications.

- The ignition timing criteria of CA10-main can be used as the control feedback parameter instead of θ_{Pmax} used in this work. R_{HLTR} can be also used as a real-time criterion to detect the partial burn region for cycle-to-cycle control purposes. Having R_{HLTR} threshold for different octane numbers, feedback control of CA10 will be possible in future.

Bibliography

[1] R. Lupul. Steady state and transient characterization of a HCCI engine with varying octane fuel. Master's thesis, University of Alberta, 2008.

[2] A. Audet. Closed loop control of HCCI using camshaft phasing and dual fuels. Master's thesis, University of Alberta, 2008.

[3] Image source:http://blogs.zdnet.com.

[4] Environment Canada National Inventory Report. Canada's greenhouse gas inventory: 1990-2003. Technical report, 2005.

[5] U. G. Department of Energy. Energy consumption by sector. Technical report, Department of Energy, 1949-2007.

[6] F. Zhao and T.W. Asmus and D.N. Assanis and J.E. Dec and J.A. Eng and P.M. Najt. Homogeneous Charge Compression Ignition (HCCI) Engines. *SAE Publication PT-94*, 2003.

[7] R.H. Stanglmaier and C.E. Roberts. Homogeneous charge compression ignition (HCCI): Benefits, compromises, and future engine applications. *SAE Paper No. 1999-01-3682.*, 1999.

[8] R.H. Thring. Homogeneous Charge Compression Ignition (HCCI) Engines. *SAE Paper No. 892068.*, 1989.

[9] G.M. Shaver, M.J. Roelle, and J.C. Gerdes. Modeling cycle-to-cycle dynamics and mode transition in HCCI engines with variable valve actuation. *Control Engineering Practice*, 14:213–222, 2006.

[10] M. Yao, Z. Zheng, B. Zhang, and Z. Chen. The Effect of PRF Fuel Octane Number on HCCI Operation. *SAE Paper No. 2004-01-2992.*, 2004.

[11] P.M. Najt and D.E. Foster. Compression-ignited homogeneous charge combustion. *SAE Paper No. 830264.*, 1983.

[12] G.M. Shaver and J.C. Gerdes. Cycle to cycle control of HCCI engines. *Proceedings of IMECE '03, 2003 ASME International Mechanical Engineering Congress and Exposition*, 2003.

[13] J. Martinez-Frias, S. Aceves, D. Flowers, and J. Smith. HCCI engine control by thermal management. *SAE Paper No. 2000-01-2869*, 2000.

[14] D. Law, D. Kemp, J. Allen, G. Kirkpatrick, and T. Copland. Controlled combustion in an ic-engine with a fully variable valve train. *SAE Paper No. 2001-01-0251.*, 2001.

[15] P. Caton and A. Simon and J.C. Gerdes and C. Edwards. Residual-effected Homogeneous Charge Compression Ignition at Low Compression Ratio Using Exhaust Reinduction. *International Journal of Engine Research*, 4:163–177, 2003.

[16] P. Kirchen, M. Shahbakhti, and C.R. Koch. A Skeletal Kinetic Mechanism for PRF Combustion in HCCI Engines. *Combustion Science and Technology*, 179:1059–1083, 2007.

[17] H. Santoso, J. Matthews, and W.K. Cheng. Managing SI/HCCI Dual-Mode Engine Operation. *SAE Paper No. 2005-01-0162.*, 2005.

[18] Koopmans, Lucien, Strm, and Hans. Demonstrating a SI-HCCI-SI Mode Change in a Volvo 5-cylinder Electronic Valve Control Engine. *SAE Paper No. 2003-01-0753.*, 2003.

[19] R. Chen and J. Turner and D. Blundell. The Transition Between Controlled Auto Ignition and Apark Ignition. *SAE Paper No. 2004-01-0939*, 2004.

[20] P. Price, R. Stone, J. Misztal, H. Xu, M. Wyszynski, T. Wilson, and J. Qiao. "Particulate Emissions From a Gasoline Homogeneous Charge Compression Ignition Engine". SAE Paper No. 2007-01-0209, 2007.

[21] R. H. Stanglmaier and C. E. Roberts. " Homogeneous Charge Compression Ignition (HCCI): Benefits, Compromises, and Future Engine Applications". *SAE Paper No. 1999-01-3682*, 1999.

[22] H. Zhao. *HCCI and CAI engines for the automotive industry.* Woodhead Publishing Limited, 2007.

[23] O. Erlandsson. Early Swedish Hot-bulb Engines - Efficiency and Performance Compared to Contemporary Gsoline and Diesel Engines. *SAE Paper No. 2002-01-0115*, 2002.

[24] H. Zhao. *Homogeneous Charge Compression Ignition (HCCI) and Controlled Auto Ignition (CAI) Engines for the Automotive Industry.* Woodhead Publishing Ltd., Brunel University UK, 2007.

[25] L. A. Gussak. "High Chemical Activity of Incomplete Combustion Products and a Method of Prechamber Torch Ignition for Avalanche Activation of Combustion in Internal Combustion Engines". SAE Paper No. 750890, 1975.

[26] S. Onishi and S. Hong Jo and K. Shoda and P. Do Jo and S. Kato. Active Thermo-atmosphere Combustion (ATAC) - A New Combustion Process for Internal Combustion Engines. *SAE Paper No. 790507*, 1979.

[27] M. Naguchi and Y. Tanaka and T. Tanaka and Y. Takeuchi. A Study on Gasoline Engine Combustion by Observation of Intermediate Reactive Products during Combustion. *SAE Paper No. 790840*, 1979.

[28] Honda Readies Activated Radical Combustion two-stroke Engine for Production Motorcyle. *Automotive Engineer, pp. 90-92, SAE Publications*, 1997.

[29] V. Stockinger and H. Schapertons and U. Kuhlmann. Investigation on a Gasoline Engine Working with Self-Ignition by Compression. *MTZ*, 53:80–85, 1992.

[30] T. Aoyama, Y. Hattori, J. Mizuta, and Y. Sato. "An Experimental Study on Premixed-Charge Compression Ignition Gasoline Engine". SAE Paper No. 1996-01-0081, 1996.

[31] T.W. Ryan and T.J. Callahan. "Homogeneous Charge Compression Ignition of Diesel Fuel". *SAE Paper No. 961160*, 1996.

[32] M. Christensen, A. Hultqvist, and B. Johansson. "Demonstarting the Multi Fuel Capability of a Homogenous Charge Compression Ignition Engine with Variable Compression Ratio". SAE Paper No. 1999-01-3679, 1999.

[33] European Federation for Transport and Environment. "Waiting for Euro 5 and Euro 6 New Emission Standards for Passenger Cars, Vans and Lorries". http://www.t-e.nu/, 2004.

[34] US Environmental Protection Agency. "2007 Emission Standard for Heavy Duty Truck and Bus Engines". http://www.epa.gov/, 2000.

[35] J. Lavy and J. Dabadie and C. Angelberger and P. Duret and J. Willand and A. Juretzka and J. Schaflien and T. Ma and Y. Lendress and A. Satre and C. Shultz and H. Kramer and H. Zhao and L. Damiano. Innovative Ultra-Low NOx Controlled Auto-ignition Combustion Process for Gasoline Engines: the 4-SPACE project. *SAE Paper No. 2000-01-1837*, 2000.

[36] H. Zhao and J. li and T. Ma and N. Ladommatos. Performance and Analysis of a 4-stroke Multi-cylinder Gasoline Engine with CAI Combustion. *SAE Paper No. 2002-01-0420*, 2001.

[37] L. Koopmans, O. Backlund, and I. Denbratt. Cycle to Cycle Variations: Their Influence on Cycle Resolved Gas Temperature and Unburned Hydrocarbons from a Camless Gasoline Compression Ignition Engine. *SAE Paper No. 2002-01-0110*, 2002.

[38] A. Furhapter. CAI - Controlled Auto Ignition - the Best Soluton for the Fuel Consumption - Versus Emission Trade-Off? *SAE Paper No. 2003-01-0754*, 2003.

[39] J. Arrafgle, B. Tormos, J. J. Laopez, and A. Garcia. "Analysis of the Potential of Biodiesel as an Alternative Fuel for Current and Future HSDI Engines". SAE Paper No. 2009-01-0480, 2009.

[40] A. Tsolakisa, A. Megaritisb, and D. Yap. "Application of Exhaust Gas Fuel Reforming in Diesel and Homogeneous Charge Compression Ignition (HCCI) Engines Fuelled with Biofuels". *Energy*, 33:462–470, 2008.

[41] R.F. Cracknell, D.J. Rickeard, J. Ariztegui, K.D. Rose, M. Muether, M. Lamping, and A. Kolbeck. "Advanced Combustion for Low Emissions

and High Efficiency Part 2: Impact of Fuel Properties on HCCI Combustion". SAE Paper No. 2008-01-2404, 2008.

[42] M. Yao, Z. Zheng, and H. Liu. "Progress and Recent Trends in Homogeneous Charge Compression Ignition (HCCI) Engines". *Progress in Energy and Combustion Science*, 35:398437, 2009.

[43] V. Hosseini and M.D. Checkel. "Reformer Gas Composition Effect on HCCI Combustion of n-Heptane, Iso-Octane, and Natural Gas". SAE Paper No. 2008-01-0049, 2008.

[44] O. Stenlåås, M. Christensen, R. Egnell, P. Tunestål, B. Johansson, and F. Mauss. "Reformed Methanol Gas as Homogeneous Charge Compression Ignition Engine Fuel". SAE Paper No. 2004-01-2991, 2004.

[45] P. Kongsereeparp and M. D. Checkel. "Study of Reformer Gas Effects on n-Heptane HCCI Combustion Using a Chemical Kinetic Mechanism Optimized by Genetic Algorithm". SAE Paper No. 2008-01-0039, 2008.

[46] A. Ghazimirsaied, M. Shahbakhti, and C. R. Koch. Partial-burn crankangle limit criteria comparison on an experimental HCCI engine. *Proceeding of Combustion Institue - Canadian Section Spring Technical Meeting, University of Montreal, Quebec*, May 11-13, 2009.

[47] R. Yu, X. S. Bai, H. Lehtiniemi, S. S. Ahmed, F. Mauss, M. Richter, M. Aldn, L. Hildingsson, B. Johansson, and A. Hultqvist. "Effect of Turbulence and Initial Temperature Inhomogeneity on Homogeneous Charge Compression Ignition Combustion". *SAE Paper No. 2006-01-3318*, 2006.

[48] A. Hultqvist, M. Christensen, B. Johansson, M. Richter, J. Nygren, J. Hult, and M. Aldjin. "The Research About the Effects of Thermal Stratification

on n-Heptane/iso-Octane-Air Mixture HCCI Combustion Using a Rapid Compression Machine". *SAE Paper No. 2006-01-3319*, 2006.

[49] J. Martinez-Frias, S.M. Aceves, D. Flowers, J.R. Smith, and R. Dibble. "Equivalence Ratio-EGR Control of HCCI Engine Operation and the Potential for Transition to Spark-ignited Operation". SAE Paper No. 2001-01-3613, 2001.

[50] L. Koopmans, H. Strom, S. Lundgren, O. Backlund, and I. Denbratt. "Demonstrating a SI-HCCI-SI Mode Change on a Volvo 5-Cylinder Electronic Valve Control Engine". SAE Paper No. 2003-01-0753, 2003.

[51] Halim Santoso, Jeff Matthews, and Wai K. Cheng. "Managing SI/HCCI Dual-Mode Engine Operation". SAE Paper No. 2005-01-0162, 2005.

[52] Y. Guezennec, C. Musardo, B. Staccia, S. Midlam-Mohler, E. Calo, P. Pisu, and G. Rizzoni. "Supervisory Control for NOx Reduction of an HEV With a Mixed-Mode HCCI/DI Engine". SAE Paper No. 2004-05-0123, 2004.

[53] S. Midlam-Mohler, S. Haas, Y. Guezennec, M. Bargende, and G. Rizzoni. "Mixed-Mode Diesel HCCI/DI With External Mixture Preparation". SAE Paper No. 2004-05-0446, 2004.

[54] M. Christensen, B. Johansson, P. Amneus, and F. Mauss. "Supercharged Homogeneous Charge Compression Ignition". SAE Paper No. 980787, 1998.

[55] Y. Iwabuchi, K. Kawai, T. Shoji, and Y. Takeda. "Trial of New Concept Diesel Combustion System Premixed Compression-Ignition Combustion". SAE Paper No. 1999-01-0185, 1999.

[56] R. Sun, R. Thomas, and C.L. Gray. "An HCCI Engine: Power Plant for a Hybrid Vehicle". SAE Paper No. 2004-01-0933, 2004.

[57] J. Hyvönen, G. Haraldsson, and B. Johansson. "Supercharging HCCI to Extend the Operating Range in a Multi-Cylinder VCR HCCI Engine". *SAE Paper No. 2003-01-3214*, 2003.

[58] J.O. Olsson, P. Tunestål, and B. Johansson. "Boosting for High Load HCCI". SAE Paper No. 2004-01-0940, 2004.

[59] J.O. Olsson, P. Tunestal, G. Haraldsson, and B. Johansson. "A Turbo Charged Dual Fuel HCCI Engine". SAE Paper No. 2001-01-1896, 2001.

[60] A. Harada, N. Shimazaki, S. Sasaki, T. Miyamoto, H. Akagawa, and K. Tsujimura. "The effects of Mixture Formation on Premixed Lean Diesel Combustion". SAE Paper No. 980533, 1998.

[61] Magnus Christensen, Bengt Johansson, and Patrick Einewall. "Homogeneous charge compression ignition (HCCI) using isooctane, ethanol and natural gas. A comparison with spark-ignition operation". SAE Paper No. 972874, 1997.

[62] F. Agrell, H.E. Ångström, B. Eriksson, J. Wikander, and J. Linderyd. "Integrated Simulation and Engine Test of Closed-Loop HCCI Control by Aid of Variable Valve Timings". *SAE Paper No. 2003-01-0748*, 2003.

[63] P. Caton, A. Simon, J. C. Gerdes, and C. Edwards. "Residual Effected Homogeneous Charge Compression Ignition at Low Compression Ratio Using Exhaust Reinduction". *International Journal of Engine Research*, (4):163–177, 2003.

[64] Shiro Yamaoka, Hiromu Kakuya, Shinji Nakagawa, Toshiharu Nogi Hitachi Research Laboratory, Atsushi Shimada, and Yusuke Kihara. "A Study of Controlling the Auto-Ignition and Combustion in a Gasoline HCCI Engine". SAE Paper No. 2004-01-0942, 2004.

[65] D. Law, D. Kemp, J. Allen, G. Kirkpatrick, and T. Copland. "Controlled Combustion in an IC-Engine with a Fully Variable Valve Train". *SAE Paper No. 2000-01-0251*, 2000.

[66] M. Jennische. *"Closed-Loop Control of Start of Combustion in a Homogeneous Charge Compression Ignition Engine"*. M.Sc. Thesis, Lund Institute of Technology, 2003.

[67] T. Milovanovic, D. Blundell, R. Pearson, J. Turner, and R. Chen. "Enlarging the Operational Range of a Gasoline HCCI Engine by Controlling the Coolant Temperature". SAE Paper No. 2005-01-0157, 2005.

[68] Y. Takeda, N. Keiichi, and N. Keiichi. "Emission Characteristics of Premixed Lean Diesel Combustion with Extremely Early Staged Fuel Injection". SAE Paper No. 961163, 1996.

[69] D. I. Handford and M. D. Checkel. "Extending the Load Range of a Natural Gas HCCI Engine using Direct Injected Pilot Charge and External EGR". SAE Paper No. 2009-01-1884, 2009.

[70] K. Nakagome, N. Shimazaki, K. Niimura, and S. Kobayashi. "Combustion and Emission Characteristics of Premixed Lean Diesel Combustion Engine". SAE Paper No. 970898, 1997.

[71] M. Christensen and B. Johansson. "Homogeneous Charge Compression Ignition with Water Injection". SAE Paper No. 1999-01-0182, 1999.

[72] R. Chen, N. Milovanovic, J. Turner, and D. Blundell. "The Thermal Effect of Internal Exhaust Gas Recirculation on Controlled Auto-Ignition". *SAE Paper No. 2003-01-0751*, 2003.

[73] G. Haraldsson, P. Tunestal, B. Johansson, and J. Hyvönen. "HCCI Combustion Phasing with Closed-Loop Combustion Control Using Variable Compression Ratio in a Multi-Cylinder Engine". *SAE Paper No. 2003-01-1830*, 2003.

[74] D. Yap, A. Megaritis, S. Peucheret, M.L. Wyszynski, and Hongming Xu. "Effect of Hydrogen Addition on Natural Gas HCCI Combustion". SAE Paper No. 2004-01-1972, 2004.

[75] H. Hu, T. Wilson, S. Richardson, M.L. Wyszynski, T. Megaritis, D. Yap, S. Golunski, and D. James. "Extension of the Boundary of HCCI Combustion Using Fuel Reforming Technology". SAE Paper No. 2004-08-0286, 2004.

[76] V. Hosseini, W. S. Neill, and M. D. Checkel. "Controlling n-Heptane HCCI Combustion with Partial Reforming: Experimental Results and Modeling Analysis". *Journal of Engineering for Gas Turbines and Power Transactions*, 131, 2009.

[77] M. Furutani, Y. Ohta, M. Kovo, and M. Hasegawa. "An Ultra-Lean Premixed Compression Ignition Engine Concept and its Characteristics". Procedding of the fourth International Symposium COMODIA 98, 1998.

[78] H. Akagawa, T. Miyamoto, A. Harada, S. Sasaki, N. Shimazaki, T. Hashizume, and K. Tsujimura. "Approaches to Solve Problems of the Premixed Lean Diesel Combustion". SAE Paper No. 1999-01-0183, 1999.

[79] P. Tunestal, J.O. Olsson, and B. Johansson. "Closed Loop Control of HCCI Engines". In Rolf Johansson and Anders Rantzer, editors, *"Nonlinear and Hybrid Systems in Automotive Control"*. Springer-Verlag, Lund, 2002.

[80] G. T. Kalghatgi. Fuel Effects in CAI Gasoline Engines. *HCCI and CAI engines for the automotive industry*. Woodhead Publishing Limited, 2007.

[81] T. Urushihara, K. Yamaguchi, K. Yoshizawa, and T. Itoh. A Study of a Gasoline-fueled Compression Ignition Engine Expansion of HCCI Operation Range Using SI Combustion as a Trigger of Compression Ignition. *SAE Paper No. 2005-01-0180.*, 2005.

[82] R.M. Wagner, J.A. Drallmeier, and C.S. Daw. Prior-Cycle Effects in Lean Spark Ignition Combustion - Fuel/Air Charge Considerations. *SAE Special Publications*, 981047:69–79, 1998.

[83] R.M. Wagner, K.D. Edwards, C.S. Daw, J.B. J.R. Green, and B.G. Bunting. On the Nature of Cyclic Dispersion in Spark Assisted HCCI Combustion. *SAE Paper No. 2006-01-0418.*, 2006.

[84] J. Bengtsson, P. Strandhv, R. Johansson, P. Tunestal, and B. Johansson. Model Predictive Control of Homogeneous Charge Compression Ignition (HCCI) Engine Dynamics. *Proceedings of the 2006 IEEE International Conference on Control Applications*, 2006.

[85] N.J. Killingsworth, S.M. Aceves, D.L. Flowers, and M. Krstic. A simple HCCI engine model for control. *Proceeding of the 2006 IEEE Conference*, 2006.

[86] K. Swan, M. Shahbakhti, and C.R. Koch. Predicting start of combustion using a modified knock integral method for an HCCI engine. *SAE Paper No. 2006-01-1086*, 2006.

[87] C.G.W. Sheppard, S. Tolegano, and R. Woolley. On the nature of autoignition leading to knock in HCCI engines. *SAE Paper No. 2002-01-2831*, 2002.

[88] Matthew Atkins. Experimental examination of the effects of fuel octane and diluent on HCCI combustion. Master's thesis, University of Alberta, 2004.

[89] M. Weinrotter. Optical diagnostics of laser-induced and spark plug-assisted HCCI combustion. *SAE Paper No. 2005-01-0129*, 2005.

[90] T. Urushihara, K. Yamaguchi, K. Yoshizawa, and T. Itoh. A study of gasoline-fueled compression ignition engine expansion of HCCI operation range using SI combustion as a trigger of compression ignition. *SAE Paper No. 2005-01-0180*, 2005.

[91] J. Hyvonen and B. Johansson. Operating conditions using spark assisted HCCI combustion during combustion mode transfer to SI in a multi-cylinder VCR-HCCI engine. *SAE Paper No. 2005-01-0109.*, 2005.

[92] J. Bengtsson. *Closed-loop control of HCCI engine dynamics*. PhD thesis, Lund Institute of Technology,, 2004.

[93] J.O. Olsson and P. Tunestal and B. Johansson. Closed-Loop Control of an HCCI Engine. *SAE Paper No. 2001-01-1031*, 2001.

[94] J.O. Olsson, P. Tunestal, and J. Ulfvik. The effect of cooled EGR on emissions and performance of a turbocharged HCCI engine. *SAE Paper No. 2003-01-0743*, 2003.

[95] M. Christensen, A. Hultqvist, and B. Johansson. Demonstrating the multi fuel capability of a homogeneous charge compression ignition engine with variable compression ratio. *SAE Paper No. 1999-01-3679*, 1999.

[96] N. Milovanovic and R. Chen. A review of experimental and simulation studies on controlled auto-ignition combustion. *SAE Paper No. 2001-01-1890*, 2001.

[97] N.B. Kaahaaina, A.J. Simon, P.A. Caton, and C.F. Edwards. Use of dynamic valving to achieve residual-affecting combustion. *SAE Paper No. 2001-01-0549*, 2001.

[98] F. Agrell, H.E. Angstrom, B. Eriksson, and J. Wikander. Transient control of HCCI through combined intake and exhaust valve actuation. *AE Paper No. 2003-01-3172*, 2003.

[99] W.R. Thomas and A.C. Matheaus. Fuel requirements for HCCI engine operation. *SAE Paper No. 2003-01-1813*, 2003.

[100] D.J. Rausen, A.G. Stefanopoulou, J-M. Kang, J.A. Eng, and W. Kuo. A mean-value model for control of homogeneous charge compression ignition (HCCI) engines. *American Control Conference*, pages 125–131, 2004.

[101] J. Bengtsson, M. Gafvert, and P. Strandh. Modeling of HCCI engine combustion for control analysis. *IEEE conference on decision and control*, page 1682, 2004.

[102] N.P. Komninos, D.T. Hountalas, and D.A. Kouremenos. Description of in-cylinder combustion processes in HCCI engines using a multi-zone model. *SAE Paper No. 2005-01-0171*, 2005.

[103] D.L. Flowers, S.M. Aceves, J. Martinez-Frias, and R.W. Dibble. Prediction of carbon monoxide and hydrocarbon emissions in iso-octane HCCI engine combustion using multizone simulations. *Proceedings of the Combustion Institute*, pages 687–694, 2002.

[104] S.C. Kong and R.D. Reitz. Numerical Study of Premixed HCCI Engine Combustion and its Sensitivity to Computational Mesh and Model Uncertainties. *Combustion Theory and Modeling*, pages 417–433, 2003.

[105] M. Embouazza, D.C. Haworth, and N. Darabiha. Implementation of detailed chemical mechanisms into multidimensional CFD using in situ adaptive tabulation: Application to HCCI engines. *SAE Paper No. 2002-01-2773*, 2002.

[106] M.R. Belmont, M.S. Hancock, and D.J. Buckingham. Statistical aspects of cyclic variability. *SAE Paper No. 860324*, 1986.

[107] J.W. Daily. Cycle-to-cycle variations: a chaotic process. *Combustion Science and Technology*, 57:149–162, 1988.

[108] Y. Moriyoshi, T. Kanimoto, and M. Yagita. Prediction of cycle-to-cycle variation of in-cylinder flow in a motored engine. *SAE Paper No. 930066*, 1993.

[109] C.S. Daw, C.E.A. Finney, and J.B. Green. A Simple Model for Cyclic Variations in a Spark-Ignition Engine. *SAE Paper No. 962086*, 1996.

[110] D.D. Brehob and C.E. Newman. Monte carlo simulation of cycle-by-cycle variability. *SAE Paper No. 922165*, 1992.

[111] M. Shahbakhti and R. Lupul and C. R. Koch. Cyclic Variations of Ignition Timing in an HCCI Engine. *Proceedings of the 2007 ASME Internal Combustion Engine Division Spring Technical Conference (Peublo, Colorado USA):*, 2007.

[112] R.M. Wagner, J.A. Drallmeier, and C.S. Daw. Origins of cyclic dispersion patterns in spark ignition engines. *Proceedings of the 1998 Technical Meet-*

ing of the Central States Section of the Combustion Institute, Lexington, Kentucky USA:213–218., 1998.

[113] C.S. Daw, J.B. J.r. Green, R.M. Wagner, C.E.A. Finney, L.I. Davis, L.A. Feldkamp, J.W. Hoard, F. Yuan, and F.T. Connolly. Controlling cyclic combustion variations in lean-fueled spark-ignition engines. *AIP Conference Proceedings*, pages 265 – 77, 2002.

[114] M. Shahbakhti and C. R. Koch. "Characterizing the Cyclic Variability of Ignition Timing in an HCCI Engine Fueled with n-Heptane/iso-Octane Blend Fuels". *International Journal of Engine Research*, 9:361–397, 2008.

[115] A. Ghazimirsaied, M. Shahbakhti, A. Audet, and C.R. Koch. HCCI engine cyclic variation characterization using both chaotic and statistical approach. *Proceeding of Combustion Institue-Canadian Section, Spring Technical Meeting, University of Toronto, Ontario*, 2008.

[116] C.S. Daw, C.E.A. Finney, M.B. Kennel, and F.T. Connolly. Cycle-by-cycle combustion variations in spark-ignited engines. *Proceeding of the Fourth Experimental Chaos Conference*, Boca Raton, Florida, 1997.

[117] R.M. Wagner, C.S. Daw, and J.B. J.r. Green. Low-order map approximations of lean cyclic dispersion in premixed spark ignition engines. *SAE Paper No. 2001-01-3559.*, 2001.

[118] L. Chew, R.L. Hoekstra, and J.F. Nayfeh. Chaos analysis on in-cylinder pressure measurements. *SAE Paper No. 942486.*, 1994.

[119] M. Shahbakhti and R. Lupul and A. Audet and C. R. Koch. Experimental Study of HCCI Cyclic Variations for Low-Octane PRF Fuel Blends. *Proceeding of Combustion Institute/Canadian Section (CI/CS) Spring Technical Conference*, Banff, Canada, 2007.

[120] C.S. Daw and C.E.A. Finney and M.B. Kennel. A Symbolic Approach for Measuring Temporal Irreversibility. *Physical Review E*, 62(2):1912–1921., 2000.

[121] J.B. Green, C.S. Daw, J.S. Armfield, and C.E.A. Finney. Time Irreversibility and Comparison of Cyclic-Variability Models. *SAE Paper No. 1999-01-0221.*, 1999.

[122] C.S. Daw, C.E.A. Finney, and E.R. Tracy. A review of symbolic analysis of experimental data. *Review of Scientific Instruments*, 74:916–930, 2003.

[123] B.G. Peter. Estimating and improving the signal-to-noise ratio of time series by symbolic dynamics. *Phys Rev E*, 64:051104, 2001.

[124] C.S. Daw, M.B. Kennel, C.E.A. Finney, and F.T. Connolly. Observing and modeling nonlinear dynamics in an internal combustion engine. *Phys. Rev. E*, 57:2811–2819, 1998.

[125] C.S. Daw and J.B. Green and R.M. Wagner and C.E.A Finney and F.T. Connolly. Synchronization of Combustion Variations in a Multi-Cylinder Spark Ignition Engine. *Proceedings of the 2000 Spring Technical Meeting of the Central States Section of the Combustion Institute:*, Edinburgh, Scotland:181–186, 2000.

[126] J.B. Green, C.S. Daw, J.S. Armfield, C.E.A. Finney, and P. Durbetaki. Time irreversibility of cycle-by-cycle engine combustion variations. *Proceedings of the 1998 Technical Meeting of the Central States Section of the Combustion Institute*, Lexington, Kentucky USA, 1998.

[127] C.S. Daw, R.M. Wagner, K.D. Edwards, and J.B. Green. Understanding the transition between conventional spark-ignited combustion and HCCI in a

gasoline engine. *31st International Symposium on Combustion (Heidelberg, Germany; August 2006)*, 2006.

[128] X. Lu, W. Chen, Y. Hou, and Z. Huang. "Study on the Ignition, Combustion and Emissions of HCCI Combustion Engines Fueled with Primary Reference Fuels". *SAE Paper No. 2005-01-0155*, 2005.

[129] M. Yao, Z. Zheng, B. Zhang, and Z. Chen. "The Effect of PRF Fuel Octane Number on HCCI Operation". *SAE Paper No. 2004-01-2992*, 2004.

[130] Z. Serinyel, L. Le Moyne, and P. Guibert. "Homogeneous Charge Compression Ignition as an Alternative Combustion Mode for the Future of Internal Combustion Engines". *International Journal of Vehicle Design*, 44(1-2):20 – 40, 2007.

[131] B. Johansson. "Homogeneous Charge Compression Ignition: The Future of IC Engines?". *International Journal of Vehicle Design*, 44(1-2):1 – 19, 2007.

[132] A. Ghazimirsaied, M. Shahbakhti, and C.R. Koch. Comparison of Crankangle Based Ignititon Timing Methods on an HCCI Engine. *Proceeding of the ASME Internal Combustion Engine Division 2010 Fall Conference, San Antonio, USA.*, 2010.

[133] A. Ghazimirsaied and M. Shahbakhti and C. R. Koch. Recognizing Partial Burn Operation in an HCCI Engine. *Proceeding of Combustion Institue - Canadian Section Spring Technical Conference, Carleton University, Ontario*, May 9-12, 2010.

[134] A. Ghazimirsaied, M. Shahbakhti, and C. R. Koch. Ignition Timing Criteria for Partial Burn Operation in an HCCI Engine. *Proceeding of Combustion*

Institue - Canadian Section Spring Technical Meeting, University of Manitoba, Winnipeg, May 8-11, 2011.

[135] A. Ghazimirsaied, M. Shahbakhti, and C.R. Koch. Nonlinear Dynamics in Cyclic Variations of Combustion Phasing in an HCCI Engine. *Proceedings of the ASME Internal Combustion Engine Division 2009 Spring Conference, Milwaukee, Wisconsin, USA*, 2009.

[136] A. Ghazimirsaied, M. Shahbakhti, and C.R. Koch. HCCI Engine Combustion Phasing Prediction Using a Symbolic-Statistics Approach. *Journal of Engineering for Gas Turbines and Power*, 132:082805 1–5, 2010.

[137] A. Ghazimirsaied and C.R. Koch. Controlling Cyclic Combustion Timing Variations Using a Symbol-Statistics Predictive Approach in an HCCI Engine. *Journal of Applied Energy*, 92:133–146, 2012.

[138] R. J. Moffat. Describing the Uncertainties in Experimental Results. *Experimental Thermal and Fluid Science*, 1:3–17, 1988.

[139] Z. Serinyel and L. Le Moyne and P. Guibert. Homogeneous Charge Compression Ignition as an Alternative Combustion Mode for the Future of Internal Combustion Engines. *International Journal of Vehicle Design*, 44:20–40, 2007.

[140] S. Tanaka and F. Ayala and J. C. Keck and J. B. Heywood. Two-stage Ignition in HCCI Combustion and HCCI Control by Fuels and Additives. *Journal of Combustion and Flame*, 132:219–239, 2003.

[141] X. Lu and W. Chen and Y. Huo and Z. Huang. Study on the Ignition, Combustion and Emissions of HCCI Combustion Engines Fueled with Primary Reference Fuels. *SAE Paper No. 2005-01-0155.*, 2005.

[142] M. D. Checkel and D. J. Dale. Computerized Knock Detection From Engine Pressure Records. *SAE Paper No. 860028.*, 1986.

[143] J.B. Heywood. *Internal Combustion Engine Fundamentals.* McGraw Hill, 1988.

[144] G. M. Rassweiler and L. Withrow. Motion Pictures of Engine Flames Correlated with Pressure Cards. *SAE Transactions*, 42:185–204, 1938.

[145] S. Matsuoka and T. Yamaguchi and Y. Umemur. Factors Influencing the Cyclic Variation of Combustion of Spark Ignition Engine. *SAE Paper No. 710586*, 1971.

[146] M.A. Ceviz and F. Yuksel. Cyclic Variations on LPG and Gasoline-Fuelled Lean Burn SI Engine. *Renewable Energy*, 32:2006, 1950-60.

[147] G.T. Kalaghatgi and R.A. Head. Combustion Limits and Efficiency in a Homogeneous Charge Compression Ignition Engines. *International Journal of Engine Research*, 7:215–236, 2006.

[148] M. Sjoberg, J.E. Dec, A. Babajimopoulos, and D. Assanis. Comparing enhanced natural thermal stratification against retarded combustion phasing for smoothing of HCCI heat-release rates. *SAE Paper No. 2004-01-2994.*, 2004.

[149] L. Xingcai and J. Libin and M. Junjun and H. Zhen. Experimental Study on the Cycle-by-Cycle Variations of Homogeneous Charge Compression Ignition Combustion using Primary Reference Fuels and their Mixtures. *Proceeding of IMechE - Part D*, 221:859–866, 2007.

[150] C. S. Daw and K. D. Edwards and R. M. Wagner and J. B. Green. Modeling Cyclic Variability in Spark-Assisted HCCI. *Journal of Engineering for Gas Turbines and Power*, 130:052801, 2008.

[151] C. Liu and G. A. Karim and A. Sohrabi and F. Xiao. Combustion and Cyclic Variation for Lean Mixture Operation. *ASME Internal Combustion Engine Spring Technical Conference*, 2006.

[152] M. Sjoberg and J. E. Dec. Comparing late-cycle autoignition stability for single- and two-stage ignition fuels in HCCI engines. *Proceeding of Combustion Institue*, 31:2895–2902, 2007.

[153] NIST/SEMATECH e-Handbook of Statistical Methods http://www.itl.nist.gov/div898/handbook/, Jan. 20, 2008.

[154] H. Lilliefors. On the Kolmogorov-Smirnov Test for Normality with Mean and Variance Unknown. *Journal of the American Statistical Association*, 62:399–402, 1967.

[155] A. N. Kolmogorov. On the Empirical Determination of a Distribution Function. *(Italian) Giornale dell'Instituto Italiano degli Attuari*, 4:83–91, 1933.

[156] N. V. Smirnov. On the Estimation of the Discrepancy Between Empirical Curves of Distribution for Two Independent Samples. *(Russian) Bulletin of Moscow University*, 2:3–16, 1939.

[157] F. Ponti. Developmnet of a Torsional Behavior Powertrain Model for Multiple Misfire Detection. *Journal of Engineering for Gas Turbines and Power*, 130, 2008.

[158] Z. Wu and A. Lee. Misfire detection using a dynamic neural network with output feedback. *SAE Paper No. 980515.*, 1998.

[159] D. Moro and P. Azzoni and G. Minelly. Misfire Pattern Recognition in High-Performance SI 12-Cylinder Engine. *SAE Paper No. 980521.*, 1998.

[160] M. Sjberg, J. E. Dec, and N. P. Cernansky. Potential of thermal stratification and combustion retard for reducing pressure-rise rates in HCCI engines, based on multi-zone modelling and experiments. *SAE Paper No. 2005-01-0113.*, 2005.

[161] J. E. Dec, W. Hwang, and M. Sjberg. An investigation of thermal stratification in HCCI engines using chemiluminescence imaging. *SAE Paper No. 2006-01-1518.*, 2006.

[162] J-O Olsson, P. Tunestal, B. Johansson, S. Fiveland, J.R. Agama, and D.N. Assanis. Compression Ratio Influence on Maximum Load of a Natural Gas-Fueled HCCI Engine. *SAE Paper No. 2002-01-0111.*, 2002.

[163] J-O. Olsson, O. Erlandsson, and B. Johansson. Experiments and simulation of a six-cylinder HCCI engine. *SAE Paper No. 2000-01-2867.*, 2000.

[164] T. Urushihara, K. Hiraya, A. Kakuhou, and T. Itoh. Parametric Study of Gasoline HCCI with Various Compression Ratios, Intake Pressures and Temperatures. *Proceeding of A New Generation of Engine Combustion Processes for the Future, Paris.*, 2001.

[165] K. Yoshizawa, A. Teraji, H. Miyakubo, K. Yamaguchi, and T. Urushihara. Study of High Load Operation Limit Expansion for Gasoline Compression Ignition Engines. *Journal of Engineering for Gas Turbines and Power*, 2006.

[166] M. J. Atkins and C. R. Koch. The effect of fuel octane and diluent on HCCI combustion. *Proc. IMechE Part D: Journal of Automobile Engineering*, 219:665 – 675, 2005.

[167] D. Choe, M. Lee, K. Lee, and M. Sunwoo. SOC detection of controlled auto-ignition engine. *SAE Paper No. 2007-01-3538*, 2007.

[168] C. J. Chiang and A. G. Stefanopoulou. Sensitivity analysis of combustion timing and duration of HCCI engines. *Proceeding of the 2006 American Control Conference, Minneapolis, USA*, 2006.

[169] W. F. Northrop, S. V. Bohac, and D. N. Assanis. Premixed low temperature combustion of biodiesel and blends in high speed compression ignition engine. *SAE Paper No. 2009-01-0133*, 2009.

[170] K. L. Knierim and S. Park and J. Ahmed and A. Kojic. Simulation of Misfire and Strategies for Misfire Recovery of Gasoline HCCI. *American Control Conference, Seattle, WA*, 2008.

[171] I. Haskara and L. Mianzo. Real-time Cylinder Pressureand Indicated Torque Estimation via Second Order Sliding Modes. *Proceedings of the American Control Conference, Arlington, VA*, 2001.

[172] E.A. VanDyne, C.L. Burckmyer, A.M. Wahl, and A.E. Funaioli. Misfire Detection From Ionization Feedback Utilizing the Smartfire Plasma Ignition Technology. *SAE Paper No. 2000-01-1377.*, 2000.

[173] F.L. Bue, A.D. Stefano, C. Giaconia, and E. Pipitone. Misfire Detection System based on the Measure of Crankshaft Angular Velocity. *Proceeding of the 11th annual AMAA conference, Berlin*, 2007.

[174] P. Azzoni and D. Moro and C.M. Porceddu-Cilione and G. Rizzoni. Misfire Detection in a High-Performance Engine by the Principal Component Analysis Approach. *SAE Paper No. 960622.*, 1996.

[175] W. Ribbens and J. Park. Road Tests of a Misfire Detection System. *SAE Paper No. 940975.*, 1994.

[176] J. Williams. An Overview of Misfiring Cylinder Engine Diagnostic Techniques Based on Crankshaft Angular Velocity Measurements. *SAE Paper No. 960039.*, 1996.

[177] A. Alkhateeb. *Robust Algorithms for Engine Misfire Detection.* PhD thesis, Oakland University, 2004.

[178] A. Oakley and H. Zhao and N. Ladommatos. Experimental Studies on Controlled Auto-ignition (CAI) Combustion of Gsoline in a 4-Stroke Engine. *SAE Paper No. 2001-01-1030.*, 2001.

[179] Z. Peng and H. Zhao and N. Ladommatos. Effects of Air/Fuel Ratios and EGR Rates on HCCI Combustion of n-heptane, a Diesel Type Fuel. *SAE Paper No. 2003-01-0747.*, 2003.

[180] J. Bengtsson, P. Strandh, R. Johansson, P. Tunestal, and B. Johansson. Closed-loop combustion control of HCCI engine dynamics. *International Journal of Adaptive Control and Signal Processing*, 18:167–179, 2004.

[181] M. Selik, R. Baraniuk, and M. Haag. Signal classifications and properties. Technical report, Work produced by The Connexions Project and licensed under the Creative Commons Attribution License, 2007.

[182] R. M. Wagner, C. S. Daw, and J. B. Green. Characterizing lean spark ignition combustion instability in terms of a low-order map. *Proceedings of the 2nd Joint Meeting of the U.S. Sections of the Combustion Institute*, Oakland, California USA, 2001.

[183] X.Z. Tang, E.R. Tracy, A.D. Boozer, A. Debrauw, and R. Brown. Symbol sequence statistics in noisy chaotic signal reconstruction. *Phys. Rev. E*, 51:3871–3889., 1995.

[184] C.E.A. Finney, J.B. J.R. Green, and C.S. Daw. Symbolic time-series analysis of engine combustion measurements. *SAE Special Publications*, 1330:1–10, 1998.

[185] X.Z. Tang, E.R. Tracy, and R. Brown. Symbol statistics and spatio-temporal systems. *Physica D*, 102, 1997.

[186] U. Asad and M. Zheng. Fast Heat Release Characterization of a Diesel Engine. *International Journal of Thermal Sciences*, 47:1688–1700, 2008.

[187] F.A. Matekunas. Modes and Measures of Cyclic Combustion Variability. *SAE Paper No. 830337.*, 92, 1983.

[188] M. Shahbakhti and A. Ghazimirsaied and C.R. Koch. Experimental Study of the Variation in a Exhaust Temperature in a HCCI Engine. *Proc. IMechE Part D: Journal of Automobile Engineering*, 224, 2010.

[189] M. Weinrotter, E. Wintner, K. Iskra, and T. Neger. Optical Diagnostics of Laser-Induced and Spark Plug-Assisted HCCI Combustion. *SAE Paper No. 2005-01-0129.*, 2005.

[190] E. Galloni. Analyses about Parameters that affect Cyclic Variation in a Spark Ignition Engine. *Applied Thermal Engineering*, 29:1131–1137, 2009.

[191] A. K. Sen and R. Longwic and G. Litak and K. Gorski. Analysis of Cycle-to-cycle Pressure Oscillations in a Diesel Engine. *Mechanical Systems and Signal Processing*, 22:362–373, 2008.

[192] L. Guo-xiu and Y. Bao-feng. Nonlinear dynamics of cycle-to-cycle combustion variations in a lean-burn natural gas engine. *Applied Thermal Engineering*, 28:611–620, 2008.

[193] A. K. Sen and J. Zheng and Z. Huang. Dynamics of Cycle-to-cycle Variations in a Natural Gas Direct-Injection Spark-Ignition Engine. *Applied Energy*, 88:2324–2334, 2011.

[194] R. K. Maurya and A. K. Agarwal. Experimental Investigation on the effect of Intake Air Temperatureand AirFuel Ratio on Cycle-to-cycle Variations of HCCI Combustionand Performance Parameters. *Applied Energy*, 88:1153–1163, 2011.

[195] M. Wendeker and J. Czarnigowski and G. Litak and K. Szabelski. Chaotic Combustion in Spark Ignition Engines. *Chaos, Solitons and Fractals*, 18:803–806, 2003.

[196] C. Diks, J.C. Van Houwelingen, F. Takens, and J. Degoede. Reversibility as a criterion for discriminating time series. *Physics Letters A*, 201:221–228, 1995.

[197] Mahdi Shahbakhti and Charles Robert Koch. Characterizing the Cyclic Variability of Ignition Timing in a HCCI Engine Fueled with N-heptane/Iso-octane Blend Fuels. *International Journal of Engine Research*, 9:361 – 397, 2008.

Appendix A

Partial Burn Crank Angle Limit Criteria Comparison on an Experimental HCCI Engine

Here, misfire and partial-burn criteria are defined using crank angle based engine parameters (such as CA1 (Crank angle at which 1 percent of fuel mass has burned), CA10, CA50 and burn duration) and investigated on an experimental HCCI single-cylinder engine at 59 operating conditions. The partial burn limit for five different blends of isooctane and n-heptane fuels is presented. The effect of different manifold pressures on the partial burn limit are investigated. Increasing the manifold pressure at each specific fuel octane number results in a lower equivalence ratio partial burn limit for the engine operating points tested. The primary aim of this section is to provide detailed investigation of the crank angle based parameters fluctuations for data points in three different regions of normal, partial burn and misfire in order to choose the proper parameters to be used as a feedback signal in future HCCI closed loop control.

The experimental engine setup is explained in 2.1 in which the engine fitted with a Mercedes E550 cylinder head are used for data collection. The tests operating conditions are listed in Table 2.5. 59 points are analyzed of which 30 are found at partial burn region, 11 at misfire and 18 at normal operating conditions region.

A.1 Determination of Partial Burn Limit Criteria

The tests operating conditions are listed in Table 2.5 which have been collected using the experimental setup fitted with a Mercedes E550 cylinder head described in section 2.1. A cycle is defined to be a partial burn cycle if its total heat release is reduced by 10% or more compared to the previous cycle [152]. An experimental operating point is considered a partial burn point if more than 15% of the cycles are partial burn cycles. Operating points with more than 30% partial burn cycles are considered to be misfire points. The process to identify partial or misfire operating points is shown in Figure A.1.

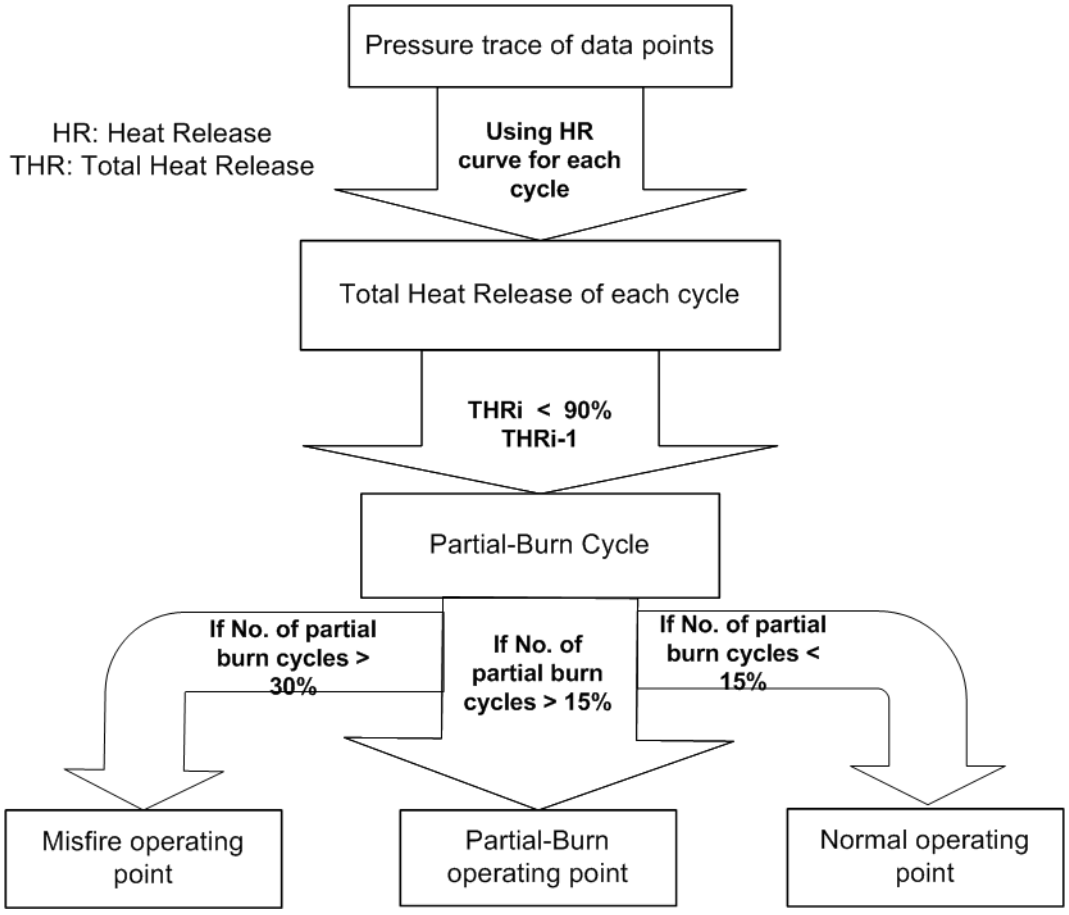

Figure A.1: Flowchart: Procedure to determine the status of HCCI operating condition

All operating points are partial burn, misfire or normal with none of the oper-

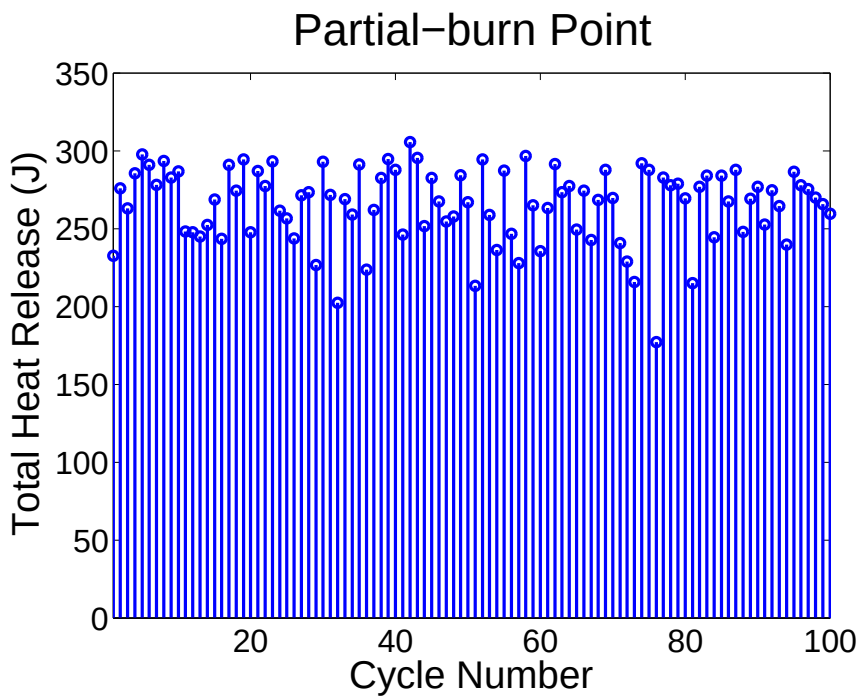

Figure A.2: Partialburn Conditions: speed 1024 rpm, T_{man} 87 °C, P_{man} 105 kPa, ON 0, λ 2.87, T 14.88 Nm

ating points used in this paper near the knock limit. Using the above criteria, 59 HCCI engine operating points are analyzed to categorize them into the different combustion regions: 30 are found to be partial burn, 11 misfire and 18 points are normal combustion.

Consecutive cycle total heat release for a partial burn and misfire operating point are shown in Figure A.2 and Figure A.3 for two operating points. The number of cycles with more than 10 percent reduction in total heat release compared to the previous cycle are 21 and 38 percent for Figure A.2 and Figure A.3 respectively. In the misfire case, Figure A.3, the number of cycles with reduction in total heat release is substantially higher compared to the partial burn point case of Figure A.2, causing a torque reduction.

The partial burn and misfire criteria is used to test data on all 59 operating points to classify their operating region. Figure A.4 compares the limits of partial

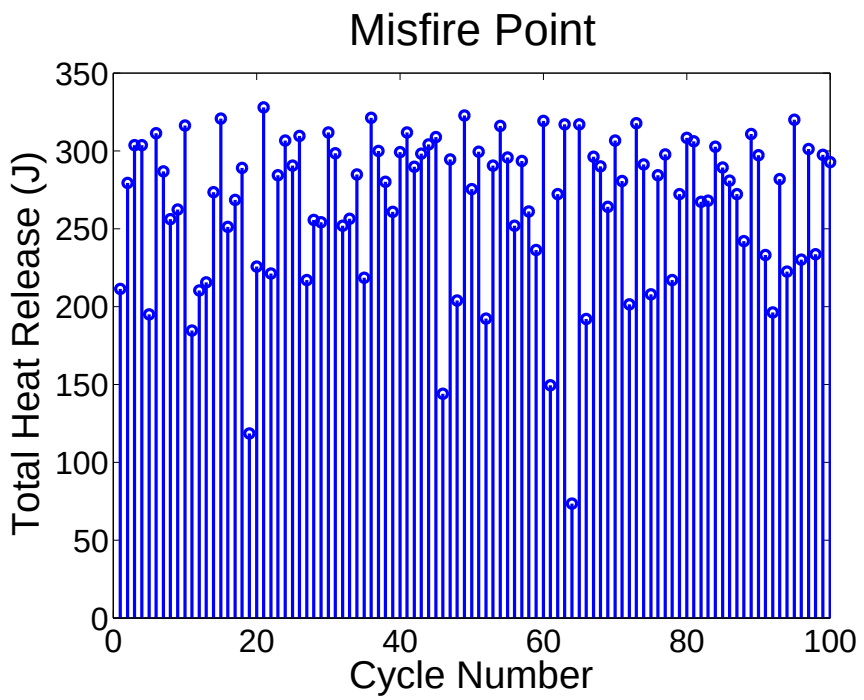

Figure A.3: Misfire Conditions: speed 1024 rpm, T_{man} 95 °C, P_{man} 115 kPa, ON 20, λ 2.90, T 8.68 Nm

burn operating conditions for five various blends of primary reference fuels. The manifold pressure ranges from 90 and 120 kPa and is plotted on the x-axis and λ (ratio of actual air to fuel ratio to stoichiometric air to fuel ratio) on the y-axis. For this engine, HCCI partial burn for each of the five octane numbers occurs in Figure A.4 above the respective lines in the unstable operating condition of engine. Partial burn boundary occurs because increasing the manifold pressure leads to higher gas pressure in the compression stroke directly effecting the time scales of the reactions leading to earlier autoignition [119] and cycle-to-cycle variation of the phasing of ignition increases with combustion-phasing retard for an HCCI engine [152]. Increasing manifold pressure extends the partial burn limit for leaner mixtures autoigniton inside the cylinder as seen in Figure A.4. Increasing the fuel octane number (higher amount of iso-octane in the mixture of iso-octane and n-heptane fuel) reduce the partial burn limit (Figure A.4) due

to the autoignition properties of the fuel [143]. This restricts the higher octane number fuels for HCCI operation for this engine. Stable operation with octane numbers 30 and 40 is not maintained at intake manifold pressures of 90 and 95 kPa.

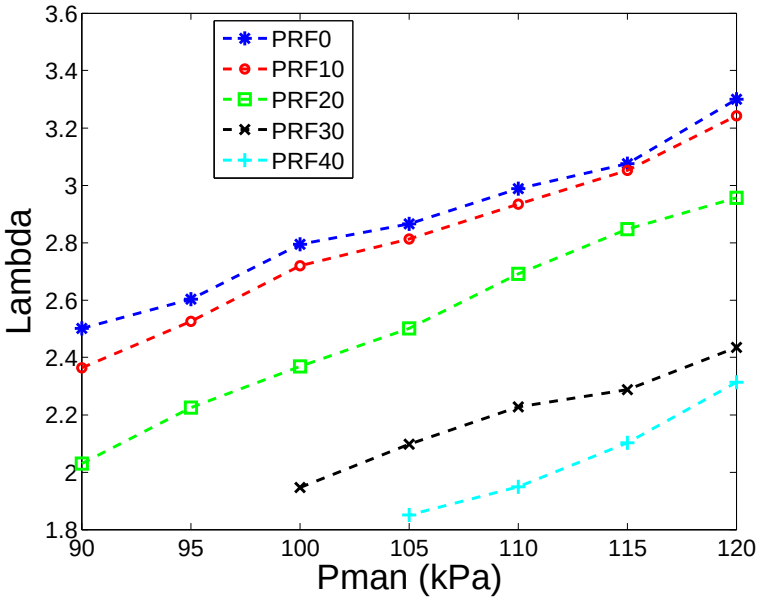

Figure A.4: HCCI partial burn boundaries as a function of λ and P_{man} for PRF0, 10, 20, 30 and 40

A.2 Misfire limit for different fuels

To recognize the misfire limit using a single parameter, several techniques using IMEP (Indicated Mean Effective Pressure) have been used [22, 152, 2]. In [152] a standard deviation of IMEP more than 2% is deemed unacceptable as this corresponds to the appearance of partial burn and misfire cycles. The coefficient of variation, is used to measure cyclic variability of engine parameters [197]. *COVImep* (Coefficient of variation of IMEP) for determining cyclic variation of IMEP have been calculated for all the operating points used in this study and categorized using previously defined normal, partial burn or misfire operation. The results are shown in Figure A.5 and

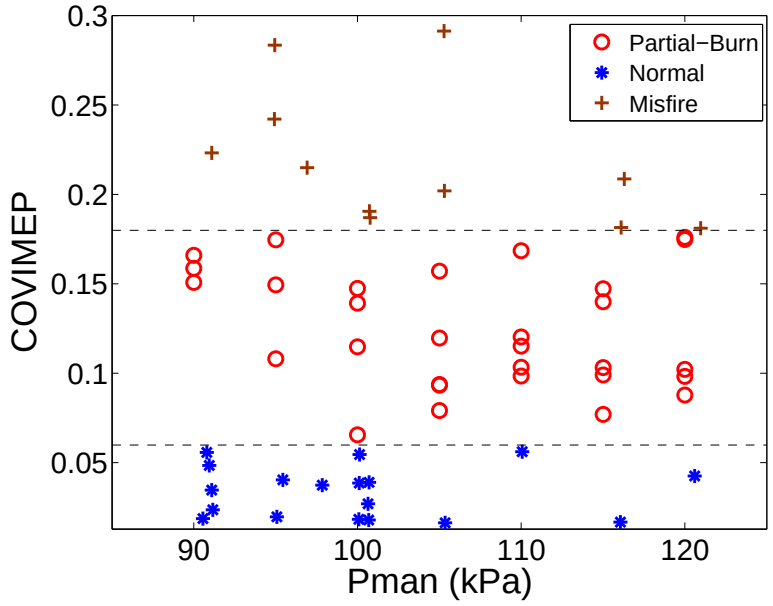

Figure A.5: Trends of change in cyclic variation of Indicated Mean Effective Pressure (IMEP) with manifold pressure

COVImep clearly distinguishes three different operating regions for the collected data points. The operating points with $0.06 < CovImep < 0.18$ are partial burn region while operating points with $CovImep > 0.18$ are the misfire region of this engine.

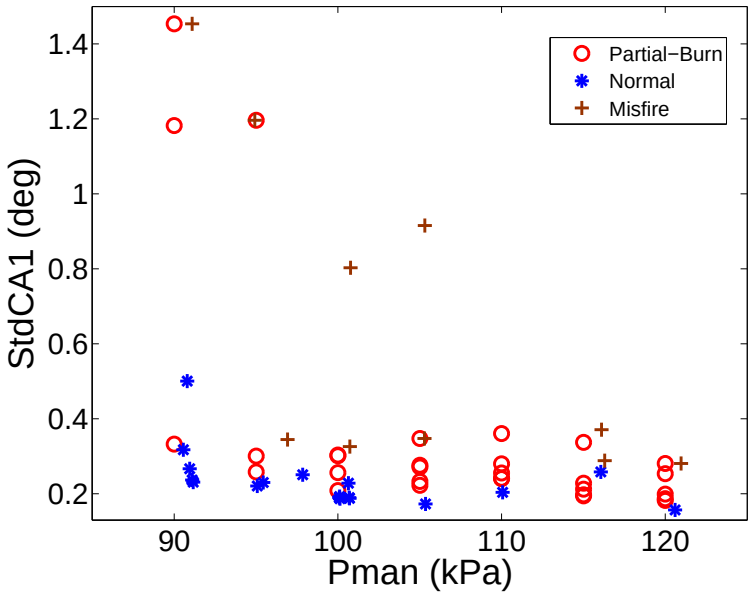

Figure A.6: Trends of change in cyclic variation of CA1 with manifold pressure

To determine the best parameter and to identify misfire conditions using an alternative to *COVImep* the crank-angle based parameters of CA1, CA10, CA50 and Burn Duration (BD) (Crank angle difference between CA10 and CA90) for all 59 operating points are shown in Figures A.6 to A.9. In Figures A.6 and A.8, no clear boundaries between the three regions of HCCI operating conditions are evident in variations of CA1 and CA50. In contrast, in Figures A.7 and A.9 three zones of normal, partial burn and misfire operations are clearly visible except that a few partial burn data points are fairly close to the boundary between normal and partial burn. In Figure A.7 all the data points with borders $1.3 < StdCA10 < 7.8$ fall in the partial burn region while the ones with $StdCA10 > 7.8$ in the misfire region. Figure A.9 shows clear boundaries between the three different operating conditions of HCCI with the data points with $3.8 < StdBD < 9$ in the partial burn zone and data points with $StdBD > 9$ in the misfire zone. In Figure A.9, StdBD has a partial burn point in the misfire region and so seems less reliable indicator compared to StdCA10 in Figure A.7.

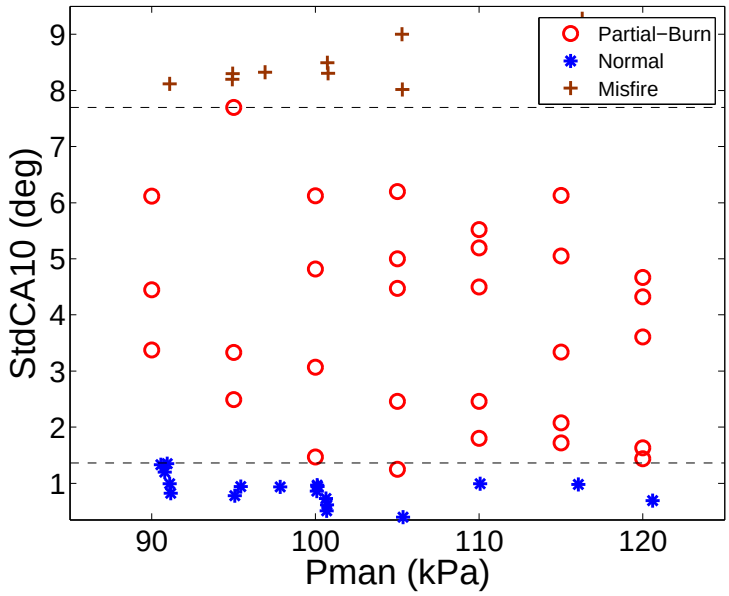

Figure A.7: Trends of change in cyclic variation of CA10 with manifold pressure

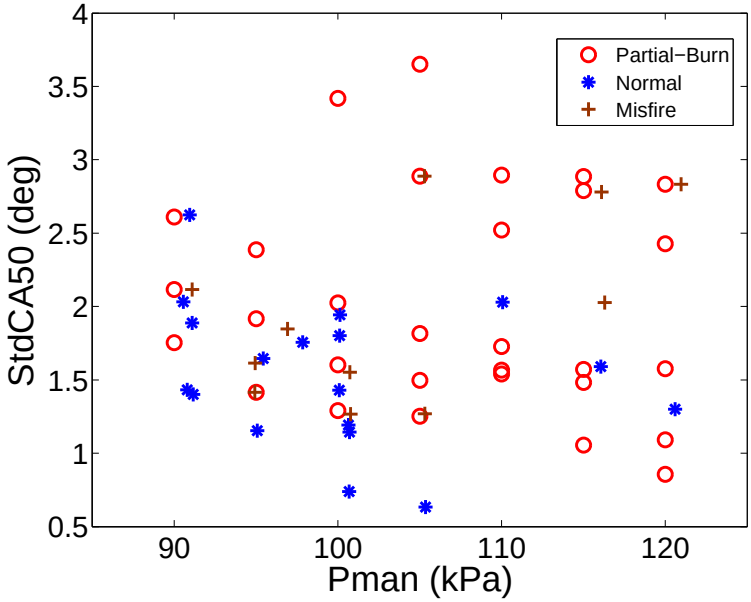

Figure A.8: Trends of change in cyclic variation of CA50 with manifold pressure

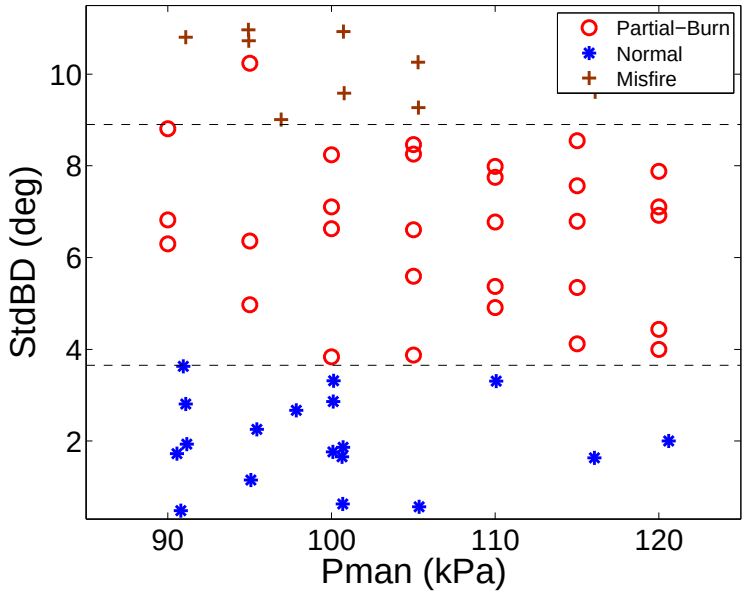

Figure A.9: Trends of change in cyclic variation of Burn Duration (BD) with manifold pressure

A.3 Summary

Experimental data from HCCI engine collected at 59 operating points is used to define a criteria for misfire limit points. The criteria for characterizing HCCI engine operation as partial burn, when 15 percent of cycles are partial burn cycles, and misfire, when more than 30 percent of the cycles are partial burn is used. Then, cyclic variation of ignition timing in an HCCI engine is investigated. Examining combustion criteria it is found that CA1 and CA50 are not effective metrics for HCCI misfire recognition. However, variations of CA10 and BD are effective measures of misfire recognition and could be used as alternatives for *COVImep* to distinguish between normal, partial burn and misfire operation of an HCCI engine.

Appendix B

Symbol Sequence Method

The principle idea of experimental data symbolization is to convert the time series values into a few possible values. Depending on the value of a given data, it is assigned to a symbolic value. The number of symbolic values is referred as the symbol-set size, which indicates the number of symbols available to symbolize the data; Figure B.1 shows a portion of time series of ignition timing for a sample point with conditions of ON 3 in Table 7.1. To illustrate the process the symbol-set size is selected as 2 and partition between symbols is located at the median of the data points. The data above the median is symbolized as 1 and the ones below the median as 0. The group of first consecutive three symbols, data points 1-3 form the symbol sequence 101, data points 2-4 form the sequence 011 and so on.

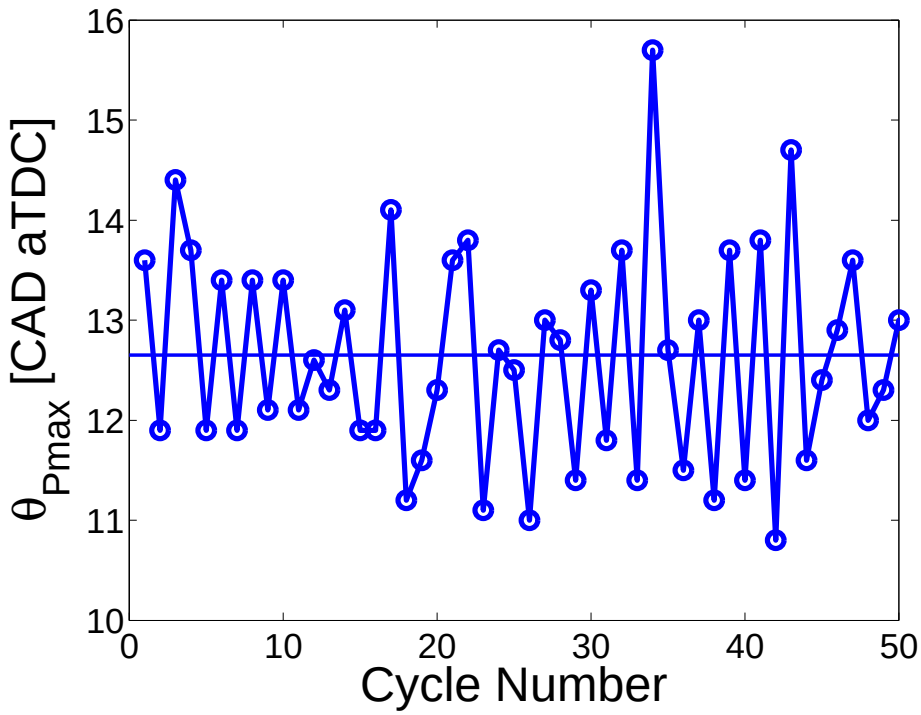

Figure B.1: Ignition timing for a sample point with conditions of ON 3 of Table 7.1.

The symbol sequence histogram of Figure B.1 is shown in Figure B.2.

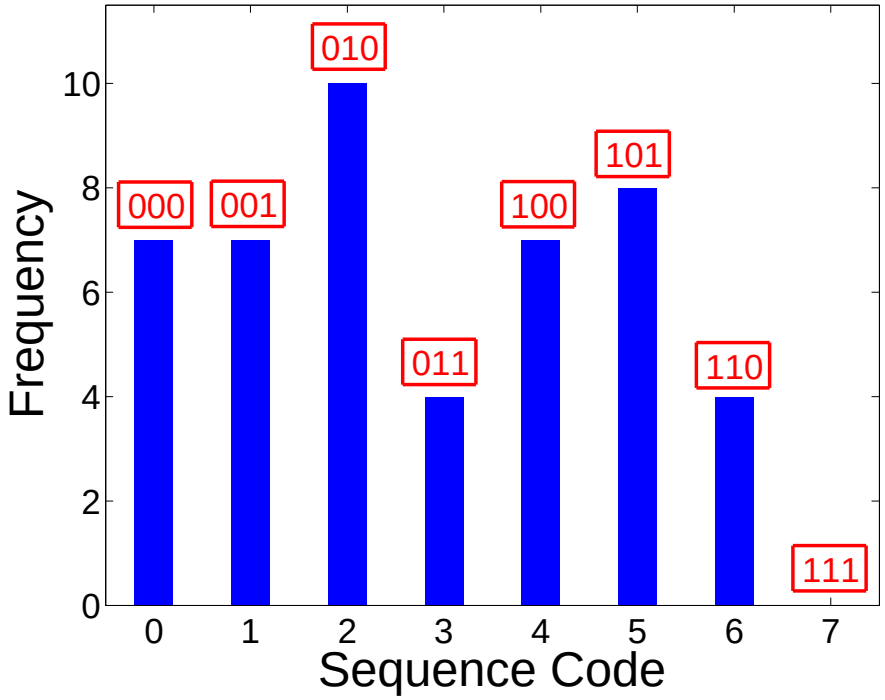

Figure B.2: Ignition timing for a sample point with conditions of ON 3 of Table 7.1.

After data symbolization, the joint probability is calculated by counting the number of occurrence of each sequence. The resulting joint frequency histograms can be used to approximate the mapping function by determining the maximum likelihood estimate for the next cycle given the occurrence of a specific set of past cycles. An example of probability of occurrence of consecutive symbols is shown below:

The probability of occurrence of three consecutive cycles P_{abc} emerges in the bottom level of the tree. The length of symbol sequence in this example is three which consists of three consecutive symbols. The sequence code is formed from converting the symbol sequences to their equivalent base-10 codes. For instance, in case of binary symbols used in this work, the symbol sequence 000 is equal to sequence code 0, 001 to 1, 010 to 2, 111 to 7 and so on. Symbol sequence

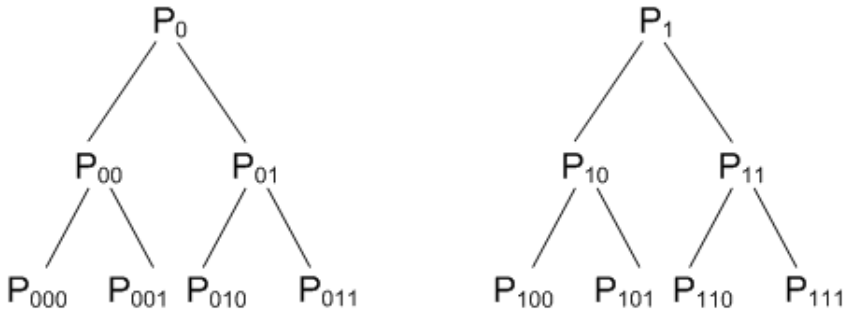

histograms used in this paper are the representation of these symbol sequence probabilistic with the sequence codes as the horizontal axis values. A completely random time series results on average in equal frequencies for histogram with equal number and equiprobable sequence codes. Deterministic data sets show deviations from the equiprobability because of existing time correlations and dependency of data points.

Appendix C

Program and Data File Summary

C.1 EXPERIMENTAL DATA AND POSTPROCESSING FILES

The following lists the script files used to study HCCI cyclic variation in Ricardo engine.

Table C.1: Postprocessing script files

File Name	**File Description**
ExpDataStruc-Build.m	Loading the values from excel spreadsheet and put them in the experimental data file format
GetHeatRelease.m	Calculating net and gross heat release using a single zone model for the Ricardo engine fitted with Rover head
GetHeatReleaseNewEngine.m	Calculating net and gross heat release using a single zone model for the Ricardo engine fitted with Mercedes head
GetHeatReleaseNewEngine_Modified _FindTotalHR.m	Finding the cycle-by-cycle Total Heat Release in addition to positive heat release until peak cumulative heat release
Import_to_Excel_Plot.m	Read all the required variables from CAS, ADAPT and DSpace and put their conditions in the excel file and also include the commands to plot the desired variables.
Cas2mat_converter.m	reads the outputs from the CAS ADAPT software for matlab file and formats it into a v4 .mat file. This requires changing the file extension and modifying the binary variable name such that it does not include any illegal characters.
DATAANALYSIS.m	combines the data from the CAS, ADAPT and dSPACE system and combines them into a single .mat file. The program also computes some general metrics such a efficiency and specific emissions and combines these into an excel sheet for quick reference.
Combustion_Analyzer_exp_batch.m	Combines all the data from CAS, ADAPT and Dspace, analyzes the data for individual cycles and gives the performance specific parameters as output

Table C.2: Postprocessing script files

File Name	**File Description**
ExpMatFile_Facilator.m	Facilitates making a workspace including the data from excel file
NIConvert.m	converts NI data to Pressure
HCCICombAnalyzer.m	Analyzes the main combustion metrics based on experiment results and engine type
pMeanCalculator.m	Calculates the average pressure signal for each cycle
pressFiltFilt.m	filters the data (usually pressure data) so that it can be more accurately differentiated to determine the ignition timing.
LHV_Finder.m	Calculates the lower heating value of used fuels
makeKinTable_Cond.m	Populate a table with calculated numbers from experimental data
ExpDataOrganizerOneFolder.m	Makes an ExpData for desired params in one folder
FolderNameFacilator.m	Selects the file directory and makes proper name for the files
Main_DataAnalyzer_Updated.m	Generates general ProcessedExpData files for processing large size experimental data
PlottingCyclicVariations.m	Plots the cyclic variations for different ignition cycle parameters based on the experimental data file format

C.2 NORMAL DISTRIBUTION AND STATISTICAL ANALYSIS FILES

The following lists the script files used to evaluate the fitted distribution of ignition timing consecutive cycles as well as performing statistical tests for different engine variables.

Table C.3: MATLAB script files

File Name	**File Description**
AutoCorrelation.m	Calculates autocorrelation of HCCI data series
DistTest.m	Checking type of data series distribution
Fitting_linear_correlation_to_data.m	Fitting linear correlation to data series
Good_Fitness_Params.m	Statistical tests to validate the goodness of prediction
Distribution_Generator.m	Generating the desired distribution shapes
ProbabilityApproach.m	Calculating the statistical parameters of experimental data

C.3 CHAOTIC ANALYSIS FILES

The following lists the script files required to perform different chaotic and non-linear technique tools on experimental data points.

Table C.4: MATLAB script files

File Name	**File Description**
Bifurcation_Diagram.m	Plots the bifurcation plot of experimental data series
BifurcationDiagramFunction.m	Generates the structure ExpData file which includes all the data files of corresponding determined directories
Lyapunov.m	determining Lyapunov exponents
Lyap of TS.m	creates a signal from non-uniformly sampled data
Fourier transform.m	Taking the Fourier transform of data series
SOC_Recursive.m	Generating return maps for ignition timings

C.4 SYMBOL-STATISTICS PREDICTIVE MODEL FILES

The following lists the MATLAB model and script files used to develop a chaotic time series which predicts cycle-to-cycle HCCI combustion timing.

Table C.5: MATLAB script files

File Name	**File Description**
Prediction.mdl (Simulink file)	Real time prediction of the time series with fixed symbol-set size and sequence length
Data_Symbol_Nonlinear_Pred _FixedSymbolSizeandSeqlength.m	Predicting the time series with fixed symbol-set size and sequence length
Data_Symbol_Nonlinear _Pred_VarSymbolSizeandSeqlength_Funcs.m	Predicting the time series with variable symbol-set size and sequence length
ChaoticPredictionRealTime.m	Regenerating the chaotic predictive models in real-time
Data_Symbolization_Primary_Version.m	Primary version of data symbolization based on symbol-statistics approach
Data_Symbolization_Tirreversibility_Calculation.m	Calculation of time irreversibility of time series based on symbol-statistics approach
Data_Symbolization_Partition_Variable.m	Variable partitioning of data series based on symbol-statistics approach
Complementary.m	Calculates and plots the Shannon entropy for different sequence lengths within the fixed directory